Inaugural dissertation

for

obtaining the doctoral degree

of the

Combined Faculty of Mathematics, Engineering and Natural Sciences of the

Ruprecht - Karls - University

Heidelberg

presented by
M. Sc. Sibylle Kanngießer
born in Marburg, Germany
oral examination: 09.12.24

Regulation of the ubiquitin ligase Ubr1 by the intrinsically disordered protein Roq1

Referees:
Prof. Dr. Hans-Walter Nickel
Prof. Dr. Sebastian Schuck

I. Summary

Many proteins have intrinsically disordered regions or are entirely disordered. Despite their lack of a stable three-dimensional structure, they are important regulators of a variety of cellular processes. The small intrinsically disordered protein Roq1 regulates SHRED, a protein quality control pathway in the budding yeast, *Saccharomyces cerevisiae*. Upon stress, Roq1 is cleaved, resulting in an exposed N-terminal arginine residue, namely R22. Via R22, Roq1 can bind to the E3 ubiquitin ligase Ubr1 as a pseudosubstrate, thereby outcompeting regular substrates. Ubr1 is the main N-recognin in yeast and recognizes proteins with destabilizing N-terminal residues through two distinct sites, the type-1 site for basic residues, and the type-2 site for hydrophobic residues. Binding of Roq1 shifts the substrate spectrum of Ubr1 from type-1 N-degron substrates to misfolded proteins, while promoting the turnover of type-2 substrates. However, the mechanism through which Roq1 reprograms Ubr1 is unclear. In this study, I built on a Roq1 mutagenesis screen that was performed prior to this study to identify SHRED-critical residues in Roq1. Analysis of the hits yielded fourteen SHRED-defective Roq1 point mutants. In addition, I identified a hydrophobic motif in the middle of the protein sequence (residues 55-58) that is necessary for Roq1 function. Specifically, these residues are required for both binding and regulating Ubr1 in vivo and in vitro. In vitro studies showed that the hydrophobic motif is important for promoting ubiquitination of misfolded substrates. In contrast, the hydrophobic motif is dispensable for the ubiquitination of regular N-degron substrates or substrates with internal degrons. Furthermore, this study demonstrates that Roq1 promotes ubiquitin chain initiation on misfolded substrates by Ubr1 dependent on the hydrophobic motif. Finally, I identified R22 and the hydrophobic motif connected by a short generic flexible linker as the minimally required building blocks of Roq1 to regulate Ubr1. Overall, this work provides mechanistic insights into how an IDP can control the substrate specificity of an E3 ligase.

II. Zusammenfassung

Viele Proteine besitzen intrinsisch ungeordnete Regionen oder sind vollständig ungeordnet. Trotz ihres Mangels einer stabilen 3D-Struktur sind sie wichtige Regulatoren verschiedenster zellulärer Prozesse. Das kleine intrinsisch ungeordnete Protein Roq1 reguliert den SHRED-Weg, einen Proteinqualitätskontrollweg in der Bäckerhefe *Saccharomyces cerevisiae*. Unter Stressbedingungen wird Roq1 gespalten, wodurch ein Arginin am N-Terminus freigelegt wird, nämlich R22. Über R22 kann Roq1 als Pseudosubstrat an die E3 Ubiquitin Ligase Ubr1 binden und so reguläre Substrate verdrängen. Ubr1 ist das Haupt-*N-Recognin* in der Hefe und erkennt Proteine mit destabilisierenden N-terminalen Resten über zwei verschiedene Bindestellen: die Typ-1 Stelle für basische Reste und die Typ-2 Stelle für hydrophobe Reste. Die Bindung von Roq1 verändert das Substratspektrum von Ubr1 von Typ-1 N-Degron-Substraten hin zu fehlgefalteten Proteinen, während gleichzeitig der Abbau von Typ-2 Substraten begünstigt wird. Der Mechanismus, durch den Roq1 Ubr1 umprogrammiert, ist noch unklar. In dieser Studie habe ich auf einem Roq1-Mutagenese-Screen aufgebaut, der bereits vor dieser Studie durchgeführt wurde, um SHRED-kritische Reste in Roq1 zu identifizieren. Die Analyse der Treffer ergab vierzehn SHRED-defekte Roq1-Punktmutanten. Am Ende habe ich ein hydrophobes Motiv in der Mitte der Proteinsequenz (Reste 55–58) identifiziert, das für die Roq1-Funktion notwendig ist. Diese Reste sind sowohl für die Bindung als auch für die Regulation von Ubr1 in vivo und in vitro erforderlich. In-vitro-Studien haben gezeigt, dass das hydrophobe Motiv besonders wichtig ist, um die Ubiquitinierung fehlgefalteter Substrate zu fördern. Im Gegensatz dazu ist das hydrophobe Motiv für die Ubiquitinierung von regulären N-Degron-Substraten oder Substraten mit internen Degrons entbehrlich. Darüber hinaus zeigt diese Studie, dass Roq1 die Initiierung der Ubiquitinkette auf fehlgefalteten Substraten in Abhängigkeit vom hydrophoben Motiv fördert. Zusätzlich habe ich die minimal erforderlichen Bausteine von Roq1 zur Regulation von Ubr1 bestimmt: R22 und das hydrophobe Motiv, verbunden durch einen kurzen generischen, flexiblen Linker. Insgesamt liefert diese Arbeit mechanistische Einblicke, wie ein IDP die Substratspezifität einer E3 Ligase steuern kann.

Table of content

Abbreviations

APS	Ammonium persulfate
BLI	Biolayer Interferometry
CRL	Cullin-RING ligases
Cryo-EM	cryo-electron microscopy
DTT	Dithiothreitol
DUB	Deubiquitinase
ER	Endoplasmic reticulum
ERAD	ER-associated protein degradation pathway
E1	Ubiquiti-activating enzyme
E2	Ubiquitin-conjugating enzyme
E3	Ubiquitin ligase
IDP	Intrinsically disordered protein
IDR	Intrinsically disordered region
OD	Optical density
PQC	Protein quality control
SDS-PAGE	Sodium dodecyl sulfate polyacrylamide gel electrophoresis
SHRED	Stress-induced homeostatically regulated protein degradation
SLiM	Short linear motif
Tm	Tunicamycin
Ub	Ubiquitin
U2BR	Ubc2-binding region
UFD	Ub-fusion degradation pathway
UPS	Ubiquitin-proteasome system
YNB	Yeast nitrogen base

1. Introduction

1.1 Protein quality control overview

Cells frequently need to adapt to changing physiological conditions. Genetic mutations or environmental stresses can cause impaired protein folding and an accumulation of misfolded proteins, threatening cell function (Balchin et al., 2016; Chen et al., 2011; Labbadia & Morimoto, 2015). The accumulation or aggregation of misfolded proteins is detrimental and is associated with various diseases, most notably neurodegeneration (Chiti & Dobson, 2006). To maintain protein homeostasis, cells must recognize aberrant and misfolded proteins and either refold or eliminate them (Wolff et al., 2014). Molecular chaperones play a critical role in this process by selectively identifying surface-exposed hydrophobic regions of misfolded proteins and facilitating their refolding (Balchin et al., 2016). Alternatively, misfolded proteins can be sequestered into specific subcellular deposits or targeted for degradation by the ubiquitin-proteasome system (UPS) (Chen et al., 2011). Ubiquitin E3 ligases are key determinants in marking proteins for destruction by the proteasome (Zheng & Shabek, 2017).

1.2 The ubiquitin-proteasome system

Protein degradation via the UPS is a fundamental regulatory mechanism in eukaryotic cells to maintain homeostasis. The selective breakdown of proteins plays a role in key regulatory mechanisms such as cell cycle progression, signal transduction, and protein misfolding (Dubiel & Gordon, 1999; Hochstrasser, 1996; Pickart & Fushman, 2004). This mechanism encloses two sequential steps: first, the conjugation of ubiquitin moieties to a substrate, and second, the degradation of the polyubiquitinated substrate by the 26S proteasome (Glickman & Ciechanover, 2002). The 26S proteasome is a 2.5 MDa multisubunit ATP-dependent protease found in the cytosol and nucleus of every cell (Forster et al., 2010; Hershko & Ciechanover, 1998). It contains two subunits with distinct functions: the 19S regulatory particle, which is equipped with ubiquitin receptors to bind ubiquitin-conjugated substrates and associated deubiquitinases (DUBs) that reverse the ubiquitin modifications. Then the substrate is unfolded and translocated to the 20S proteolytic core particle with the help of ATPases followed by substrate proteolysis (Finley, 2009; Finley et al., 2016). The fate of a ubiquitinated substrate is determined by the type of lysine residues used to link ubiquitin molecules (Hershko & Ciechanover, 1998). Ubiquitin has seven lysines (K6, K11, K27, K29, K33, K48, K63) and the N-terminal methionine (M1) that can be used for chain initiation and elongation (Ikeda & Dikic, 2008). A minimum of four ubiquitin moieties linked through K48 is required to promote

proteasomal degradation (Ciechanover & Schwartz, 1998). On the other hand, K63-linkages mainly serve as non-proteolytic signals and play a role in DNA repair and signal transduction pathways (Grabbe & Dikic, 2009). K11-chains have also been described to be recognized by the proteasome during mitosis, while other ubiquitin linkages are less likely to mediate degradation (Komander & Rape, 2012). Unlike polyubiquitination, monoubiquitination typically serves as a non-proteolytic signal in intracellular signaling, DNA repair, and signal transduction pathways (Hicke et al., 2005).

Ubiquitin is a highly conserved 76 amino acid (8 kDa) eukaryotic protein that is covalently linked to acceptor proteins through the sequential action of three enzymes: a ubiquitin-activating enzyme (E1), a ubiquitin-conjugating enzyme (E2), and a ubiquitin ligase (E3). First, the E1 enzyme activates ubiquitin in an ATP-dependent step. The activated ubiquitin is transferred to the E2 enzyme, which forms a thioester bond with the C-terminal carboxyl group of ubiquitin via its active site cysteine. Finally, the E3 ligase catalyzes the ubiquitin transfer of ubiquitin to the substrate by mediating the simultaneous interaction of E2~Ub and the substrate. The thioester bond from E2~Ub is orientated such that the incoming substrate lysine can make a nucleophilic attack on the C-terminal ubiquitin glycine, G76 (Plechanovova et al., 2012). As a result, an isopeptide bond between the lysine amino group of the substrate and the C-terminal carboxyl group of ubiquitin is formed (Ciechanover, 1994; Hochstrasser, 1995).

All E2 enzymes contain a catalytic domain with an active site cysteine that is used to form a thioester with ubiquitin. This region has been shown to be structurally conserved (Cook et al., 1997; Pickart, 2001; Tong et al., 1997; Worthylake et al., 1998).

Eukaryotes have three major types of E3 ligases: HECT (homologous to the E6-AP carboxyl terminus), RING (really interesting new gene) and HECT/RING hybrid ligases called RING-between-RING (RBR). RING E3 ligases mediate a direct transfer of ubiquitin from E2~Ub to the substrate, whereas HECT E3 ligases catalyze ubiquitination through an E3~Ub thioester intermediate (Deshaies & Joazeiro, 2009). RBR E3 ligases utilize a hybrid mechanism in which the RING1 domain first binds the E2 of the E2~Ub conjugate and then the RING2 forms a HECT-like E3~Ub thioester intermediate (Cotton & Lechtenberg, 2020). In all cases substrate specificity is determined by the E3 ligase as the substrate-binding unit (Cowan & Ciulli, 2022). RING ligases are well conserved across species, with about 600 different human RING ligases (Deshaies & Joazeiro, 2009). Within this family, the multisubunit cullin-RING E3 ligases (CRLs) are the largest family with more than 200 members. CRLs assemble with numerous substrate receptors, such as F-box, BTB and SOCS/BC-box proteins, allowing them to bind a

variety of different substrates (Petroski & Deshaies, 2005). Additionally, a new class of enzymes, the E4 enzymes, has been identified. E4 enzymes work in concert with E1, E2, and E3 enzymes to extend ubiquitin chains of already modified proteins, thereby promoting polyubiquitination (Hoppe, 2005; Koegl et al., 1999).

1.3 The RING E3 ligase Ubr1

1.3.1 The N-degron pathway

The N-degron pathway is a branch of the UPS and is critical for the regulated degradation of proteins within a cell. This pathway targets proteins based on the identity of their N-terminal residue, called N-degron. N-degrons were the first degradation signals of short-lived proteins discovered in 1986 and are initially generated by proteolytic cleavage (Rao et al., 2001; Varshavsky, 2011). This selective degradation has been shown to regulate a variety of cellular processes like oxygen sensing, peptide transport, apoptosis, DNA repair and the removal of misfolded proteins (Dissmeyer et al., 2018; Eldeeb et al., 2018; Varshavsky, 2011). For example, during apoptosis, caspases cleave cellular proteins to produce proapoptotic Ct-fragments with destabilizing N-termini. Therefore, the N-degron pathway regulates apoptosis by destroying proapoptotic fragments (Piatkov et al., 2012).

In eukaryotes, the Arg/N-degron pathway targets unacetylated N-terminal residues. This pathway differentiates between primary, secondary, and tertiary substrates based on whether the N-terminal residue requires modification before recognition by an E3 ligase. Therefore, initially most degrons are pro-N-degrons. For example, N-terminal Asn, Gln, Asp, Glu, and Cys are secondary and tertiary destabilizing residues and require enzymatic modifications, such as Nt-deamidation and Nt-arginylation, to become primary degrons (Brower & Varshavsky, 2009; Tasaki et al., 2012; Varshavsky, 2011). Hence, primary unmodified basic residues like Arg, Lys and His, and bulky hydrophobic residues like Leu, Phe, Tyr, Trp, Ile, and Met (if Met is followed by a hydrophobic residue) are directly recognized by a cognate E3 ligase (Choi et al., 2010; Varshavsky, 2008) (**Figure 1**).

In *Saccharomyces cerevisiae*, the 225 kD RING E3 ligase Ubr1 is the sole E3 ligase involved in the Arg/N-degron pathway, where it has been extensively studied. Ubr1 employs two distinct binding sites to recognize N-terminal residues, the type-1 site (for basic residues), and the type-2 site (for bulky, hydrophobic residues) (Xia, Webster, et al., 2008). These binding sites are embedded within the UBR-box domain, with Ubr1 preferentially binding the residue arginine via a shallow and acid surface groove (Choi et al., 2010; Matta-Camacho et al., 2010).

Additionally, Ubr1 was found to act in concert with the HECT-type E3 ligase Ufd4 and the corresponding E2 enzymes Rad6 and Ubc4/5. Although Ufd4 cannot recognize N-degrons itself, it increases the processivity of polyubiquitination by Ubr1 (Hwang et al., 2010).

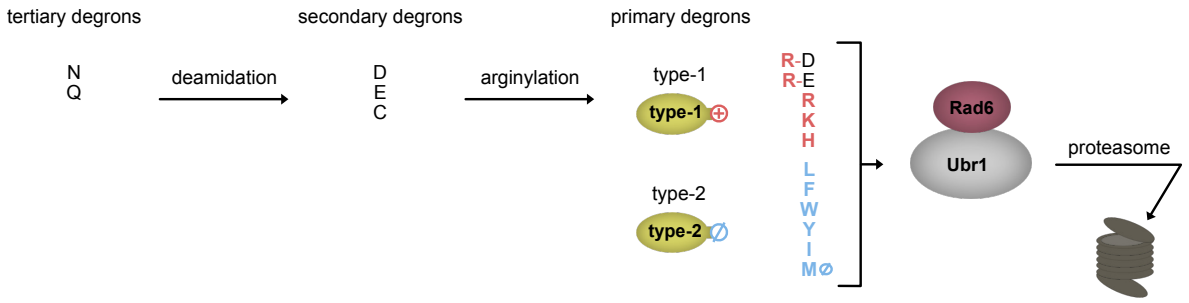

Figure 1: The Arg/N-degron pathway in *S. cerevisiae*.
Nt-residues are classified in primary, secondary or tertiary degrons. Tertiary degrons need to undergo two rounds of modification and secondary degrons one, whereas primary degrons can be recognized by the E3 ligase directly. Type-1 and type-2 define the two categories of N-degron substrates with either basic (red) or bulky, hydrophobic (blue) residues, with methionine followed by a hydrophobic residue (Φ). Degrons are recognized by Ubr1, the E3 ligase and N-recognin, in complex with Rad6, the E2 enzyme, and proteins are marked for proteasomal degradation. Nt-residues are shown in the single-letter code. Based on (Varshavsky, 2011).

1.3.2 Physiological Ubr1 substrates

Typically, Ubr1, as the major player of the N-degron pathway, targets proteins with destabilizing N-terminal residues. However, Ubr1 also has some physiological substrates with internal degrons, such as Cup9. Cup9 represses the transcription of the di/tripeptide importer Ptr2 (Cai et al., 2006). While the substrate-binding sites of Ubr1 that target N-degrons are always accessible, a third site on Ubr1, that targets Cup9, is autoinhibited. The autoinhibition of Ubr1 can be allosterically reversed through binding of short peptides to the N-degron binding sites. Imported di- or tripeptides with destabilizing N-terminal residues bind to the type-1 and type-2 sites of Ubr1, which allosterically activates the otherwise autoinhibited Cup9-binding site. This activation increases the proportion of Ubr1 molecules that can target Cup9 for polyubiquitination, leading to the rapid degradation of Cup9 and the subsequent de-repression of the PTR2 gene. This positive-feedback loop enables *S. cerevisiae* to detect extracellular peptides and respond by enhancing their uptake (Byrd et al., 1998; Du et al., 2002; Turner et al., 2000; Xia, Turner, et al., 2008). Thus, Ubr1 activity is closely linked to an environmental signal and is allosterically regulated by peptides.

Another example is Mgt1, a DNA alkyltransferase, involved in DNA repair by demethylating lesions in double-stranded DNA in *S. cerevisiae*. Mgt1 is targeted by both the N-degron pathway, via Ubr1/Rad6, and the UFD pathway, via Ufd4/Ubc4. Unlike Cup9, the interaction with Ubr1 does not require cognate dipeptides (Hwang et al., 2009).

Chk1, a mitotic checkpoint kinase and client of Hsp90, is also a Ubr1 and Ufd4 substrate with an internal degron. It has been shown, that Ubr1 and Hsp90 compete for Chk1, depending on the presence of an Nt-acetylase. In absence of this Nt-acetylase normally acetylated proteins, including Hsp90, lack this modification and are destabilized. Without protection by Hsp90, Chk1 is rapidly degraded by Ubr1 through the N-degron pathway (Oh et al., 2017).

1.3.3 Degradation of misfolded proteins

Misfolded proteins are targeted by the cellular quality control machinery, which refolds, sequesters or degrades them upon recognition (Buchberger et al., 2010). Ubr1 has also been shown to be part of quality control systems that function to selectively eliminate misfolded proteins in the nucleus or cytosol (Eisele & Wolf, 2008). In yeast, these systems include the Hsp70 chaperone-assisted import of misfolded cytosolic proteins into the nucleus, followed by their degradation by both the E3 ligase San1 and Ubr1 (Heck et al., 2010; Prasad et al., 2010). Thus, Ubr1 can directly interact with misfolded proteins, a process which is further supported by molecular chaperones that present these substrates to Ubr1. In addition, Ubr1 also participates in PQC through the endoplasmic reticulum-associated degradation pathway (ERAD), which recognizes and degrades ER membrane proteins (Stolz et al., 2013). Overall, these functions demonstrate that Ubr1 also has functions beyond the N-degron pathway.

1.3.4 Mode of action

Ubr1 mediates the ubiquitination of its substrates through a process that involves distinct structural rearrangements. This process was elucidated in 2021 by Man Pan and colleagues, who obtained cryo-EM structures of the first and second ubiquitin transfer steps of Ubr1 in complex with Rad6 (E2), ubiquitin and N-degron peptides using chemical strategies. Ubr1 primarily catalyzes K48-linked ubiquitination and partial K63-linked ubiquitination. Compared to multisubunit CRLs, Ubr1 was shown to exhibit faster kinetics for the initiation step and slower kinetics for chain elongation (Pan et al., 2021; Saha & Deshaies, 2008). The overall structure of apo Ubr1 resembles a sailboat (**Figure 2**). The base is formed by a helical scaffold containing the type-1 and type-2 sites for N-degron substrate binding while Rad6 is bound by both the RING domain and the U2BR (Ubc2/Rad6 binding region). Ubr1 forms an interface with the backside of Rad6 through non-covalent interactions, positioning the Rad6~Ub thioester bond close to the substrate lysine in a so-called closed conformation (Pan et al., 2021). The unifying concept is, that E3 ligases activate the thioester of the E2~Ub conjugate by holding the ubiquitin in a folded-back position, extending the C-terminal tail of

ubiquitin. Thus, E3 ligases provide a scaffold to ensure optimal ubiquitin transfer from the E2 to the substrate and promote closed conformations (Plechanovova et al., 2012).

After the initial ubiquitin transfer, subsequent chain elongation involves structural rearrangements. The ubiquitin-binding loop of Ubr1, which is disordered in the initiation complex, becomes structured and binds the acceptor ubiquitin while Rad6 is released (**Figure 2**). The ubiquitin loop then further participates in the recruitment of another Rad6~Ub by providing an anchor for newly conjugated ubiquitin. Therefore, when comparing the initiation and elongation complexes, the U2BR together with Rad6 undergoes a displacement of about 18 Å, while the rest of the Ubr1 structure remains unchanged. This is the key to make the Rad6~Ub thioester approachable by the K48 of ubiquitin-degron for elongation (Pan et al., 2021).

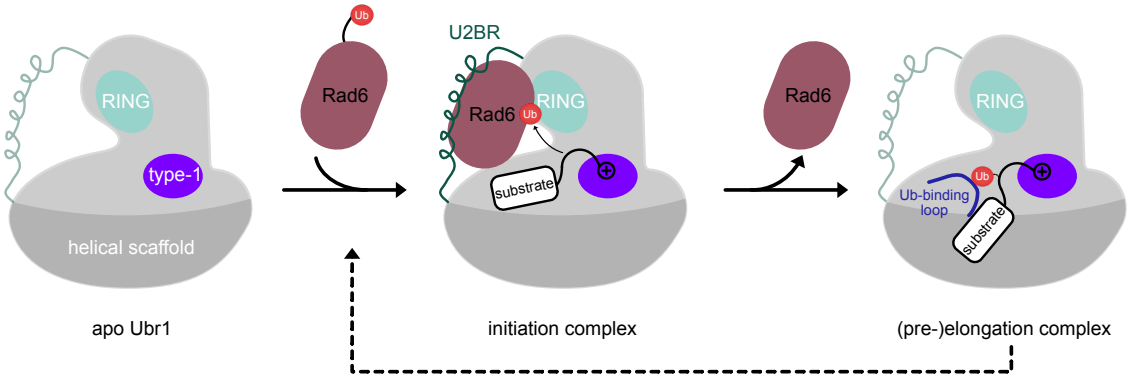

Figure 2: Mode of ubiquitination by Ubr1.
The type-1 substrate binds to the type-1 site of Ubr1 via its positively charged N-terminal residue. Rad6~Ub binds to Ubr1 through two sites: the RING domain and the U2BR (Ubc2/Rad6-binding region). In the initiation complex, the U2BR undergoes structural rearrangements. The ubiquitin-binding loop, embedded in the helical scaffold of Ubr1, is disordered and becomes structured upon Rad6~Ub binding and binds to the initial acceptor ubiquitin once conjugated to the substrate. After ubiquitin transfer, the U2BR moves away, Rad6 is released and Ubr1 can bind a newly charged Rad6 molecule. Based on (Pan et al., 2021).

1.3.5 Conservation and disease

In contrast to the yeast N-degron pathway, the mammalian genome encodes for at least four N-recognins: Ubr1, Ubr2, Ubr4 and Ubr5. Ubr1 and Ubr2 are highly sequelogous (similar in sequence) to each other and to yeast Ubr1 (Tasaki et al., 2012; Varshavsky, 2011). Moreover, a double deletion in mice has been shown to be lethal (Tasaki et al., 2005). The mammalian homolog of Ubr1 is involved in a broader array of functions, including the regulation of cardiovascular development, neurogenesis, and apoptosis (An et al., 2006). The lack of Ubr1, coupled with the presence of other N-recognins like Ubr2, is associated with the Johanson-Blizzard syndrome (JBS). This condition is characterized by symptoms like pancreatic

insufficiency, inflammation, multiple malformations, and mental retardation (Zenker et al., 2005). Moreover, similar to how Ubr1 controls peptide uptake in yeast by degrading Cup9, mammalian Ubr1 acts as an amino acid sensor to control hepatic steatosis. In the presence of amino acids, Ubr1 targets Plin2, a lipid droplet protein, for degradation (Zhang et al., 2022; Zhao et al., 2023). Along this line, a previous study has shown that patients with hepatic steatosis can reduce liver fat through a high-protein diet (Markova et al., 2017). This underlines that a thorough understanding of Ubr1 regulation in cells is crucial for developing strategies to cure Ubr1-related diseases.

1.4 Regulation of E3 ligases

E3 ligases perform a large variety of functions within cells. Hence, their activity needs to be tightly controlled (Vittal et al., 2015). The most prominent regulatory mechanisms are outlined below.

1.4.1 Phosphorylation

Phosphorylation plays a critical role in regulating E3 ligase activity. For instance, the anaphase promoting complex (APC) E3 ligase is activated by phosphorylation (Zhang et al., 2016). This modification alters the conformation of the enzyme, thereby assisting to stabilize the closed conformation of E2~Ub on the E3 ligase or positioning the bound E2 closer to the substrate (Dou et al., 2012).

The properties of Ubr1 in regulating peptide import have also been shown to involve a phosphorylation cascade in vivo. Ubr1 is initially phosphorylated at S300 by the Yck1/Yck2 kinases of the casein kinase type-1 family. This modification primes Ubr1 for further phosphorylation by Mck1, a Gsk3-type kinase, on S296, S292, T288 and Y277. However, the phosphorylation on S300 was shown to be mainly relevant to promote peptide import (Hwang & Varshavsky, 2008). Notably, not only E3 ligases but also substrates can be modified. Substrate degrons can either be generated through proteolytic cleavage or post-translational modification (PTM) (Cowan & Ciulli, 2022).

1.4.2 Ubiquitin-like modification

The most abundant class of RING ligases are the CRLs which contain a cullin at their core (Petroski & Deshaies, 2005). Structural studies of the human CRL Skp1-Cul1-F-box protein (SCF) revealed a ~50 Å gap between the bound substrate and the active site of E2~Ub docked

to SCF (Zheng et al., 2002). To bridge this gap, the SCF cullin must undergo modification by the ubiquitin-like protein Nedd8 (Pan et al., 2004; Saha & Deshaies, 2008). The covalent binding of Nedd8, known as neddylation, activates chain initiation by inducing substantial conformational rearrangements that bring the bound E2~Ub and the naked substrate into closer proximity. Moreover, neddylation improves the recruitment of the E2 enzyme and also increases the probability of tetraubiquitin chain transfer to the substrate (Duda et al., 2008; Saha & Deshaies, 2008).

1.4.3 Complex assembly

E3 ligases can form homo- or heterotypic assemblies involving either the same or different E3 ligases (Balaji & Hoppe, 2020). The oligomeric state can regulate the activity of E3 ligases, resulting in activation or inactivation. In addition, potentially multiple degrons can be recognized in a single substrate (Tang et al., 2007).

RING-homodimerization activates the RING ligase cIAP2 (Inhibitor of apoptosis). It is postulated, that changes in the RING domain are associated with E2 binding. Accordingly, dimeric cIAP2 exhibits a higher affinity for E2~Ub compared to its monomer, thereby enhancing polyubiquitination. In the cIAP2 dimer both E3 molecules recruit an E2 symmetrically, unlike in asymmetric assemblies where only one unit binds the E2 (Feltham et al., 2011; Mace et al., 2008).

The breast cancer tumor suppressor (BRCA1) exists as a RING heterodimer with BARD1 to provide E3 ligase activity (Brzovic et al., 2001). Only one of the monomer subunits binds the E2 enzyme, BRCA1, while the other has stabilizing functions and potentially interacts with substrates (Metzger et al., 2014). Thus, RING dimerization is a complex and crucial mode to control E3 ligase activity.

1.4.4 Substrate recognition through receptor units

CRLs are multisubunit E3 ligases which exhibit an immense plasticity in substrate specificity. They are characterized by the presence of a cullin subunit to bind a substrate receptor and a RING protein to recruit E2~Ub. Cul1-7 define the CRL subfamilies, which differ in their substrate receptor unit and RING protein (Bulatov & Ciulli, 2015). A well-studied example is the SCF (Skp1-Cul1-F-box protein) E3 ligase family. Sixty-nine F-box proteins have been identified to act as substrate receptors for SCF E3 ligases in humans (Cenciarelli et al., 1999; Jin et al., 2004; Winston et al., 1999). They bind to Skp1 through an F-box domain and to the substrate through protein-protein interaction motifs, like WD-40 (Zheng et al., 2002). The main

substrates targeted by SCF complexes are regulators of cyclin-dependent kinases (CDKs) or regulators of gene transcription, thereby controlling cellular proliferation (Zheng et al., 2016).

1.4.5 Autoinhibition

All three classes of E3 ligases have also been shown to be regulated by autoinhibitory mechanisms (Buetow & Huang, 2016). For example, the RBR E3 ligase Parkin is autoinhibited by its ubiquitin-like (Ubl) domain to suppress substrate binding (Chaugule et al., 2011). The kinase PINK1 activates Parkin through phosphorylation of the Ubl domain, leading to parkin activation (Shiba-Fukushima et al., 2012). Parkin then ubiquitinates mitochondrial outer membrane proteins and induces their degradation or mitophagy (Narendra et al., 2008; Tanaka et al., 2010).

The mechanism of Ubr1 to control peptide uptake in cells by degrading Cup9 also involves autoinhibition. The synergistic binding of two dipeptides to both the type-1 and type-2 site of Ubr1 leads to the unmasking of another substrate binding site. The hereby induced allosteric rearrangements involve the release of a C-terminal fragment (1678-1950) of Ubr1 that is normally bound to the N-terminal half of Ubr1(1-1140). Finally, this aspect of autoinhibition has also been observed with mouse Ubr1 (Du et al., 2002).

1.5 PROTACS and molecular glues

An emerging modality in drug discovery is targeted protein degradation by so-called proteolysis-targeting chimeras (PROTACs) or molecular glues. The function of PROTACs is to induce proximity between an E3 ligase and a protein of interest (POI), forming a ternary complex. The POI is then ubiquitinated and degraded by the proteasome. Thus, PROTACs are composed of a ligand that binds the target POI, followed by a chemical linker and a ligand for an E3 ligase. Computational, fragment- or structure-based approaches are used to design plausible ligands. The first generation of PROTACs was reported in the early 2000s (Sakamoto et al., 2001). Today, E3 ligases like cereblon (CRBN), von Hippel-Lindau (VHL) and inhibitors of apoptosis (IAPs) are used as therapeutic target for PROTACs (Itoh et al., 2010; Winter et al., 2015; Zengerle et al., 2015).

In contrast to PROTACs, molecular glues mediate de novo protein-protein interactions between an E3 ligase and a *neo*-substrate (Ramachandran & Ciulli, 2021). The plant hormone auxin is the first notable example. Auxin binds to an F-box protein of the SCF E3 ligase and builds a substrate-binding site for Aux/IAAs, auxin transcriptional repressors. This activates the

transcription of auxin-regulated genes. By enhancing the substrate interaction of SCF by filling in a hydrophobic cavity at the SCF-substrate interface, auxin acts as a molecular glue and controls plant growth (Tan et al., 2007). Similarly, non-natural molecular glues like thalidomide and its immunomodulatory drugs (IMiD) analogues lenalidomide and pomalidomide, have been found to extend the survival of patients with multiple myeloma (Ramachandran & Ciulli, 2021; Singhal et al., 1999). They target cereblon (CRBN), a CRL ligase substrate receptor (Ito et al., 2010). Binding modulates the substrate specificity of CRL to target specific B cell transcription factors for degradation (Fischer et al., 2014; Kronke et al., 2014). Molecular glues have also been specifically designed to rescue impaired degradation of substrates caused by mutation of E3 ligases during disease (Simonetta et al., 2019).

To facilitate the degradation of a broader range of proteins and for higher selectivity, expanding the E3 ligase toolbox becomes an important objective. There are more than 600 E3 ligases in mammalian cells that can potentially be hijacked for targeted protein degradation. This has the potential to develop degraders with a wider range of cell- or tissue-specific expression (Ishida & Ciulli, 2021).

1.6 Disordered proteins

Molecular interactions play a crucial role in determining the fate and function of a cell and are largely mediated by proteins that convey cellular information. Typically, these interactions occur through well-structured folded domains often separated by intrinsically disordered regions (IDRs). IDRs are unable to acquire a stable tertiary structure since they generally lack hydrophobic amino acids to form a hydrophobic core to build a structured domain. Despite the lack of a three-dimensional structure, they actively participate in diverse functions of proteins (van der Lee et al., 2014). Accordingly, a protein that is entirely disordered is referred to as an intrinsically disordered protein (IDP) (Holehouse & Kragelund, 2024).

Many proteins are composed of a higher number of IDRs than structured regions. In fact, 33 % of the eukaryotic proteome have functionally relevant disordered sequences (Ward et al., 2004). Chromatin and transcription regulators, in particular, are vastly enriched in protein disorder (Cermakova & Hodges, 2023; Tompa et al., 2015). In contrast, proteins predominantly composed of folded domains are commonly involved in metabolic and homeostasis regulating processes (Cermakova & Hodges, 2023). Despite their lack of any stable structure, IDRs are involved in a wide range of interactions. This includes molecular switches, scaffolding, oligomer assembly, subnuclear localization by selective partitioning of proteins into diverse

phase-separated condensates in the nucleus, and degron regulation (Cermakova & Hodges, 2023; Sabari et al., 2020). These interactions are often regulated by post-translational modifications (PTMs) such as phosphorylation, which can change the energy landscape (Aoki et al., 2020; Dyson & Wright, 2005). IDRs can bind to other biomolecules through one of the three mechanisms (**Figure 3**): (**A**) coupled folding and binding in which either the entire IDR folds upon binding to its binding partner or only a subregion, following the concept of induced fit or conformational change (Arai et al., 2015; Robustelli et al., 2020); (**B**) Fuzzy binding, which involves static disorder (e.g. during amyloid fibril assembly) or dynamic disorder, where the complex is rapidly rearranged (Berlow et al., 2022; Yang et al., 2022); and (**C**) Binding between two IDRs to form fully disordered complexes involving short-lived and electrostatic interactions (Schuler et al., 2020).

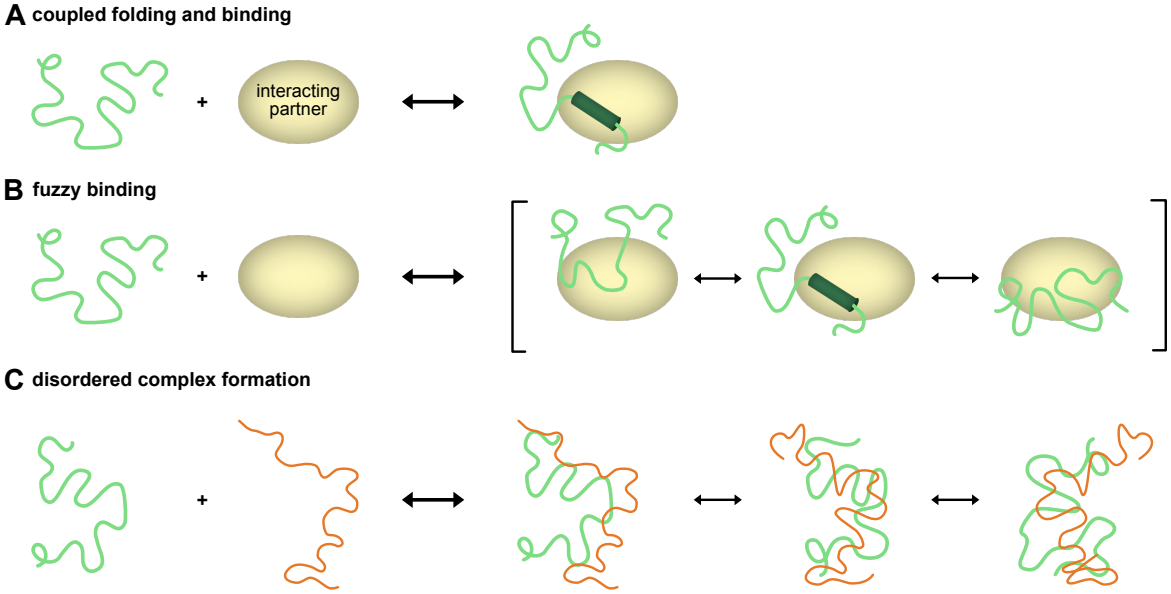

Figure 3: Binding mechanisms of proteins with disorder.
(**A**) IDRs (or a subregion) of a protein can fold upon binding to an interacting partner. (**B**) Multiple ensembles from static to dynamic and from full to segmental disorder are formed when IDRs undergo fuzzy binding interactions. (**C**) Interaction of two disordered partners leads to the formation of fully disordered complexes without adopting any structure. Based on (Holehouse & Kragelund, 2024).

These mechanisms are often assisted by so-called short linear motifs (SLiMs), a small functional unit found within IDRs (Davey et al., 2012; Kumar et al., 2020). They typically consist of 3–15 amino acids (Van Roey et al., 2014; Zanzoni et al., 2019) and even single mutations in SLiMs can have destructive consequences for the cell (Meszaros et al., 2017). Unlike the generally poor conservation of IDRs, SLiMs are more likely to be conserved (Davey et al., 2015). The first SLiMs to be described were targeting signals, such as the KDEL motif,

an ER retention signal, or the nuclear localization signal (NLS) (Dingwall & Laskey, 1991; Munro & Pelham, 1987). Over time, it has become evident that SLiM interactions are involved in nearly every aspect of cell biology, including vesicle trafficking, cell cycle regulation and RNA and protein degradation systems (Giangreco et al., 2021; Robinson, 2004; Van Roey et al., 2012). A drawback of the extensive use of SLiMs in cells is the vulnerability, as intracellular pathogens often hijack cellular pathways by mimicking motifs of host cell interactions (Meszaros et al., 2021).

1.7 An IDP controls the SHRED pathway in yeast

Different stress responses exist to counteract protein misfolding. In the yeast *S. cerevisiae,* proteotoxic stress activates the SHRED pathway for stress-induced homeostatically regulated protein degradation. This pathway is controlled by Roq1, a small IDP that binds and regulates the substrate specificity of the E3 ligase Ubr1 (Szoradi et al., 2018). Under non-stress conditions, Ubr1 determines the half-life of many proteins by recognizing their N-terminal amino acid residues as part of the N-degron pathway (**Figure 4**). To do this, Ubr1 has two distinct binding sites: a type-1 binding site to recognize basic N-terminal residues; and a type-2 binding site to bind bulky, hydrophobic N-terminal residues. However, various stress conditions upregulate the transcription of the *ROQ1* gene and the Roq1 protein is then proteolytically cleaved by the HtrA-type protease Ynm3. As a result, the C-terminal cleavage fragment, termed Roq1(22-104), exposes a positively charged arginine residue (R22) at its new N-terminus. This arginine enables Roq1(22-104) to bind to the type-1 binding site of Ubr1 as a pseudosubstrate and promotes the degradation of misfolded proteins, thereby increasing cellular stress resistance. At the same time, Roq1(22-104) outcompetes regular type-1 N-degron substrates and promotes the turnover of type-2 N-degron substrates. Thus, SHRED represents a protein quality control pathway in which an IDP comprehensively reprograms the substrate specificity an E3 ligase. However, the underlying molecular mechanism is unknown.

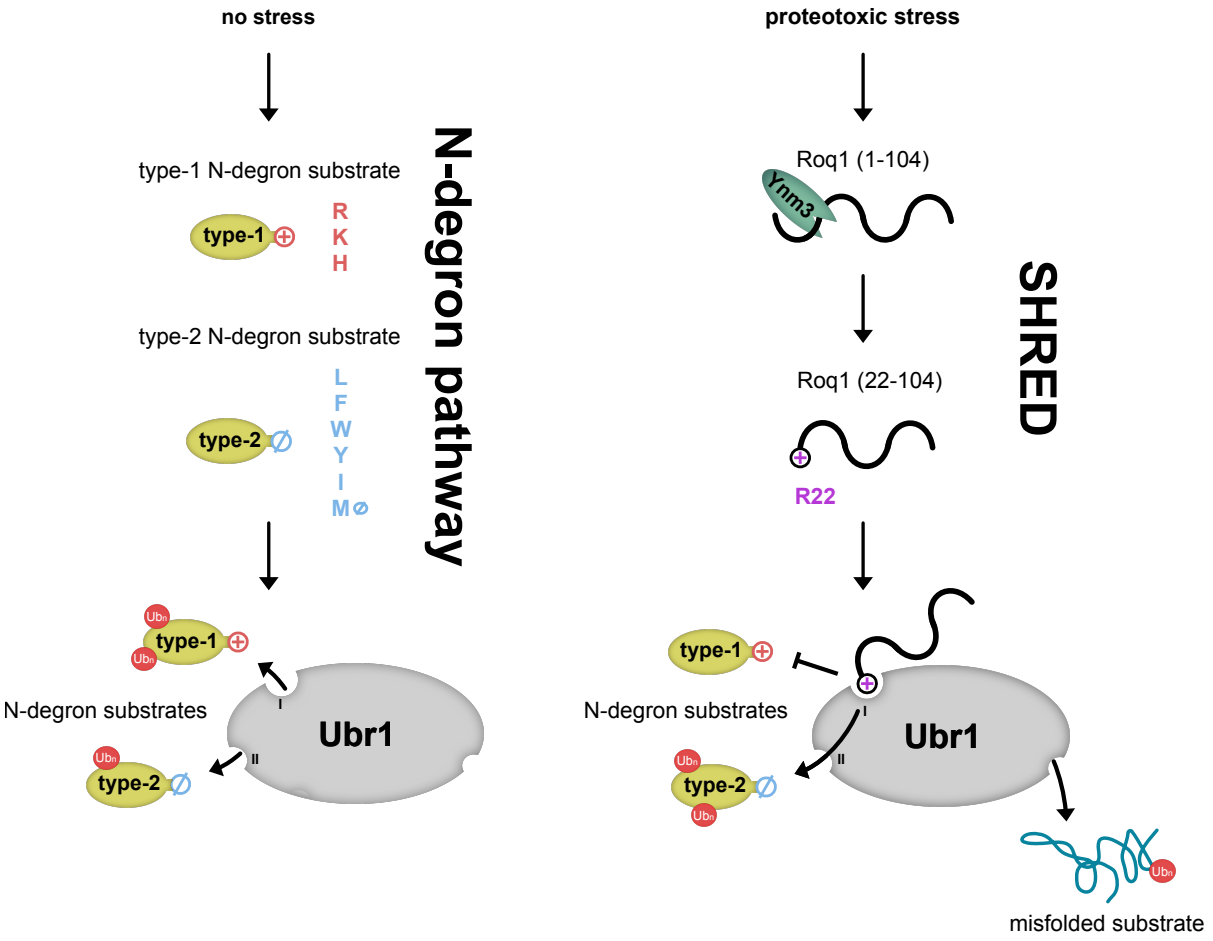

Figure 4: The N-recognin Ubr1 and the SHRED pathway in yeast.
Under non-stress conditions, Ubr1 targets and ubiquitinates substrates with destabilizing N-terminal residues via two distinct sites: the type-1 site for basic residues (R=Arg, K=Lys, H=His) and the type-2 site for bulky, hydrophobic residues (L=Leu, F=Phe, W=Trp, Y=Tyr, I= Ile). Stress upregulates levels of Roq1, which is proteolytically cleaved by the protease Ynm3. Via its new N-terminus (R22) Roq1(22-104) can bind to the type-1 site of Ubr1, where it outcompetes the binding of regular type-1 N-degron substrates. Roq1 binding also enhances the ubiquitination of type-2 N-degron substrates and more importantly changes the substrate specificity of Ubr1 towards misfolded cytosolic proteins in a pathway named SHRED (Szoradi et al., 2018).

1.8 The IDP Roq1

Roq1 consists of only 104 amino acids (**Figure 5A**). It belongs to the protein family of hydrophilins, involved in desiccation tolerance in yeast, and is defined by high hydrophilicity and a high glycine content (Battaglia et al., 2008; Dang & Hincha, 2011).

The Roq1 protein is predicted to be almost entirely disordered and therefore lacks a defined structure. Some parts are less disordered than others: One containing the Ynm3 cleavage site with R22 and one in the middle of the protein sequence (residues 50-65) (**Figure 5B+C**). In addition, Roq1 is poorly conserved, with sequence homologs found only in closely related species (**Figure 5D**). Consistent with the disorder prediction, two regions show the highest

sequence conservation. Among this is the Ynm3 cleavage site and a hydrophobic region in the middle of the protein sequence.

Apart from R22 of Roq1 no other motif was known to regulate Ubr1. However, Roq1 binds the type-1 site of Ubr1 without being a substrate itself, raising the question if and which other sites in Roq1 are relevant for its function.

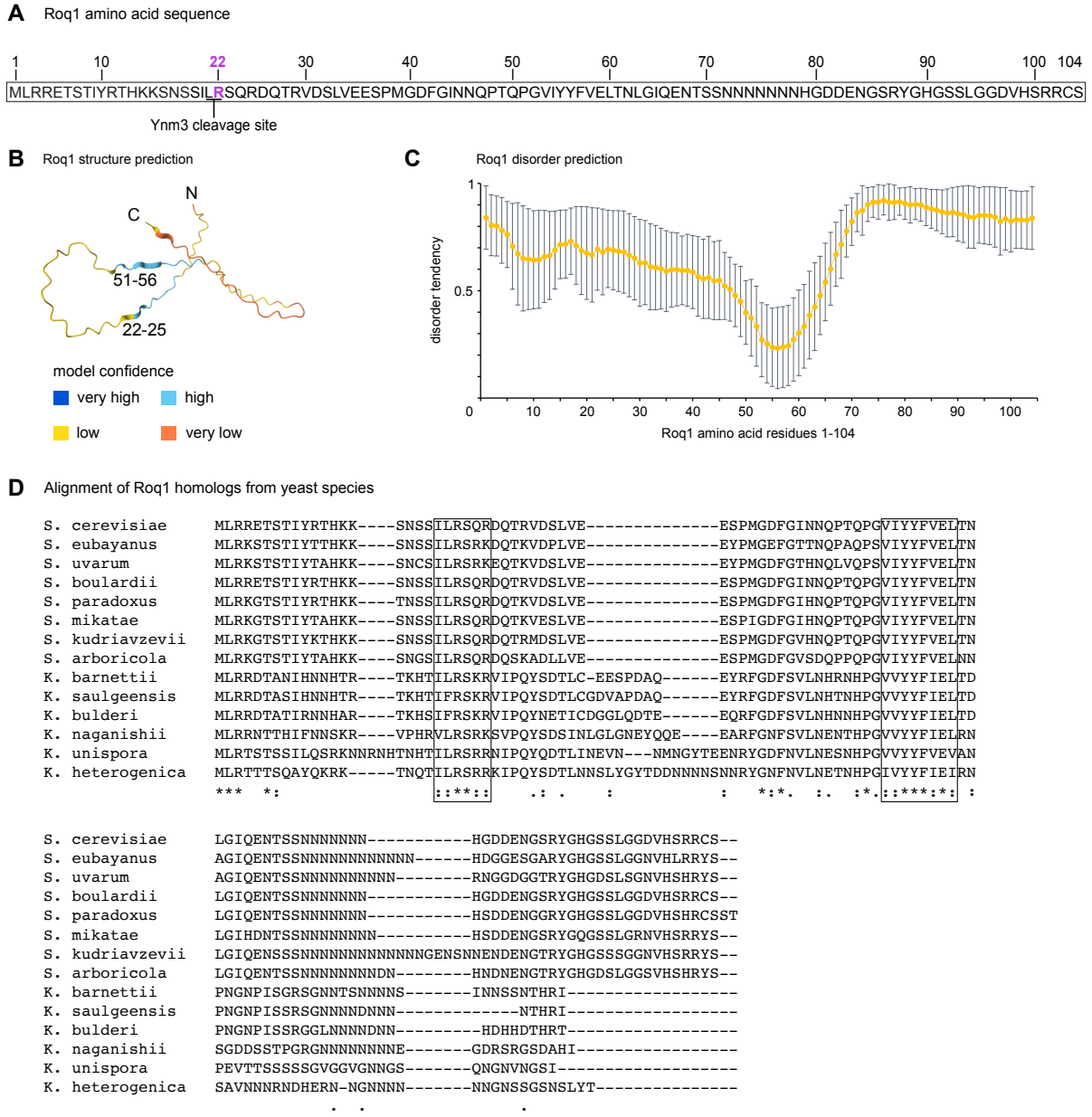

Figure 5: Features of the IDP Roq1.

A) Schematic amino acid sequence of Roq1(1-104). **B**) Roq1 structure prediction by AlphaFold (Varadi et al., 2024). **C**) Roq1(1-104) protein disorder plot. **D**) Sequence alignment with Roq1 homologs from fourteen yeast species with residues fully conserved (*), strongly conserved (:) and weakly conserved (.). R22 and a hydrophobic region of Roq1 are more conserved and marked by a box.

1.9 Aim of this thesis

E3 ligases are key regulators of the ubiquitin-proteasome system (UPS) by marking proteins for degradation to prevent their accumulation and associated diseases. Therefore, a detailed understanding of the regulation of E3 ligases is fundamental. In yeast, it has been shown that under stress the E3 ligase Ubr1 changes its substrate specificity from N-degron substrates to misfolded proteins in a pathway named SHRED. This is mediated by Roq1, a small IDP that is proteolytically cleaved and binds Ubr1 as a pseudosubstrate via its new N-terminus. How exactly Roq1 is able to control the substrate specificity of this E3 ligase remains unknown.

The overall aim of this project was to elucidate how Roq1 comprehensively reprograms Ubr1. This study was preceded by a genetic mutagenesis screen of Roq1. I then studied a set of uncharacterized Roq1 point mutations to

1) identify SHRED-critical residues in Roq1.
2) identify residues required for Ubr1 binding and regulation.
3) understand the mechanism of Ubr1 reprogramming by Roq1.

1.10 Contributions

In this project, my primary focus was the identification of SHRED-critical elements in Roq1 in order to understand the mechanism of Ubr1 reprograming. All experiments presented here were designed and performed by me, unless noted otherwise in the figure legends. Experiments performed in collaboration with colleagues are pointed out in the main text.

This work was a joint project with my fellow graduate student Niklas Peters. He focused on reconstituting the SHRED pathway in vitro to understand the reprograming of Ubr1 by Roq1. Therefore, he purified all necessary components and established a ubiquitination assay. Later, I also purified components following Niklas Peters' protocols and applied ubiquitination assays as well.

My work built on the Master thesis of Oliver Pajonk, who initiated the Roq1 mutagenesis screen. The biolayer interferometry studies of Roq1 and Ubr1 (**Figure 12**) were performed with initial assistance from Carola Sparn (Nickel lab, BZH). The photo-crosslinking experiment (**Figure 13**) was carried out in collaboration with Niklas Peters and with the help of Jörg Malsam (Söllner lab, BZH).

2. Materials and Methods

2.1 Materials

2.1.1 Yeast and *E. coli* growth media and plates

Table 1. Recipe for 10x synthetic complete amino acid mix (100 ml) for yeast media.

Component	Amount	Component	Amount
adenine	0.5 g	leucine	4 g
alanine	2 g	lysine	2 g
para-aminobenzoic acid	0.2 g	methionine	2 g
arginine	2 g	phenylalanine	2 g
asparagine	2 g	proline	1 g
aspartic acid	2 g	serine	2 g
cysteine	2 g	threonine	2 g
glutamic acid	2 g	tyrosine	2 g
glutamine	2 g	tryptophan	2 g
glycine	2 g	uracil	2 g
histidine	2 g	valine	2 g
isoleucine	2 g		

100 ml of 10 x amino acid mixes were combined with stocks of 20 % glycose (100 ml), 10 x YNB (without ammonium sulfate) (100 ml) and 500 ml of water to prepare final 1 L of 1 x SCD medium. Drop-out media (SC-URA) were prepared by omitting the respective amino acid (uracil) from the complete amino acid mix.

Table 2. Liquid media for culturing yeast.

Medium	Composition
SCD	0.69 % (w/v) yeast nitrogen base 0.2 % (w/v) amino acid mix (table above) 2 % (w/v) glucose
YPD	1 % (w/v) yeast extract 2 % (w/v) peptone 2 % (w/v) glucose

Table 3. Liquid media for culturing *E. coli.*

Medium	Composition
LB	1 % (w/v) tryptone 0.5 % (w/v) yeast extract 1 % (w/v) NaCl
2x YT	1.6 % (w/v) tryptone 1 % (w/v) yeast extract 0.5 % (w/v) NaCl

Table 4. Plates.

Plates	Composition
SCD	SCD medium 2 % (w/v) agar
LB + ampicillin	LB medium 1.5 % (w/v) agar 100 µg/ml ampicillin
LB + kanamycin	LB medium 1.5 % (w/v) agar 50 µg/ml kanamycin

Table 5. Enzymes, kits and standards.

Enzyme	Supplier
Dpn1	NEB
Taq DNA polymerase	Sigma
Opti Taq DNA polymerase	Roboklon
Allin Mega polymerase	HighQ
Q5 High-fidelity DNA polymerase	NEB
T4 DNA ligase	NEB
Kit or standard	**Supplier**
GeneRuler 1 kb Plus DNA ladder	Thermo Fisher Scientific
PageRuler Plus Prestained Protein Ladder	Thermo Fisher Scientific

Table 6. Antibodies.

primary antibodies	Supplier
rat anti-HA (clone 3F10)	Roche
mouse anti-FLAG (clone M2)	Merck
mouse anti-GFP (clones 7.1/13.1)	Roche
Strep-Tactin HRP (conjugate)	Iba Lifesciences
mouse anti-Pho8 (clone 1D3A10)	Abcam
goat anti-Luciferase	Merck
anti-ALFA IRDye 800CW (conjugate)	NanoTag Biotechnologies

secondary antibodies	Supplier
donkey anti-rat HRP	Jackson ImmunoResearch
goat anti-mouse HRP	Thermo Fisher Scientific
rabbit anti-goat HRP	Jackson ImmunoResearch

2.1.2 Chemicals and reagents

Table 7. Buffers and solutions used in this study.

Buffer/Solution	Composition
30 % acrylamide mix	29.2 % (w/v) acrylamide 0.8 % (w/v) N,N'-methylen-bisacrylamide (ratio 37.5:1)
49.5 % acrylamide mix	46.5 % (w/v) acrylamide, 3 % (w/v) N,N'-methylen-bisacrylamide (ratio 15.5:1)
1x anode buffer	1 M Tris-HCl pH 8.9
10 % (w/v) APS	in water
Betaine	5 M in water with 0.5 % (w/v) Orange G
Biotinylation reaction buffer (Rad6)	50 mM HEPES pH 7.5 150 mM NaCl 10 mM $MgCl_2$
Biotinylation reaction buffer (Roq1)	25 mM HEPES pH 7.5 25 mM KCl 5 mM $MgCl_2$
BLI assay buffer	50 mM HEPES pH 7.5 150 mM NaCl 10 mM MgCl2

	0.02 % (v/v) bovine serum albumin (BSA) buffer 0.05 % (v/v) Tween
Blotting buffer (1x)	25 mM Tris 192 mM glycine 20 % (v/v) ethanol
10 % bovine serum albumin (BSA) buffer	50 mM HEPES pH 7.5 150 mM NaCl 10 mM MgCl2 10 % (w/v) bovine serum albumin (BSA)
1x cathode buffer	100 mM Tris 100 mM Tricine 0.5 % SDS
Co-IP lysis buffer	25 mM HEPES pH 7.5 100 mM NaCl 0.5 mM EDTA 1 % (v/v) triton X-100 1 mM PMSF complete protease inhibitors
Colony PCR buffer (10x)	200 mM Tris-HCl pH 8.8 100 mM $(NH_4)_2SO_4$ 100 mM KCl 25 mM $MgCl_2$
Complete protease inhibitors (25x)	1 tablet in 2 ml water
Dithiothreitol (DTT)	1 M in water
DNA loading dye (5x)	50 % (v/v) glycerol 10 % (v/v) 10x TAE buffer 0.05 (w/v) Orange G
dNTPs	10 mM of each in water
20 % Glucose stock	20 % (w/v) in water, autoclaved
30 % Glycerol stock	30 % (w/v) in water, autoclaved
Guanidinium chloride (GuHCl) buffer	30 mM Tris pH 7.4 50 mM KCl 5 mM $MgCl_2$ 10 mM DTT 7.5 M guanidinium chloride (GuHCl)
HPDP-Biotin	4 mM in DMSO

Lithium acetate	1 M in water, filter sterilized
Luciferase dilution buffer	30 mM Tris pH 7.4 50 mM KCl 5 mM $MgCl_2$ 1 mM DTT
NHS-PEG4 biotin	20 mM in water
Phenylmethylsulfonyl fluoride (PMSF)	1 M in water
Polyethylene glycol (PEG) 3350	50 % (w/v) in water, filter sterilized
Ponceau S	0.1 % (w/v) Ponceau S 5 % (v/v) acetic acid
Running buffer (1x)	0.1 % SDS 25 mM Tris 192 mM glycine
Salmon sperm DNA	10 mg/ml in water
Separating gel buffer	2 M Tris-HCl pH 8.8
Sodium dodecyl sulfate (SDS)	15 % (w/v) in water
3x solution B	3 M Tris-HCl pH 8.5 0.3 % SDS
Stacking gel buffer	0.5 M Tris-HCl pH 6.8
SDS-PAGE sample buffer (4x)	278 mM Tris pH 6.8 44.4 % (v/v) glycerol 4.4 % (w/v) LDS 0.02 % (w/v) bromophenol blue 0.1 volumes β-mercaptoethanol, added fresh
Yeast cell lysis buffer	50 mM HEPES pH 7.5 0.5 mM EDTA
TAE buffer (50x)	2 M Tris 1 M acetic acid 50 mM EDTA
TBS/Tween (TBST) buffer (1x)	10 mM Tris pH 7.4 150 mM NaCl 0.1 % (v/v) Tween
Trehalose buffer	30 mM Tris pH 7.4 50 mM KCL

	5 mM MgCl2 1 mM DTT 200 mM trehalose
Tunicamycin	1 mg/ml in DMSO
Ubiquitination assay buffer	50 mM HEPES pH 7.5 0.15 M NaCl 10 mM $MgCl_2$ 5 mM ATP
10 x YNB (without ammonium sulfate) stock	6.9 % (w/v) in water, autoclaved

Table 8. Buffers used for protein purification.

Buffer/Solution	Composition
Roq1 lysis buffer	50 mM Bis-Tris pH 6.0 500 mM NaCl 20 mM imidazole 5 mM MgCl2 2 mM beta-ME 1 mM PMSF EDTA-free protease inhibitors
Roq1 wash buffer	50 mM Bis-Tris pH 6.0 500 mM NaCl 50 mM imidazole 5 mM MgCl2 2 mM beta-ME
Roq1 ATP wash buffer	50 mM Bis-Tris pH 6.0 500 mM NaCl 50 mM imidazole 5 mM MgCl2 5 mM ATP 2 mM beta-ME
Roq1 high salt wash buffer	50 mM Bis-Tris pH 6.0 750 mM NaCl 50 mM imidazole 5 mM MgCl2 2 mM beta-ME
Roq1 elution buffer	50 mM Bis-Tris pH 6.0 150 mM NaCl 250 mM imidazole 2 mM beta-ME

Roq1 dialysis buffer	50 mM Bis-Tris pH 6.0 150 mM NaCl 2 mM beta-ME
Roq1 SEC buffer	50 mM Bis-Tris pH 6.0 150 mM NaCl
Ubr1 lysis buffer	50 mM HEPES pH 7.5 200 mM NaCl 10 % glycerol 0.5 % NP-40 1 mM PMSF complete protease inhibitors
Ubr1 buffer A	50 mM HEPES pH 7.5 1 M NaCl 10 % glycerol 0.5 % NP-40 complete protease inhibitors
Ubr1 buffer B	50 mM HEPES pH 7.5 200 mM NaCl 10 % glycerol
Ubr1 elution buffer	50 mM HEPES pH 7.7 200 mM NaCl 10 % glycerol 1 mg/ml FLAG peptide
Pho8* lysis buffer	50 mM HEPES pH 7.5 500 mM NaCl 5 mM $MgCl_2$ 10 mM Imidazole 10 % glycerol 0.4 % CHAPS 1 mM PMSF EDTA-free protease inhibitors
Pho8* wash buffer	50 mM HEPES pH 7.5 500 mM NaCl 5 mM $MgCl_2$ 10 mM Imidazole 10 % glycerol
Pho8* ATP wash buffer	50 mM HEPES pH 7.5 500 mM NaCl 5 mM $MgCl_2$ 10 mM Imidazole 10 % glycerol 10 mM ATP

Pho8* IMAC A	50 mM HEPES pH 7.5 500 mM NaCl 5 mM $MgCl_2$ 10 % glycerol
Pho8* IMAC B	50 mM HEPES pH 7.5 500 mM NaCl 5 mM $MgCl_2$ 500 mM Imidazole 10 % glycerol
Pho8* maltose buffer	50 mM HEPES pH 7.5 150 mM NaCl 10 mM $MgCl_2$ 10 mM maltose
Pho8* dialysis buffer	50 mM HEPES pH 7.5 150 mM NaCl 10 mM $MgCl_2$ 2 mM beta-ME
Pho8* SEC buffer	50 mM HEPES pH 7.5 150 mM NaCl 10 mM $MgCl_2$
Rad6 lysis buffer	50 mM NaH_2PO_4 pH 8.0 300 mM NaCl 5 mM $MgCl_2$ 10 mM Imidazole 2 mM beta-ME 1 mM PMSF EDTA-free protease inhibitors
Rad6 wash buffer	50 mM NaH_2PO_4 pH 8.0 300 mM NaCl 20 mM Imidazole 2 mM beta-ME
Rad6 ATP wash buffer	50 mM NaH_2PO_4 pH 8.0 750 mM NaCl 20 mM Imidazole 2.5 mM ATP 2 mM beta-ME
Rad6 high salt wash buffer	50 mM NaH_2PO_4 pH 8.0 750 mM NaCl 20 mM Imidazole 2 mM beta-ME

Rad6 elution buffer	50 mM NaH_2PO_4 pH 8.0 300 mM NaCl 250 mM Imidazole 2 mM beta-ME
Rad6 dialysis buffer	50 mM NaH_2PO_4 pH 8.0 300 mM NaCl 2 mM beta-ME
Rad6 SEC buffer	25 mM HEPES pH 7.5 25 mM KCl 5 m $MgCl_2$ 1 mM DTT
Sfa1 lysis buffer	50 mM NaH_2PO_4 pH 8.0 300 mM NaCl 2 mM beta-ME 1 mM PMSF EDTA-free protease inhibitors
Sfa1 wash buffer	50 mM NaH_2PO_4 pH 8.0 300 mM NaCl 20 mM Imidazole 2 mM beta-ME
Sfa1 ATP wash buffer	50 mM NaH_2PO_4 pH 8.0 300 mM NaCl 20 mM Imidazole 5 mM ATP 2 mM beta-ME
Sfa1 elution buffer	50 mM NaH_2PO_4 pH 8.0 300 mM NaCl 250 mM Imidazole 2 mM beta-ME
Sfa1 dialysis buffer	50 mM NaH_2PO_4 pH 8.0 150 mM NaCl 2 mM beta-ME
Sfa1 Strep elution buffer	50 mM NaH_2PO_4 pH 8.0 300 mM NaCl 2.5 mM Desthiobiotin

2.1.3 Tris-glycine PAGE gel recipes

Table 9. Recipe for Tris-glycine gels.

	Separating gel (7.5 %)	Stacking gel (4 %)
H_2O	3.2 ml	1.2 ml
separating/stacking buffer	1.2 ml	0.5 ml
30 % acrylamide mix	1.5 ml	0.27 ml
15 % SDS	40 µl	13 µl
10 % APS	60 µl	20 µl
TEMED	6 µl	2 µl

Table 10. Recipe for 7.5-15% Tris-glycine step gradient gels.

	Separating gel (7.5 %)	Stacking gel (15 %)
H_2O	3.2 ml	1.7 ml
separating/stacking buffer	1.2 ml	1.2 ml
30 % acrylamide mix	1.5 ml	3 ml
15 % SDS	40 µl	40 µl
10 % APS	60 µl	60 µl
TEMED	6 µl	6 µl

2.1.4 Tris-tricine PAGE gel recipes

In contrast to tris-glycine SDS PAGE gels are run with 1x Anode and 1x Cathode buffer (**Table 7**) instead of the common Running buffer (Schagger, 2006).

Table 11. Recipe for Tris-tricine gels.

	Separating gel (16 %)	Stacking gel (4 %)
H_2O	1.58 ml	1.13 ml
3x solution B	2 ml	0.67 ml
40 % acrylamide mix	2.41 ml	0.2 ml
10 % APS	30 µl	20 µl
TEMED	3 µl	2 µl

7.5-16 % tris-tricine step gradient gel for co-immunoprecipitation experiments (Roq1 input and precipitate). 1.5 ml were used per layer of gel, respectively, with a stacking gel on top (see recipe in **Table 11**).

Table 12. Recipe for 7.5-16 % tris-tricine step gradient gel.

	Separating gel (16 %)	**Separating gel (12 %)**	**Separating gel (8 %)**
H_2O	1.58 ml	2.2 ml	2.8 ml
3x solution B	2 ml	2 ml	2 ml
40 % acrylamide mix	2.41 ml	1.8 ml	1.2 ml
10 % APS	30 µl	30 µl	30 µl
TEMED	3 µl	3 µl	3 µl

2.2 Methods

2.2.1 Yeast and *E. coli* Plasmids

Table 13. Yeast plasmids used in this study.

Yeast plasmid	alias	Source
pRS316-P_{Roq1}-Roq1	pSS254	(Szoradi et al., 2018)
pRS305-P_{ADH}-Rtn1-Pho8*-FLAG-GFP	pSS174	(Szoradi et al., 2018)
pRS416-P_{GPD}-Roq1-HA(74)	pSS649	(Szoradi et al., 2018)
pRS416-P_{GPD}-Ub-Roq1(22-104)-HA(74)	pSS764	(Szoradi et al., 2018)
pRS416-P_{GPD}-Ub-Roq1(22-104)(E36K)-HA(74)	pSS1067	Sibylle Kanngießer
pRS416-P_{GPD}-Ub-Roq1(22-104)(M39K)-HA(74)	pSS1068	Sibylle Kanngießer
pRS416-P_{GPD}-Ub-Roq1(22-104)(G40C)-HA(74)	pSS1069	Sibylle Kanngießer
pRS416-P_{GPD}-Ub-Roq1(22-104)(N45K)-HA(74)	pSS1070	Sibylle Kanngießer
pRS416-P_{GPD}-Ub-Roq1(22-104)(Q50K)-HA(74)	pSS1071	Sibylle Kanngießer
pRS416-P_{GPD}-Ub-Roq1(22-104)(I54K)-HA(74)	pSS1072	Sibylle Kanngießer
pRS416-P_{GPD}-Ub-Roq1(22-104)(Y55H)-HA(74)	pSS1073	Sibylle Kanngießer
pRS416-P_{GPD}-Ub-Roq1(22-104)(Y55N)-HA(74)	pSS1074	Sibylle Kanngießer
pRS416-P_{GPD}-Ub-Roq1(22-104)(Y55D)-HA(74)	pSS1075	Sibylle Kanngießer
pRS416-P_{GPD}-Ub-Roq1(22-104)(Y56N)-HA(74)	pSS1076	Sibylle Kanngießer
pRS416-P_{GPD}-Ub-Roq1(22-104)(V58E)-HA(74)	pSS1077	Sibylle Kanngießer
pRS416-P_{GPD}-Ub-Roq1(22-104)(N62K)-HA(74)	pSS1078	Sibylle Kanngießer
pRS416-P_{GPD}-Ub-Roq1(22-104)(I65K)-HA(74)	pSS1079	Sibylle Kanngießer
pRS416-P_{GPD}-Ub-Roq1(22-104)(E67K)-HA(74)	pSS1080	Sibylle Kanngießer
pRS416-P_{GPD}-Ub-Roq1(22-104)(I54R)-HA(74)	pSS1463	Sibylle Kanngießer
pRS416-P_{GPD}-Ub-Roq1(22-104)(E36A)-HA(74)	pSS1133	Sibylle Kanngießer
pRS416-P_{GPD}-Ub-Roq1(22-104)(M39A)-HA(74)	pSS1134	Sibylle Kanngießer
pRS416-P_{GPD}-Ub-Roq1(22-104)(N45A)-HA(74)	pSS1135	Sibylle Kanngießer
pRS416-P_{GPD}-Ub-Roq1(22-104)(Q50A)-HA(74)	pSS1136	Sibylle Kanngießer
pRS416-P_{GPD}-Ub-Roq1(22-104)(I54A)-HA(74)	pSS1137	Sibylle Kanngießer
pRS416-P_{GPD}-Ub-Roq1(22-104)(N62A)-HA(74)	pSS1139	Sibylle Kanngießer
pRS416-P_{GPD}-Ub-Roq1(22-104)(I65A)-HA(74)	pSS1140	Sibylle Kanngießer
pRS416-P_{GPD}-Ub-Roq1(22-104)(E67A)-HA(74)	pSS1141	Sibylle Kanngießer
pRS416-P_{GPD}-Ub-Roq1(22-104)(V53E)-HA(74)	pSS1187	Sibylle Kanngießer
pRS416-P_{GPD}-Ub-Roq1(22-104)(I54E)-HA(74)	pSS1142	Sibylle Kanngießer
pRS416-P_{GPD}-Ub-Roq1(22-104)(Y56D)-HA(74)	pSS1188	Sibylle Kanngießer
pRS416-P_{GPD}-Ub-Roq1(22-104)(F57D)-HA(74)	pSS1177	Sibylle Kanngießer
pRS416-P_{GPD}-Ub-Roq1(22-104)(L60E)-HA(74)	pSS1143	Sibylle Kanngießer
pRS416-P_{GPD}-Ub-Roq1(22-104)(Y55A)-HA(74)	pSS1138	Sibylle Kanngießer
pRS416-P_{GPD}-Ub-Roq1(22-104)(Y56A)-HA(74)	pSS1189	Sibylle Kanngießer
pRS416-P_{GPD}-Ub-Roq1(22-104)(F57A)-HA(74)	pSS1176	Sibylle Kanngießer
pRS416-P_{GPD}-Ub-Roq1(22-104)(V58A)-HA(74)	pSS1190	Sibylle Kanngießer

pRS416-P_{GPD}-Ub-Roq1(22-104)(Y55A,Y56A,F57A,V58A)-HA(74)	pSS1300	Sibylle Kanngießer
pRS415-P_{ADH1}-FLAG-Ubr1	pSS930	(Szoradi et al., 2018)
pRS416-P_{GPD}	pSS027	(Mumberg et al., 1995)
pRS316-P_{ROQ1}-Ub-Roq1(22-104)	pSS756	(Szoradi et al., 2018)
pRS316-P_{ROQ1}-Ub-Roq1(22-104)-HA(74)	pSS1124	Rafael Salazar
pRS416-P_{GPD}-Ub-Roq1(22-104) -HA(74)(R22A,Y55A,Y56A,F57A,V58A)	pSS1301	Sibylle Kanngießer
pRS306N-P_{ROQ1}-Roq1	pSS1292	Rafael Salazar
pRS306N-P_{ROQ1}-Ub-Roq1(22-104)	pSS1293	Rafael Salazar
pRS306N-P_{ROQ1}-Ub-Roq1(22-60)	pSS1305	Rafael Salazar
pRS416-P_{GPD}-Ub-Roq1(22-60)	pSS1333	Rafael Salazar
pRS416-P_{GPD}-Ub-Roq1(22-38)(49-60)	pSS1359	Sibylle Kanngießer
pRS416-P_{GPD}-Ub-Roq1(22-32)(37-38)(49-60)	pSS1368	Sibylle Kanngießer
pRS416-P_{GPD}-Ub-Roq1(22-29)(37-38)(49-60)	pSS1369	Sibylle Kanngießer
pRS416-P_{GPD}-Ub-Roq1(22-26)(37-38)(49-60)	pSS1370	Sibylle Kanngießer
pRS416-P_{GPD}-Ub-Roq1(22-23)GGSGGSGGSG(51-60)	pSS1428	Sibylle Kanngießer
pRS416-P_{GPD}-Ub-Roq1(22-23)GSPGSPGGSG(51-60)	pSS1429	Sibylle Kanngießer
pRS316-Proq1-Ub-Roq1(22-104)-HA(74)-CYCterm	pSS1124	Sibylle Kanngießer
pRS416-GPD-Ub-yjl144(R22A)(22-104)-HA(74)	pSS927	Tamas Szoradi
p316-Pyjl144-Ub-yjl144(R22A)(22-104)-CYCterm	pSS827	Tamas Szoradi
pRS316	pSS009	Peter Walter
pRS416-GPD	pSS027	Peter Walter

Table 14. *E. coli* plasmids used in this study.

***E. coli* plasmid**	**alias**	**Source**
pCA528	pSS685	(Andreasson et al., 2008)
pCA528-Roq1(22-104)	pSS850	Tamas Szoradi
pCA528-Pho8*-MBP	pSS1240	Niklas Peters
pCA528-Roq1(22-60)(R22A)-HA	pSS1412	Sibylle Kanngießer
YEplac181-P_{ADH1}-FLAG-Ubr1	pSS1478	(Xia, Webster, et al., 2008)
pCA528-Rad6	pSS1212	Axel Mogk
pCA528-Roq1(22-104)-ALFA	pSS1375	Niklas Peters
pCA528-Roq1(22-104)(Y55amber)-ALFA	pSS1496	Sibylle Kanngießer
pCA528-Roq1(22-104)(Y56amber)-ALFA	pSS1497	Sibylle Kanngießer
pCA528-Roq1(22-104)(R22A)	pSS1081	Niklas Peters

pCA528-Roq1(22-104) (Y55A,Y56A,F57A,V58A)	pSS1283	Sibylle Kanngießer
pCA528-Roq1(22-104) (R22A,Y55A,Y56A,F57A,V58A)	pSS1285	Sibylle Kanngießer
pCA528-Roq1(22-104)(Y55D)	pSS1173	Sibylle Kanngießer
pCA528-Roq1(22-104)(Y56D)	pSS1206	Sibylle Kanngießer
pCA528-Roq1(22-104)(F57D)	pSS1207	Sibylle Kanngießer
pCA528-Roq1(22-104)(V58E)	pSS1208	Sibylle Kanngießer
pCA528-Sfa1-Strep	pSS1263	Sibylle Kanngießer
pCA528-Roq1(22-60) 4A-HA	pSS1417	Sibylle Kanngießer
pCA528-Roq1(22-60)(V58E)-HA	pSS1416	Sibylle Kanngießer
pCA528-Roq1(22-29)(37-38)(49-60) (= 22 aa)	pSS1456	Sibylle Kanngießer
pCA528-Roq1(22-23 GGSGGSGGSG(51-60)	pSS1454	Sibylle Kanngießer
pCA528-Roq1(22-23)GSPGSPGGSG(51-60)	pSS1455	Sibylle Kanngießer

Table 15. Oligonucleotides for cloning generated in this study.

Oligonucleotide	Sequence
Roq1_I54K fw	gctctacaaagtagtatttcacgccgccag
Roq1_I54K rev	acacagcctggcgtgaaatactac
FLAG fw_new	gattacaaggacgacgatgacaag
ADH rev_new	tctagagcggccagcttggagt
Ubr1 fw	tccgttgctgatgatgatttaggat
Roq1-22 fw	aggagccagcgggacca
Ubi-Roq1-22 rev	ctggtcccgctggctcctaccacctcttagccttagca
GPD-Ubi fw	accagaacttagtttcgacggattctagaactagtatgc
Roq1_V58E fw	gcctaaattagtcagctcttcaaagtagtatatcacgcca
Roq1_V58E rev	tggcgtgatatactactttgaagagctgactaatttaggc
Roq1_Y55H fw	gctctacaaagtagtgtatcacgccaggctgtgtag
Roq1_Y55H rev	ctacacagcctggcgtgatacactactttgtagagc
Roq1_Q50K fw	cacgccaggctttgtaggctggttattgatccc
Roq1_Q50K rev	gggatcaataaccagcctacaaagcctggcgtg
Roq1_G40C fw	tgatcccgaaatcgcacatgggagactcctc
Roq1_G40C rev	gaggagtctcccatgtgcgatttcgggatca
Roq1_Y56N fw	agtcagctctacaaagttgtatatcacgccaggct
Roq1_Y56N rev	agcctggcgtgatatacaactttgtagagctgact
Roq1_E67K fw	gttattattactgcttgtgtttttctgtatgcctaaattagtcagct
Roq1_E67K rev	agctgactaatttaggcatacagaaaaacacaagcagtaataataac
Roq1_M39A_fw	ggtagaggagtctcccgcgggcgatttcgggatc
Roq1_M39A_rev	gatcccgaaatcgcccgcgggagactcctctacc
Roq1_Y55A_fw	cctacacagcctggcgtgatagcctactttgtagagctgac
Roq1_Y55A_rev	gtcagctctacaaagtaggctatcacgccaggctgtgtagg
Roq1_N62A_fw	gatatactactttgtagagctgactgctttaggcatacaggaaaacacaagc

Roq1_N62A_rev	gcttgtgttttcctgtatgcctaaagcagtcagctctacaaagtagtatatc
Roq1_I65A_fw	ctttgtagagctgactaatttaggcgcacaggaaaacacaagcagtaataat
Roq1_I65A_rev	attattactgcttgtgttttcctgtgcgcctaaattagtcagctctacaaag
Roq1_E67A_fw	gctgactaatttaggcatacaggcaaacacaagcagtaataataaca
Roq1_E67A_rev	tgttattattactgcttgtgtttgcctgtatgcctaaattagtcagc
Roq1_Y55N fw	ctacacagcctggcgtgataaactactttgtagagc
Roq1_Y55N rev	gctctacaaagtagtttatcacgccaggctgtgtag
Roq1_Y55F_fw	acagcctggcgtgatattctactttgtagagctg
Roq1_Y55F_rev	cagctctacaaagtagaatatcacgccaggctgt
Roq1_E36A_fw	ttccttggtagaggcgtctcccatgggcg
Roq1_E36A_rev	cgcccatgggagacgcctctaccaaggaa
Roq1_N45A_fw	gctgtgtaggctggttagcgatcccgaaatcgccca
Roq1_N45A_rev	tgggcgatttcgggatcgctaaccagcctacacagc
Roq1_Q50A_fw	tcacgccaggcgctgtaggctggttattgatccc
Roq1_Q50A_rev	gggatcaataaccagcctacagcgcctggcgtga
Roq1_I54A_fw	cagctctacaaagtagtatgccacgccaggctgtgtaggc
Roq1_I54A_rev	gcctacacagcctggcgtggcatactactttgtagagctg
Roq1_I54E_fw	gtcagctctacaaagtagtactccacgccaggctgtgtaggct
Roq1_I54E_rev	agcctacacagcctggcgtggagtactactttgtagagctgac
Roq1_Y56D_fw	agtcagctctacaaagtcgtatatcacgccaggct
Roq1_Y56D_rev	agcctggcgtgatatacgactttgtagagctgact
Roq1_L60E_fw	tttcctgtatgcctaaattagtctcctctacaaagtagtatatcacgc
Roq1_L60E_rev	gcgtgatatactactttgtagaggagactaatttaggcatacaggaaa
Roq1_E67A_fw_new	agttattattactgcttgtgtttgcctgtatgcctaaattagtcagc
Roq1_E67A_rev_new	gctgactaatttaggcatacaggcaaacacaagcagtaataataact
Roq1_Y55D_fw	ctacacagcctggcgtgatagactactttgtagagc
Roq1_Y55D_rev	gctctacaaagtagtctatcacgccaggctgtgtag
Roq1_V53E_fw	ctacaaagtagtatatctcgccaggctgtgtagg
Roq1_V53E_rev	cctacacagcctggcgagatatactactttgtag
Roq1_Y56F_fw	tagtcagctctacaaagaagtatatcacgccaggc
Roq1_Y56F_rev	gcctggcgtgatatacttctttgtagagctgacta
Roq1_Y56A_fw	aattagtcagctctacaaaggcgtatatcacgccaggctgtg
Roq1_Y56A_rev	cacagcctggcgtgatatacgcctttgtagagctgactaatt
Roq1_F57D_fw	cctaaattagtcagctctacatcgtagtatatcacgccaggctg
Roq1_F57D_rev	cagcctggcgtgatatactacgatgtagagctgactaatttagg
Roq1_F57A_fw	cctaaattagtcagctctacagcgtagtatatcacgccaggctg
Roq1_F57A_rev	cagcctggcgtgatatactacgctgtagagctgactaatttagg
Roq1_V58A_fw	gcctaaattagtcagctctgcaaagtagtatatcacgcca
Roq1_V58A_rev	tggcgtgatatactactttgcagagctgactaatttaggc
pCA528linkstrep fw	ggtggttcgggtggtggttc
Roq1 up res74_fw	ggaaaacacaagcagtaataataac
Roq1 down R22_rev	caaggaatccactctagtctgg
Roq1(22-104) R22A fw	ggctaagaggtggtgcgagccagcgggacc

Roq1(22-104) R22A rev	ggtcccgctggctcgcaccacctcttagcc
Y55amber_fw	acagcctggcgtgatatagtactttgtagagctg
Y55amber_rev	cagctctacaaagtactatatcacgccaggctgt
Roq1-LVEE_fw	ccagactagagtggattcctctcccacacagcctggc
Roq1-LVEE_rev	caggctgtgtgggagaggaatccactctagtctggtccc
Roq1-VDSLVEE_fw	cagcgggaccagactagatctcccacacagcctggc
Roq1-VDSLVEE_rev	ccaggctgtgtgggagatctagtctggtcccgctggc
Roq1-QTRVDSLVEE_fw	gtaggagccagcgggactctcccacacagcctggc
Roq1-QTRVDSLVEE_rev	caggctgtgtgggagagtcccgctggctcctacc
Roq1(22-60)HA 58E fw	cgtatgggtacagctcttcaaagtagtatatcacgc
Roq1(22-60)HA 58E rev	gcgtgatatactactttgaagagctgtacccatacg
Roq1(22-60)4A fw	tacccatacgatgttcctgactatgcgtgaactaatttaggcatacagg
Roq1(22-60)4A rev	tcacgcatagtcaggaacatcgtatgggtacagctctgcagctgcagc
Roq1 GGS linker fw	tctggtggctccggtcctggcgtgatatactactttgtagagctg
Roq1 GGS linker rev	tccgcctgaacctccgctcctaccacctcttagccttagcac
Roq1 GSP linker fw	cctgggggatccggtcctggcgtgatatactactttgtagagctg
Roq1 GSP linker rev	agaacctggtgatccgctcctaccacctcttagccttagcac
Roq1 pCA GGS_rev	tccgcctgaacctccgctcctaccaccaatctgttctctgtgag
Roq1 pCA GSP_rev	agaacctggtgatccgctcctaccaccaatctgttctctgtgag
pCAminimal Roq1_fw	agatctcccacacagcctggcgtgatatactactttgtagagctg
pCAminimal Roq1_rev	agtctggtcccgctggctcctaccaccaatctgttctctgtgag
Y56 amber fw	gcctggcgtgatatactagtttgtagagctgactaat
Y56 amber rev	attagtcagctctacaaactagtatatcacgccaggc
SUMO_Sfa1_fw	cacagagaacagattggtggtatgtccgccgctactgttgg
Sfa1_Strep_rev	gaaccaccacccgaaccacctttatttcatcagacttcaag

Oligonucleotide design for gene deletion or tagging in yeast was done according to (Janke et al., 2004; Longtine et al., 1998).

2.2.2 Molecular cloning

Plasmids used in this study are listed in **Table 13** and **14** and were in general generated using Gibson assembly and site-directed mutagenesis. Note, that pRS416-P_{GPD}-Roq1 variants were expressed as ubiquitin Roq1(22-104) fusions (e.g. pRS416-P_{GPD}-Ub-Roq1(22-104)) which are processed by cells to make Roq1(22-104) protein.

Oligonucleotides used for cloning and generating yeast strains were purchased from Sigma-Aldrich or Integrated DNA Technologies (IDT) and are listed in **Table 15**. The following polymerases were used for standard PCR reactions: OptiTaq (Roboklon), Q5 (NEB) or Allin Mega polymerase (HighQ) to amplify larger fragments. 1 % agarose gels with stain G (Serva) were used to analyze PCR products. To extract DNA the gel extraction a kit from miniBio was

used. Gibson assembly of two DNA fragments was employed according to Gibson (Gibson, 2011). For this, the respective vector was linearized, gel-purified and digested with Dpn1 and combined with insert (PCR product, gblock) in a 1:2 molar ratio and incubated in a total volume of 20 µl Gibson mix at 50 °C for 60 min. Phosphorylated oligonucleotides (5'Phos) were used when sequences were to be removed or added and the vector was re-ligated using T4 ligase (NEB). Oligonucleotides to introduce point mutations were designed using the Quikchange site-directed mutagenesis tool from Agilent. Generated constructs were then transformed into competent competent *E. coli* DH5a cells and plasmids were isolated using the mini-prep kit from miniBio.

Gibson mix

320 µl	5x Gibson buffer (500 mM Tris-HCl pH 7.5, 50 mM MgCl2, 1 mM dGTP, 1 mM dATP, 1 mM dTTP, 1 mM dCTP, 50 mM DTT, 5 mM nicotinamide adenine dinucleotide (NAD), 25 % PEG-8000)
0.64 µl	T5 exonuclease (10 U/µl, NEB)
20 µl	Phusion DNA polymerase (2 U/µl, NEB)
160 µl	Taq DNA ligase (40 U/µl, NEB)
700 µl	H_2O

Table 16. List of *Escherichia coli* strains used in this study.

Strain	Relevant genotype	Source
DH5α	F^- φ80*lac*ZΔM15 Δ(*lac*ZYA-*arg*F) U169 *rec*A1 *end*A1 *hsd*R17(r_K^-, m_K^+) *pho*A *sup*E44 λ^-*thi*-1 *gyr*A96 *rel*A1	Schuck lab
BL21 DE(3) Rosetta	F^- *ompT* *hsdS*$_B$(r_B^- m_B^-) *gal* *dcm* (DE3) pRARE (Cam^R)	Matthias Mayer (ZMBH)

2.2.3 Yeast methods

Table 17. Yeast strains used in this study.

Strain	Relevant genotype	Source
SSY2908	ubr1::nat-P_{GPD}-FLAG-UBR1 pep4Δ	Ilia Kats
SSY835	his3::Pgpd-BFP-hph Δyjl144w::kan leu2::Padh-Rtn1Pho8*-GFP-LEU2	(Szoradi et al., 2018)
SSY837	his3::Pgpd-BFP-hph Δubr1::nat Δyjl144w::HIS3 leu2::Padh-Rtn1Pho8*-GFP-LEU2	Sebastian Schuck
SSY1180	Δsan1::kan	Tamas Szoradi
SSY1181	Δubr1::nat Δsan1::kan	Tamas Szoradi
SSY795	his3::Pgpd-BFP-hph	(Schmidt et al., 2019)
SSY792	ubr1Δ::nat roq1Δ::HIS3	(Szoradi et al., 2018)
SSY2959	ubr1Δ::nat roq1Δ::HIS3 leu2::P_{ADH}-FLAG-Ubr1-LEU2	Sibylle Kanngießer
SSY3091	Δubr1::nat Δyjl144w::HIS3 Δrad6::TRP1 leu2::Padh-FLAG-Ubr1-Cycterm-LEU2	Sibylle Kanngießer
SSY3543	his3::Pgpd-BFP-hph roq1Δ::kan leu2::P_{ADH}-Rtn1Pho8*-GFP-LEU2 ura3::nat	Rafael Salazar
SSY3544	his3::Pgpd-BFP-hph roq1Δ::kan leu2::P_{ADH}-Rtn1Pho8*-GFP-LEU2 ura3::P_{ROQ1}-Roq1-nat	Rafael Salazar
SSY3545	his3::Pgpd-BFP-hph roq1Δ::kan leu2::P_{ADH}-Rtn1Pho8*-GFP-LEU2 ura3::P_{ROQ1}-Ub-Roq1(22-104)-nat	Rafael Salazar
SSY3551	his3::Pgpd-BFP-hph roq1Δ::kan leu2::P_{ADH}-Rtn1Pho8*-GFP-LEU2 ura3::P_{ROQ1}-Ub-Roq1(22-60)-nat	Rafael Salazar

2.2.4 Transformation of yeast

Yeast strains used in this study are listed in **Table 17** and are based on the *Saccharomyces cerevisiae* W303 mating type a as parental strain.

For flow cytometry experiments I used the strain SSY835 which was generated by Tamas Szoradi previously (Szoradi et al., 2018). I then transformed this strain with centromeric plasmids carrying Roq1 variants (**Table 13**).

For co-immunoprecipitation experiments with Roq1 and Ubr1 I generated the strain SSY2959 (ubr1Δ::nat roq1Δ::HIS3 leu2::P_{ADH}-FLAG-Ubr1-LEU2). I amplified the P_{ADH}-FLAG-Ubr1 cassette from the plasmid pRS415-P_{ADH}-FLAG-Ubr1 and integrated it into the *leu2* locus of the strain SSY792 (Szoradi et al., 2018). Rad6 was deleted in SSY2959 using the kITRP marker cassette to generate SSY3091 (Δubr1::nat Δyjl144w::HIS3 Δrad6::TRP1 leu2::Padh-FLAG-Ubr1-Cycterm-LEU2).

For experiments that investigated the requirement of Roq1's C-terminal region in yeast Rafael Salazar (master student) generated SSY3543, 3544, 3545 and 3551 using integral plasmids based on pRS306 (**Table 13**).

For yeast transformations, cells were grown overnight and backdiluted the next day in 5 ml YPD medium. At an OD_{600} of 1, cells were pelleted at 1,000 xg for 5 min, washed with 1 ml of water and pelleted again at 10,000 xg for 2 min. After adding transforming DNA (1/10 of PCR product or 100-500 ng centromeric, 250 ng integrative plasmid DNA) to the pellet, cells were mixed with 360 µl transformation mix (**Table 18**) followed by a heat-shock at 42 °C for 40 min. After incubation cells were pelleted again, taken up in 1 ml YPD medium and 100 µl of cell suspension were plated on an appropriate selective plate. When auxotrophic markers were used for selection, cells were plated directly. When antibiotics were used, the cells were incubated at 30 °C for 6 h to allow expression of the marker cassette prior plating. Correct integration of the DNA was verified using colony PCR and the Sigma Taq polymerase. For colony PCR oligonucleotides were used that anneal in the used marker cassette and upstream of the locus in the chromosome. Cells transformed with centromeric plasmid DNA could directly be used for downstream experiments once colonies had grown on the plate.

Table 18. Yeast transformation mix.

Component	Volume
50 % (w/v) PEG	240 µl
1 M Lithium acetate	36 µl
freshly boiled 10 mg/ml salmon sperm DNA	10 µl
transforming DNA	1 µl
water	74 µl

To freeze down either yeast or *E. coli* strains, cells were grown to saturation and mixed with 30 % (w/v) glycerol in a 1:1 ratio (final 15 %).

2.2.5 Yeast cell lysis for Western

Cells were lysed by bead beating. Ten or twenty ODs were pelleted at 3,000 xg at 4 °C for 5 min. Cells were resuspended in 1 ml cold water and either snap-frozen in liquid nitrogen and stored at -70 °C or immediately processed. For direct lysis pellets were resuspended in 200 µl cold lysis buffer (50 mM HEPES pH 7.5, 0.5 mM EDTA) containing 1 mM PMSF and complete protease inhibitors (Roche) and transferred into pre-cooled 2 ml screw-capped tubes with 0.7 g 1 mm glass beads. To lyse cells a FastPrep 24 (MP Biomedical) was used to vortex cells for 40 s at 6 m/s. Lysates were collected by piercing the tubes at the bottom, placing them on fresh microfuge tubes and centrifuging them at 1000 xg for 10 s. After addition and mixing of 20 µl of 15 % (w/v) SDS, lysates were incubated at 65 °C for 5 min (**note**: this step was omitted when co-immunoprecipitation experiments were performed). Finally, the lysate was cleared at 16,000 xg at 4 °C for 10 min to pellet cell debris. After transferring the lysate to a fresh tube, the protein concentration was determined. Samples were kept on ice throughout the whole process to avoid post-lysis degradation.

2.2.6 Flow cytometry-based SHRED reporter assay

SHRED activity in yeast was determined using a flow cytometry-based assay that monitors the degradation of the fluorescently labelled SHRED model substrate Rtn1-Pho8*-GFP upon stress. Cells expressing the reporter and cytosolic BFP (SSY835) - harboring Roq1 pRS416-based plasmids - were grown to saturation in 1 ml SC-URA medium in 96-deep well plates at 30 °C. Cells were back-diluted in 1 ml SC-URA medium with 1, 2 and 4 µl of saturated culture and placed in a programmable incubator (Memmert) at 14 °C. At midnight the temperature was increased to 30 °C to allow cells to reach an OD_{600} of 0.5 in the morning. Cells were then diluted to an OD_{600} of 0.05 in 1 ml SC-URA and either left untreated or were treated with a final concentration of 2 µg/ml tunicamycin (Merck). After 5 h of incubation at 30 °C the fluorescence from 100 µl of cell suspension was determined with a FACS Canto flow cytometer (BD Biosciences) equipped with a high-throughput sampler. The measured GFP fluorescence from Rtn1-Pho8*-GFP was first corrected for background autofluorescence by subtracting the fluorescence of identically treated cells not expressing the reporter (SSY795). Corrected GFP fluorescence values were then normalized to constitutively expressed cytosolic BFP to control for differences in protein translation. The resulting GFP/BFP ratios of

tunicamycin-treated cells were then divided by the respective ratios of untreated cells to assess the effect of the stress treatment. Finally, the reporter levels were analyzed as a percentage of the levels at time point 0.

2.3 Biochemistry methods

2.3.1 Protein determination

Protein concentrations were determined using (1) BCA or (2) Bradford assay:
(1) To determine the protein concentration of total yeast cell lysates the BCA assay from Pierce was used in a 96-well format in duplicates. A reference series from 0 to 20 µg BSA was set up in 150 µl water (10 µl BSA stock solutions ranging from 0 to 2 mg/ml and 140 µl water). Samples to be measured were pipetted to empty wells and 150 µl water – x µl sample were added. The concentration of the sample was aimed to be ideally in the middle of the standard curve obtained from the BSA reference series. 150 µl of mixed BCA reagents A and B were added (ratio 50:1) to both the reference series and the sample and mixed. After incubation at 37 °C for a minimum of 20 and a maximum of 120 min absorbance at 562 nm was measured using a TECAN sunrise (Tecan, Switzerland) or a PHERAsar FSX (BMG Labtech, Germany) plate reader.

(2) To determine concentrations of recombinant purified proteins a 1:5 dilution of the Bradford reagent concentrate from Biorad in water was used. A duplicate reference series was prepared with wells containing 0-5 µg BSA (5 µl BSA stock solution from stock solutions ranging from 0 to 1 mg/ml) and wells containing 5 µl of diluted or undiluted sample. 200 µl diluted Bradford reagent was added to each well and incubated at room temperature for 5 min. Absorbance was measured at 595 nm using a PHERAsar FSX (BMG Labtech, Germany) or a TECAN spark (Tecan, Switzerland) plate reader.

2.3.2 Western blot with total yeast cell lystate

Ten ODs of cells were lysed as described in **2.2.5** and protein concentrations were determined with a BCA kit from Pierce (**2.3.1**). Equal amounts of protein lysate were supplemented with final 1x sample buffer and were then separated on either tris-glycine or tris-tricine SDS-PAGE gels, the latter was used when handling the small protein Roq1. The gel compositions are listed under **2.1.3** and **2.1.4**.

Proteins were separated at constant 200 V and then transferred to nitrocellulose membranes by standard wet blotting (BioRad) at 100 V for 1 h. Membranes were then stained with Ponceau S (0.1% (w/v) Ponceau S, 5% (v/v) acetic acid) for 1 min to validate the transfer and then incubated with 5 % milk in TBST (5 % milk in TBS when using LI-COR system) for 1 h. Membranes were probed with primary antibodies or HRP conjugates (**Table 6**) following the instructions of the manufacturer. After rinsing the membranes three times for 5 min with TBST HRP-coupled or fluorescent (LI-COR) secondary antibodies were added, and membranes were incubated for 1 h at room temperature. Again, membranes were rinsed three times for 5 min with TBST. To develop the membranes, they were incubated with SuperSignal West Pico Plus substrate for 5 min in the dark (Thermo Fisher Scientific) and finally chemiluminescence was detected with an Amersham Imager 600 (GE HealthCare). Fluorescence was detected with an Odyssey CLx imaging system (LI-COR). Acquired images were analyzed using Fiji.

4x sample buffer	278 mM Tris-HCl, pH 6.8, 4.4% (w/v) LDS, 44.4% glycerol, 0.02% (w/v) bromophenol blue

2.3.3 Co-immunoprecipitation

Twenty ODs of cells in mid-log phase were harvested and lysed by bead beating in 500 µl cold IP buffer (25 mM HEPES pH 7.5, 100 mM NaCl, 1% Triton X-100, 0.5 mM EDTA) containing 1 mM PMSF and protease inhibitors as mentioned in **2.2.5**. Lysates were cleared at 16,000 xg for 10 min at 4 °C and 3 % of the lysate were kept for Roq1 input samples. 30 % of the lysate was used to precipitate FLAG-Ubr1 with 20 µl anti-FLAG M2 affinity gel (Sigma) to collect Ubr1 input samples. 50 % of the lysate was used to co-immunoprecipitate Roq1(22-104)-HA(74) and FLAG-Ubr1 with 30 µl anti-HA affinity matrix (Sigma) at 4 °C for 30 min. Anti-HA and anti-FLAG beads were both washed three times with 1 ml cold IP buffer and bound proteins were eluted with 1x sample buffer (volumes: 20 µl for Ubr1 pulldown, 15 µl for IP) at 65 °C for 5 min. Roq1 input (10 µl) and co-immunoprecipitated samples (15 µl) were separated on 7.5 – 16 % tris-tricine step-gradient gels whereas 15 % of Ubr1 input samples (10 µl) were run on 7.5 % tris-glycine gels. Roq1 and Ubr1 were detected using mouse anti-FLAG or rat anti-HA antibody as primary antibodies and anti-mouse HRP and anti-rat HRP as secondary antibodies (**Table 6**).

2.3.4 Protein expression and purification

Note: The here mentioned purification protocols were all initially established by Niklas Peters. For **FLAG-Ubr1** expression, yeast cells (SSY2908) lacking the protease Pep4 and expressing FLAG-tagged Ubr1 from a ADH promoter on the yeast chromosome, were grown in 12 L YPD medium to an OD_{600} = 2 at 30 °C. Cells were collected at 3500 xg for 15 min, washed with cold PBS, snap-frozen in liquid nitrogen and stored at -70 °C.

FLAG-Ubr1 was then purified as described by Varshavsky and colleagues (Du et al., 2002). Yeast cell pellets from 12 L cultures were resuspended in 60 ml lysis buffer (50 mM HEPES pH 7.5, 0.2 NaCl, 10 % glycerol, 0.5 % NP-40, 1 mM PMSF, complete protease inhibitors (Roche) and lysed by passing through a microfluidizer (Microfluidics M-110L) at 1200 bar 10 times. The lysate was collected and cleared at 4 °C at 11,200 xg for 30 min. Per 30 ml of supernatant 0.9 ml of in buffer A (50 mM HEPES pH 7.5, 1 M NaCl, 10 % glycerol, 0.5% NP-40) pre-equilibrated anti-FLAG agarose beads (Thermo Fisher Scientific) were added and incubated at 4 °C for 2 h. Beads were collected at 1,000 xg for 5 min and were then washed with 20 ml of cold buffer A (50 mM HEPES pH 7.5, 1 M NaCl, 10 % glycerol, 0.5% NP-40) and 20 ml of cold buffer B (50 mM HEPES pH 7.5, 0.2 M NaCl, 10% glycerol). Finally, FLAG-Ubr1 was eluted in five rounds with 500 µl buffer B containing 1 mg/ml FLAG peptide (Thermo Fisher Scientific). 1x Bradford solution (BioRad) was used to select protein-containing eluates to be pooled. Amicon Ultra centrifugal filter units with a molecular weight cut-off (MWCO) of 100 kDa were used to concentrate FLAG-Ubr1. Concentrated protein was immediately snap-frozen in liquid nitrogen and stored at -70 °C.

Roq1 variants were purified from *E. coli* BL21 (DE3) cells harboring pCA528-based plasmids encoding for Roq1 variants with N-terminal His_6-SUMO tag (**Table 14**). Cells were grown in 6 L 2xYT medium supplemented with 25 µg/ml kanamycin and 34 µg/ml chloramphenicol to an OD of 0.7 at 37 °C. To induce Roq1 expression IPTG (ZellBio) was added to a final concentration of 1 mM. After 3 h of induction cells were harvested at 3500 xg for 15 min, washed once with cold water, snap-frozen in liquid nitrogen and stored at -70 °C.

E. coli cell pellets from 6 L His_6-SUMO-Roq1 expressing cultures were resuspended in 60 ml of lysis buffer (50 mM Bis-Tris pH 6.0, 500 mM NaCl, 20 mM imidazole, 5 mM $MgCl_2$, 2 mM 2-mercaptoethanol, 1 mM PMSF, protease inhibitors without EDTA (Roche)). A spatula tip of DNase (Merck) was added, and the cell suspension was stirred at 4 °C for 30 min. Cells were

disrupted by 6 passages through a microfluidizer (Microfluidics M-110L). Cell lysate was cleared at 4 °C at 11,200 xg for 30 min. For IMAC, 30 ml of supernatant were incubated with 1.5 g Ni-IDA beads (Machery-Nagel) at 4 °C for 60 min. Beads were then applied to a 25 ml gravity flow column and washed as follows: 50 ml lysis buffer, 50 ml wash buffer (50 mM Bis-Tris pH 6.0, 50 mM imidazole, 500 mM NaCl, 5 mM $MgCl_2$, 2 mM 2-mercaptoethanol), 50 ml wash buffer with 5 mM ATP, 100 ml wash buffer with 750 mM NaCl and 50 ml wash buffer. Bound protein was then eluted with five times 5 ml elution buffer containing a high concentration of imidazole (50 mM Bis-Tris pH 6.0, 150 mM NaCl, 250 mM imidazole, 2 mM 2-mercaptoethanol). Eluates were collected in 1-2 ml fractions and protein-containing fractions, as determined by Bradford (BioRad), were pooled. 30 ml of eluate were mixed with 25 µl of SUMO protease Ulp1-His_6 (4 mg/ml) to remove the N-terminal His_6-SUMO tag and dialyzed with a dialysis tube with a 3 kDa MWCO against dialysis buffer (50 mM Bis-Tris pH 6.0, 150 mM NaCl, 2 mM 2-mercaptoethanol) at 4°C overnight. Uncleaved His_6-SUMO-Roq1, free His_6-SUMO and Ulp1-His_6 were removed by incubation with Ni-IDA beads at 4 °C for 30 min. Beads were again collected with a gravity flow column and the flow-through was concentrated to a volume of 2 ml to load onto a Hiload 16/600 Superdex S30 prep grade size exclusion column (Cytiva) equilibrated with SEC buffer (50 mM HEPES pH 7.5, 150 mM NaCl). Protein-containing fractions were pooled, concentrated, 10% (v/v) glycerol was added, the protein was snap-frozen and stored at -70 °C.

Pho8*-MBP was purified from *E. coli* BL21 (DE3) harboring pCA528-His_6-SUMO-Pho8*-MBP (pSS1240). Cells were grown in 6 L LB medium supplemented with 25 µg/ml kanamycin and 34 µg/ml chloramphenicol to an OD of 0.7 at 37 °C. To induce Pho8* expression the temperature was reduced to 30 °C and IPTG (ZellBio) was added to a final concentration of 1 mM. After 3 h of induction cells were harvested at 3500 xg for 15 min, washed once with cold water, snap-frozen in liquid nitrogen and stored at -70 °C.

Cells were lysed as above in 75 ml of lysis buffer (50 mM HEPES pH 7.5, 500 mM NaCl, 5 mM $MgCl_2$, 10% glycerol, 10 mM imidazole and 0.4% CHAPS, 1 mM PMSF, protease inhibitors without EDTA (Roche)). Cells were lysed with the microfluidizer, cell lysate was cleared, and the supernatant was applied to a HisTrap FF crude affinity chromatography column (GE HealthCare) equilibrated with IMAC A buffer (50 mM HEPES pH 7.5, 500 mM NaCl, 5 mM $MgCl_2$, 10% glycerol). First, the column was washed with 10 volumes of IMAC A containing 10 mM Imidazole. This was repeated with additional 10 mM ATP included. The

protein was eluted with IMAC buffer containing 125 mM Imidazole. Eluates with protein were pooled and combined with Ulp1 and 2 mM 2-mercaptoethanol and dialyzed overnight in dialysis buffer (50 mM HEPES pH 7.5, 150 mM NaCl, 10 mM $MgCl_2$, 2 mM 2-mercaptoethanol). The dialysate was further purified with amylose resin (NEB) equilibrated with dialysis buffer. To elute bound proteins dialysis buffer containing 10 mM maltose was used. The eluate was concentrated using 30 kD MWCO filtration units and loaded onto a Hiload 16/60 Superdex S200 size exclusion prep grade column equilibrated with SEC buffer (50 mM HEPES pH 7.5, 150 mM NaCl, 10 mM $MgCl_2$). Protein-containing fractions were pooled, concentrated, 10 % (v/v) glycerol was added, the protein was snap-frozen in liquid nitrogen and stored at -70 °C.

Rad6 was purified from *E. coli* BL21 (DE3) harboring pCA528-His_6-SUMO-Rad6 (pSS1212). Cells were grown in 2 L 2xYT medium supplemented with 25 µg/ml kanamycin and 34 µg/ml chloramphenicol to an OD of 0.7 at 37 °C. To induce Rad6 expression IPTG (ZellBio) was added to a final concentration of 1 mM. After 4 h of induction cells were harvested at 3500 xg for 15 min, washed once with cold water, snap-frozen in liquid nitrogen and stored at -70 °C.

Cells were lysed as above in 25 ml of lysis buffer (50 mM NaH_2PO_4 pH 8.0, 300 mM NaCl, 5 mM $MgCl_2$, 10 mM imidazole, 2 mM 2-mercaptoethanol, 1 mM PMSF, protease inhibitors without EDTA (Roche)). After dialysis and removal of His_6-SUMO, Rad6 dialysate was concentrated to 2.5 ml using 10 kD MWCO filtration units and loaded on a Hiload 16/60 Superdex S75 prep grade size exclusion column (GE HealthCare). The column was equilibrated in SEC buffer (25 mM HEPES pH 7.5, 25 mM KCl, 5 mM $MgCl_2$, 1 mM DTT). Protein-containing fractions were pooled, concentrated, 10 % (v/v) glycerol was added, the protein was snap-frozen in liquid nitrogen and stored at -70 °C.

Sfa1-StrepII was purified from *E. coli* BL21 (DE3) harboring pCA528-His_6-SUMO-Sfa1-StrepII (pSS1263). Cells were grown in 2 L 2xYT medium supplemented with 25 µg/ml kanamycin and 34 µg/ml chloramphenicol to an OD of 0.7 at 37 °C. Sfa1 expression was induced by adding IPTG (ZellBio) to a final concentration of 1 mM and incubation at 37 °C for 3 h. Cells were harvested at 3500 xg for 15 min, washed once with cold water, snap-frozen in liquid nitrogen and stored at -70 °C.

Cells were lysed as above in 20 ml of lysis buffer (50 mM NaH_2PO_4 pH 8.0, 300 mM NaCl, 2 mM 2-mercaptoethanol, 1 mM PMSF, protease inhibitors without EDTA (Roche)). After

overnight dialysis and removal of His_6-SUMO, Sfa1 dialysate was applied onto a StrepTrap column (Cytiva) and protein-containing fractions were pooled, concentrated, 10 % (v/v) glycerol was added, the protein was snap-frozen in liquid nitrogen and stored at -70 °C.

Table 19. Protein beads/resins used in this study.

Protein beads/resins	Supplier
Pierce™ anti-FLAG agarose beads	Thermo Fisher Scientific
Protino Ni-IDA beads	Macherey-Nagel
anti-HA affinity matrix	Sigma
anti-FLAG M2 affinity gel	Sigma
ALFA Selector CE magnetic beads	NanoTag Biotechnologies

2.3.5 Photo-crosslinking

For photo-crosslinking of the Roq1-Ubr1 complex we used the pEVOL/pET system (Young et al., 2010). *E. coli* BL21(DE3) harboring pEVOL-pBpF, encoding for an amber tRNA synthetase/tRNA pair, and pCA528 Roq1(22-104)-ALFA plasmids with either the Y55amber or Y56amber mutation were used. Cells were grown in 2 L 2xYT medium supplemented with 25 µg/ml kanamycin and 34 µg/ml chloramphenicol, 50 mM phosphate buffer (pH 7.2) and 1 mM p-benzoyl-L-phenylalanine (Bpa, Bachem). When cultures reached an OD_{600} of 0.5 L-arabinose (Merck) was added to 0.25 % (w/v) and this was repeated at OD_{600} = 0.8. Final expression of the Roq1 variants was induced with 1 mM IPTG (ZellBio) at 37° for 5 h.

Via the N-terminal His_6-SUMO, Roq1 was first purified by IMAC, cleaved by Ulp1 (as described for Roq1 purification) and then immobilized with 250 µl of ALFA Selector CE magnetic beads (50% slurry, NanoTag Biotechnologies) in 16 ml dialysate at 4 °C for 2 h. Beads were then collected by centrifugation at 4°C at 1000 xg for 5 min and washed three times with 500 µl wash buffer (50 mM HEPES, pH 7.5, 0.15 M NaCl, 10 mM $MgCl_2$).

Beads with immobilized Roq1(22-104)-ALFA were then incubated with 150 µl wash buffer containing 170 nM FLAG-Ubr1 at 4°C overnight to allow Roq1-Ubr1 complex formation. After washing the beads, Roq1 was eluted with 2 x 25 µl wash buffer containing 800 µM ALFA peptide (NanoTag Biotechnologies). The eluate was split and 20 µl eluate were kept as -UV control. The other 20 µl were irradiated on ice with a UV-LED lamp (Opsytec Dr. Gröbel GmbH) at 365 nm with 15 cycles of 1 s irradiation at 25 W/cm^2 followed by a 2 s break. All samples were then resolved on a 7.5-15% step gradient Tris-glycine SDS-PAGE gel and photo-crosslinking was analyzed by Western blotting.

2.3.6 Protein staining

Recombinant proteins in SDS-PAGE gels were visualized by staining with InstantBlue Coomassie solution (Abcam). Gels were rinsed with water once and then incubated with staining solution with gentle agitation at room temperature for 15 min. For destaining gels were again rinsed with water.

2.3.7 Biolayer interferometry

Protein-protein interactions were analyzed by biolayer interferometry with the OctetRed96e system from Sartorius. One interactant ("ligand") was immobilized on the surface of a biosensor and the other remained in solution ("analyte"). In this study, both Roq1 and Rad6 were biotinylated and immobilized on streptavidin biosensors (Sartorius) that had been hydrated in assay buffer (50 mM HEPES, 150 mM NaCl, 10 mM $MgCl_2$, 0.05 % Tween-20, 0.02 % BSA) for 10 min prior use. Binding assays were performed in black 96-well plates (Greiner) in 200 µl at 1000 rpm according to the dip and read principle. In preparation for the assays a loading scout was performed to determine the optimal loading concentration of the ligand to allow for adequate analyte binding and assess assay step times. To do so, one analyte concentration was set, and different ligand concentrations were titrated. Finally, assays were set up with (1) an initial wash step of the unloaded biosensors in assay buffer for 1 min, followed by (2) a loading/immobilization step with 1.25 µg/ml Roq1 or 0.5 µg/ml Rad6, respectively, for 10 min, (3) another wash step for 1 min, (4) a baseline step for data normalization for 1 min and to assess assay drift, and (5) an association step with Ubr1 as analyte in solution for 5 min. Up to seven concentrations of Ubr1 were run in parallel (200, 100, 50, 25, 12.5, 6.25, 3.13 nM). An additional sensor was included as a non-specific binding control (NSB) with buffer without Ubr1. Unspecific binding of Ubr1 to unloaded sensors was controlled for at the very beginning.

To test the effect of RA and LA dipeptides on Ubr1-Roq1 interaction, 100 nM Ubr1 and 400 µM dipeptide were used. On the other hand, to test the effect of Roq1 on Ubr1-Rad6 association, 100 nM Ubr1 and 200 nM or 1 µM Roq1 were used. Data were evaluated with the Data Analysis HT 12.0 software (Sartorius).

2.3.8 Protein biotinylation

Roq1(22-104) variants were biotinylated at the single cysteine in Roq1 at the C-terminus, C103. EZ-Link™ HPDP-Biotin (Thermo Fisher Scientific) specifically reacts with reduced

sulfhydryl (-SH) groups to form reversible disulfide bonds and was incubated with Roq1 at a 1.2-fold molar excess at room temperature for 90 min in reaction buffer (25 mM HEPES pH 7.5, 25 mM KCl, 5 mM $MgCl_2$) at a total volume of 100 µl. 0.5 ml 7k MWCO Zeba spin desalting columns (Thermo Fisher Scientific) equilibrated in the before mentioned reaction buffer were used to remove non-reacted biotin.

For the biotinylation of Rad6 a 1.2-fold molar excess of the amino-reactive EZ-Link™ NHS-PEG4-Biotin (Thermo Fisher Scientific) was used. 2 mg/ml Rad6 and biotin were incubated at room temperature for 30 min in reaction buffer (50 mM HEPES pH 7.5, 0.15 M NaCl, 10 mM $MgCl_2$) in a total volume of 100 µl. For removal of unbound biotin 0.5 ml 7k MWCO Zeba spin desalting columns were used as for Roq1. Both Roq1 and Rad6 were snap-frozen in 10 % glycerol and stored at -80 °C. To quickly assess their functionality after biotinylation they were both individually subjected to a ubiquitination assay with Pho8* in comparison with the respective unmodified molecule. Roq1 and Rad6 were both still functional after biotinylation (data not shown).

2.3.9 Ubiquitination assay

Ubiquitination reactions were originally set up by my colleague Niklas Peters as follows: 0.1 µM Ube1 (R&D Systems), 4 µM Rad6, 0.25 µM Ubr1, 80 µM wild-type or lysine-free ubiquitin (MoBiTec), and 0.2 µM substrate protein in reaction buffer (50 mM HEPES pH 7.5, 0.15 M NaCl, 10 mM $MgCl_2$, 5 mM ATP) were combined in a total volume of 10 µl in a 0.5 ml PCR tube. Roq1 wild-type and mutants were used at 2.5 µM unless noted otherwise. RA (arginine-alanine) and LA (leucine-alanine) dipeptides (peptides & elephants) were used at a final concentration of 1 mM. Reactions were incubated at 30°C and stopped with SDS-PAGE sample buffer containing DTT at indicated times. Samples were incubated at 65°C for 5 min and either stored at -20 °C or directly loaded onto SDS-PAGE gels for Western blotting. The whole reaction (10 µl) was separated on an SDS-PAGE gel. To resolve ubiquitinated species we exclusively used 7.5 % tris-glycine SDS-PAGE gels and wet protein transfer was performed for 1.5 h at 100 V.

2.3.10 Chemical denaturation of Luciferase

To use Luciferase as misfolded model substrate in ubiquitination assays, the protein needed to be unfolded prior to the assay. This protocol was originally established by my colleague Niklas Peters.

To unfold recombinant firefly Luciferase (Promega, 237 µM) the protein was diluted 4-fold in denaturation buffer (30 mM Tris pH 7.4, 50 mM KCl, 5 mM $MgCl_2$, 7.5 M guanidinium chloride, 10 mM DTT) and incubated for 30 min on ice for unfolding. Unfolded Luciferase was stabilized by diluting the protein 100-fold in buffer containing trehalose (30 mM Tris pH 7.4, 50 mM KCl, 5 mM $MgCl_2$, 0.2 M trehalose, 1 mM DTT) as described by (Singer & Lindquist, 1998). To eliminate formed aggregates, samples were centrifuged at 4 °C at 13,200 g for 30 min and the supernatant was subsequently used for ubiquitination assays with Luciferase at a final concentration of 150 nM.

When handling folded Luciferase, the protein was treated in the same procedure except guanidinium chloride was omitted in the first step.

2.4 Bioinformatic analyses of Roq1

To predict the structure of full-length Roq1(1-104) the AlphaFold Protein Structure Database was used (Varadi et al., 2024). To predict the disorder of full-length Roq1 twelve prediction algorithms were averaged using DisEMBL, NetsurfP 3.0, PONDR VSL2, Metapredict, AIUPred, DISpro, Espritz, MFDp, IsUnstruct, PrDOS, IUPred3 and RONN (Kurgan, 2022).

The search for Roq1 sequence homologs was carried out with the protein-protein BLAST search on the NCBI home page and alignments were performed with CLUSTALW. AlphaFold3 predictions from Roq1(22-60) were further analyzed using UCSF ChimeraX (Abramson et al., 2024; Meng et al., 2023).

3. Results

3.1 Roq1 mutagenesis screen

A screen was sought to identify additional SHRED-critical features in Roq1 besides R22 in an unbiased and comprehensive manner using the full-length HA-tagged Roq1 protein.

Prior to this work, Oliver Pajonk had performed a Roq1 mutagenesis screen as part of his master thesis project. He used error-prone PCR and generated a pooled plasmid library of mutant versions of Roq1. *S. cerevisiae* cells lacking Roq1 and expressing the SHRED-reporter Rtn1-Pho8*-GFP were transformed with the resulting PCR products and plated on solid medium. Colonies with functional Roq1 had an intact SHRED pathway resulting in a loss of fluorescence due to degradation of the reporter upon stress as originally described by Szoradi et al., 2018. However, cells with a SHRED defect caused by a Roq1 mutation retained the fluorescent reporter and could be visually screened by Oliver Pajonk (20.000 colonies). 279 selected colonies were then validated for SHRED-activity by flow cytometry with a reporter degradation assay and 151 strains remained with a strong SHRED defect. I then carried out the further analysis of these strains by confirming the expression of Roq1, retrieving the plasmids and sequencing their Roq1 variants. **Figure 6** depicts the basic principle of the assay, and a more detailed description can be found in the Materials and Methods section.

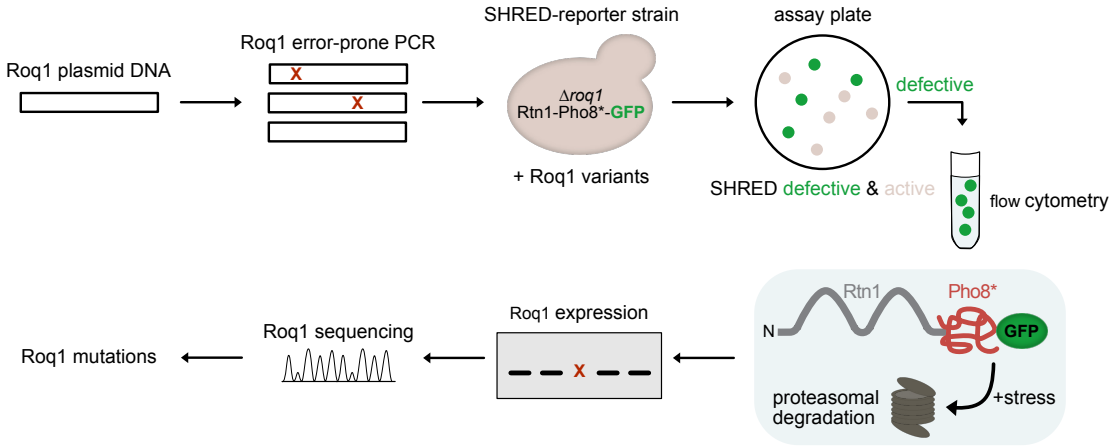

Figure 6: Workflow of the Roq1 mutagenesis screen.
Roq1(1-104) plasmid DNA was mutagenized via error-prone PCR to introduce individual point mutations to Roq1. The created library of Roq1 variants was used to transform the SHRED-reporter strain lacking endogenous Roq1 and expressing the fluorescent SHRED substrate Rtn1-Pho8*-GFP (Δroq1 Rtn1-Pho8*-GFP). Cells were plated onto selective plates and formed colonies were visually screened for an accumulation of the reporter (SHRED-defective) and validated by flow cytometry with a reporter degradation assay. Selected cells were checked for Roq1 expression by Western blotting and finally plasmids from SHRED-defective cells were retrieved and sequenced.

3.1.1 Validation of the Roq1 mutagenesis screen hits

As mentioned above, I tested the expression of 151 uncharacterized Roq1 variants that caused a SHRED defect in yeast by Western blotting. This step was necessary to sort out mutations that simply destabilized Roq1 protein levels in cells. These mutations were most likely not involved in Ubr1 regulation. In the end, 44 strains still expressed Roq1, and the majority did not. I retrieved the plasmids from these strains and sequenced them to determine the underlying Roq1 mutation. I identified mutations causing a C-terminal frameshift in Roq1 and putative chromosomal mutations but excluded them from the further analysis. Identified double mutations were split into two single point mutations to identify the driving mutation. Some single point mutations were identified multiple times. The mutations were then applied to the cleavage mimic Roq1(22-104) to exclude mutations that affect the cleavage of full-length Roq1(1-104) by Ynm3 and again validated with the SHRED-reporter degradation assay. Finally, I identified fourteen single point mutations in Roq1 which resulted in an impaired degradation of Rtn1-Pho8*-GFP in cells as measured by flow cytometry (**Figure 7A**). All fourteen Roq1 variants were still detectable by Western blot with varying abundance (**Figure 7B**). Noteworthy, all Roq1 variants were generally expressed under the control of the strong GPD promoter in yeast since wild-type Roq1 expressed from its endogenous *ROQ1* promoter is essentially undetectable. Thus, all tested mutant variants were in principle abundant enough to induce SHRED. As a side note, Roq1 often appears as a double band in Western blots with an additional, higher molecular weight band that has not been characterized to date (Szoradi et al., 2018).

The fourteen hits from the screen were divided into two groups: (1) lysine mutations, where one residue in the otherwise lysine-free Roq1(22-104) was substituted with a lysine. (2) polar mutations, where a hydrophobic residue was replaced by a polar or charged residue. Interestingly, the polar mutations were found to cluster in the more ordered region of Roq1. Finally, a G40C mutation was identified that did not fall into either of the two groups and was not further analyzed (**Figure 7C**).

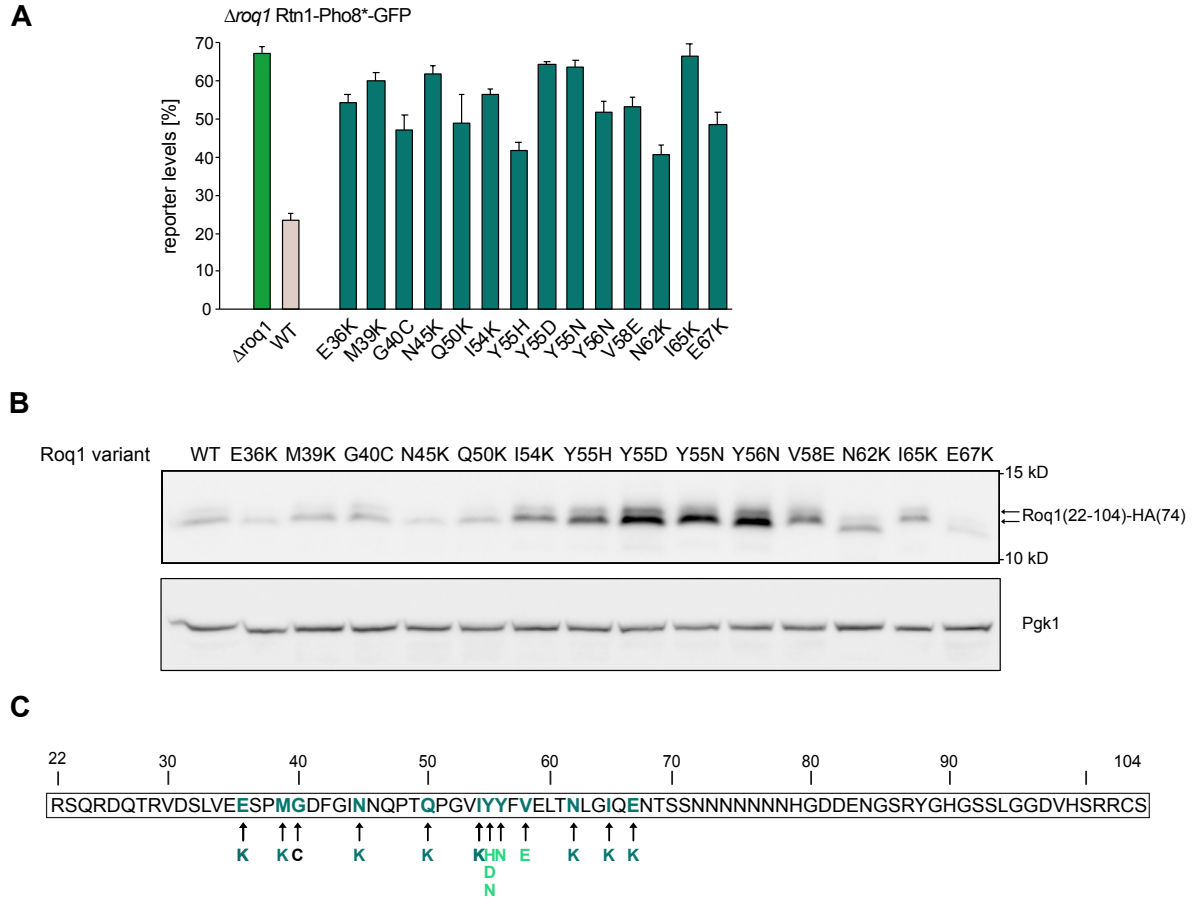

Figure 7: Fourteen individual point mutations in Roq1 cause a SHRED-defect in yeast.
A) Remaining reporter levels after 5 h of tunicamycin treatment measured by flow cytometry. Cells with an empty plasmid (Δroq1) and cells with a plasmid encoding wild-type Roq1 (WT) were used as controls. Roq1(22-104) point mutants were expressed from a plasmid under control of the strong GPD promoter. Geometric mean ± SEM, n=3. **B**) Western blot of HA-tagged Roq1(22-104) and Pgk1 as loading control. 40 µg protein from total yeast cell lysates were resolved on a 16 % tris-tricine SDS-PAGE gel. **C**) Schematic of the Roq1(22-104) sequence with point mutations identified by the Roq1 mutagenesis screen. Lysine mutations are highlighted in dark green and polar mutations in light green.

3.1.2 Characterization of lysine mutations in the lysine-free Roq1(22-104)

Polyubiquitination marks proteins for degradation by conjugating ubiquitin to a substrate lysine, the most common ubiquitin acceptor (Swatek & Komander, 2016). However, Roq1(22-104) is completely lysine-free, and the screen identified a SHRED defect in cells expressing Roq1 variants with a residue replaced by a lysine. Furthermore, they were shown to be less abundant than other candidates (**Figure 7B**).

To first test, whether the mutated residue as such is required for Roq1 function, I individually changed all lysine mutations to alanine. I used the reporter degradation assay to assess the function of the Roq1 variants during SHRED and showed that the alanine mutations did not

disturb Roq1 function (**Figure 8A**). To further distinguish whether the positive charge or the lysine residue by itself is disruptive, I changed I54, which belongs to the group of Roq1 lysine mutations, to an arginine, I54R. I observed that reporter levels still decreased during treatment when Roq1(I54R) was present, but this was not the case for I54K (**Figure 8B**). This implies that the lysine by itself inactivates Roq1. Possibly, the newly introduced lysine in Roq1 allows ubiquitination of Roq1 by Ubr1, thereby dampening its regulatory function. Thus, I analyzed the protein levels of a few lysine variants in comparison to wild-type Roq1 in Δubr1 cells. It turned out that ablation of Ubr1 only had marginal stabilizing effects on the Roq1 lysine variants (**Figure 8C**). Consequently, the ubiquitination of Roq1 lysine variants by Ubr1 is unlikely to be causative for the impaired activity. Alternatively, attachment of ubiquitin to Roq1 could cause steric hindrance of the Roq1-Ubr1 interaction.

I concluded that the affected residues are not critical for Roq1 function and therefore I did not explore this group further.

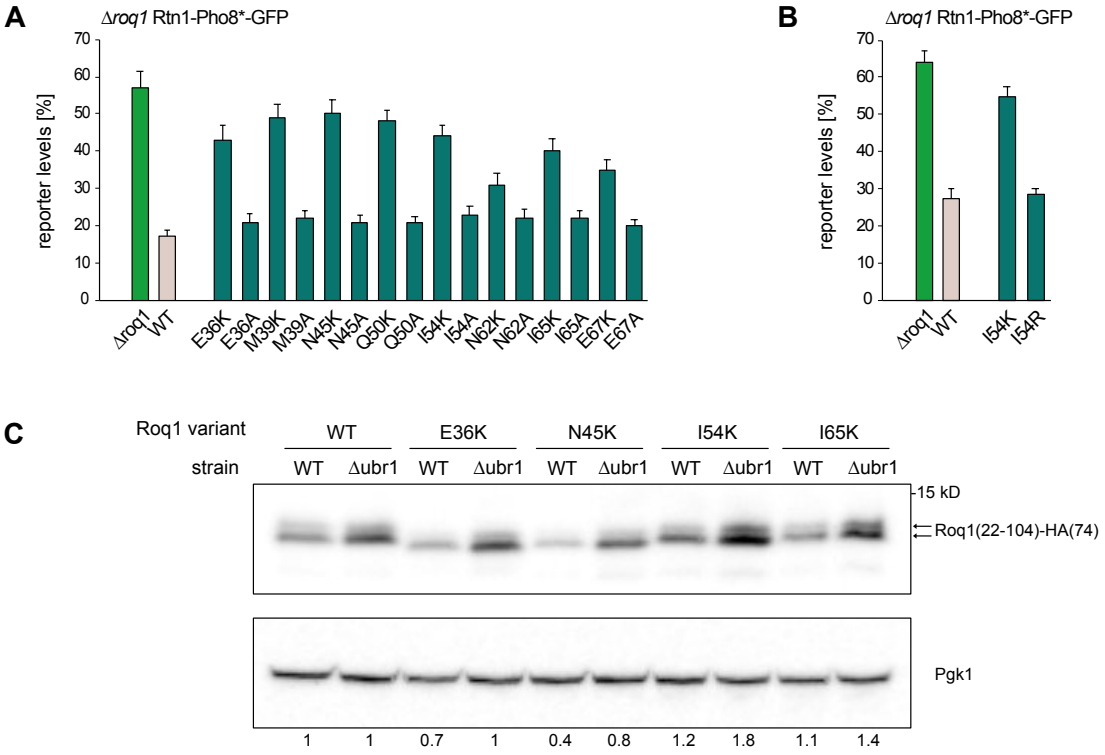

Figure 8: Lysine mutations inactivate Roq1.

A) Remaining reporter levels after 5 h of tunicamycin treatment measured by flow cytometry. Cells with an empty plasmid (Δroq1) and cells with a plasmid encoding wild-type Roq1(WT) were used as controls. Roq1(22-104) point mutants were expressed from a plasmid under control of the strong GPD promoter. Geometric mean ± SEM, n=3. **B)** As in A. **C)** Western blot of HA-tagged Roq1(22-104) and Pgk1 used as loading control. Wild-type or Δubr1 cells expressed Roq1(22-104) variants as indicated. 40 µg protein from total yeast cell lysates were resolved on a 16 % tris-tricine SDS-PAGE gel. Protein levels were normalized to levels of the reference strain (WT or Δubr1) with Roq1 WT.

3.1.3 Roq1 contains a SHRED-critical hydrophobic motif

The second group of Roq1 screen hits were polar mutations. Here, polar or charged residues were introduced for residues at position 55-58 in the predicted more ordered region of Roq1. As a result, hydrophobic residues were changed to charged residues, inactivating Roq1 in vivo. To explore this hydrophobic region further, I individually mutated the neighboring residues (V53-L60) to a charged residue, such as aspartic acid. This allowed me to define Y55-Y56-F57-V58 as four hydrophobic residues in a consecutive order that are required for Roq1-mediated SHRED activity in vivo (**Figure 9A**). Individual substitution of these residues with an alanine rescued SHRED activity suggesting that the negative charge is responsible for disabling Roq1 function. However, the simultaneous mutation of all four residues 55-58 to alanines completely abolished Roq1 function during SHRED (**Figure 9B**). Therefore, the residues Y55-Y56-F57-V58 together form a second SHRED-critical feature in Roq1(22-104), and we named it the hydrophobic motif (**Figure 9C**).

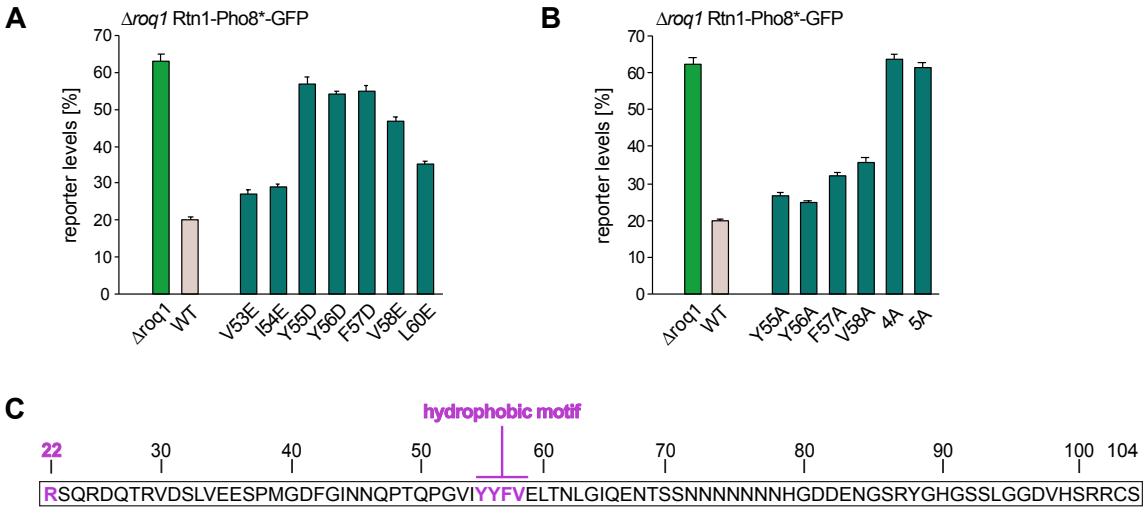

Figure 9: Roq1 contains a functionally relevant hydrophobic motif.
A) Remaining reporter levels after 5 h of tunicamycin treatment measured by flow cytometry. Cells with an empty plasmid (Δroq1) and cells with a plasmid encoding wild-type Roq1(WT) were used as controls. Roq1(22-104) point mutants were expressed from a plasmid under control of the strong GPD promoter. Geometric mean ± SEM, n=3. **B**) As in A but with Roq1 variants lacking the hydrophobic motif (4A) and lacking both R22 and the hydrophobic motif (5A) with 4A = Y55A, Y56A, F57A, V58A and 5A = R22A + 4A. **C**) Schematic of the Roq1(22-104) sequence, R22 and the hydrophobic motif (Y55-Y56-F57-V58) are highlighted in pink.

Notably, Roq1(22-104) protein levels increased with a mutation in the hydrophobic motif (**Figure 7B**). This indicates that the hydrophobic motif may have a dual function in cells contributing to both Roq1 stability and regulating Ubr1. Since it is already known from yeast that Roq1 is short-lived and that Ubr1 plays a very minor role in the turnover of wild-type

Roq1, other E3 ligases must be involved in Roq1 turnover (Szoradi et al., 2018). The E3 ligase San1 has been described to function together with Ubr1 in cytosolic quality control (CytoQC), targeting misfolded cytosolic proteins in a redundant manner (Fredrickson & Gardner, 2012). In general, San1 recognizes five contiguous hydrophobic residues on its substrates (Fredrickson et al., 2011). Therefore, I tested whether Roq1 levels are stabilized in Δsan1 cells and whether this stabilization is dependent on the hydrophobic motif. However, ablation of San1 even caused a slight destabilization of Roq1 wild-type and Y55D variant (**Figure 10**). Eventually this was due to upregulation of Ubr1 in these cells. Thus, San1 is not directly involved in Roq1 degradation.

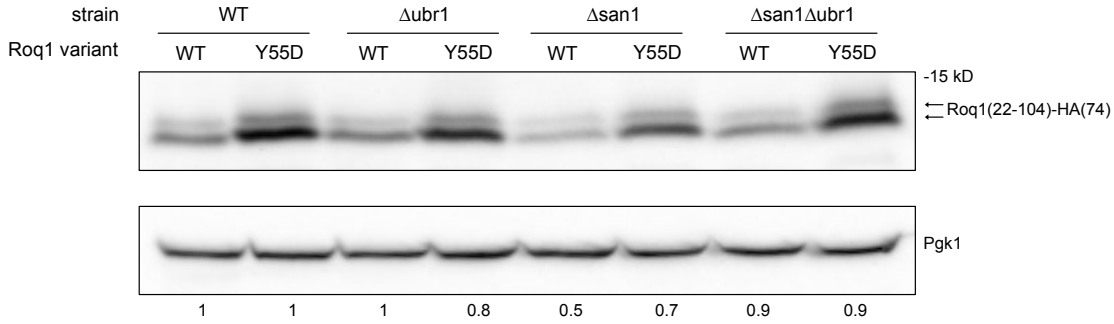

Figure 10: The hydrophobic motif is not a degron for the E3 ligase San1.
Western blot of HA-tagged Roq1(22-104) and Pgk1 used as loading control. Wild-type (WT), Δubr1, Δsan1 or Δubr1Δsan1 cells expressed Roq1(22-104) variants as indicated. 40 µg protein from total yeast cell lysates were resolved on a 16 % tris-tricine SDS-PAGE gel. Protein levels were normalized to levels in the wild-type strain (Roq1 WT or Y55D).

3.2 The role of Roq1's hydrophobic motif

The following section deals with the functional characterization of the newly identified hydrophobic motif of Roq1. Here, I examined whether the hydrophobic motif is required to bind and reprogram Ubr1.

3.2.1 Roq1 interacts with Ubr1 through a heterobivalent binding mechanism

Previously, I have shown that the hydrophobic motif consisting of Y55-Y56-F57-V58 is required for Roq1 function during SHRED in yeast. Succeeding, I asked whether the hydrophobic motif plays a role for the binding of Roq1 with Ubr1 and performed co-immunoprecipitation experiments. I used Δ*roq1* cells stably expressing P_{ADH}-FLAG-Ubr1 and alongside various HA-tagged Roq1(22-104) variants, wild-type and point mutants (R22A, Y55D, Y56D, F57D, V58E) were expressed from a centromeric plasmid. Roq1 with the R22A mutation was used as a negative control for Ubr1 binding corroborating previous findings

(Szoradi et al., 2018). Additionally, a plasmid without Roq1 was used to control for nonspecific binding of Ubr1 to anti-HA agarose beads.

As expected, Ubr1 co-precipitated with wild-type Roq1 and Roq1 with the R22A mutation almost completely abolished Ubr1 binding. Roq1 with mutations that introduced a negative charge in the hydrophobic motif reduced the binding of Ubr1. The V58E mutation was an exception. Roq1 with the V58E mutation could still bind substantial amounts of Ubr1 suggesting that this specific residue has functions beyond Ubr1 binding (**Figure 11A**). Moreover, the substitution of the hydrophobic motif with four alanines reduced the binding of Roq1 to Ubr1 whilst an additional R22A mutation abolished it (**Figure 11B**).

Notably, Roq1 with polar mutations was more abundant than wild-type Roq1, which I also observed earlier, suggesting an additional role of the hydrophobic motif in Roq1 stability. However, also the R22A mutation seemed to stabilize Roq1 in cells. In addition, the F57D mutation in Roq1 resulted in a changed migration behavior within the gel. Apparently, a single change in charge can already cause Roq1 to migrate at a different molecular weight.

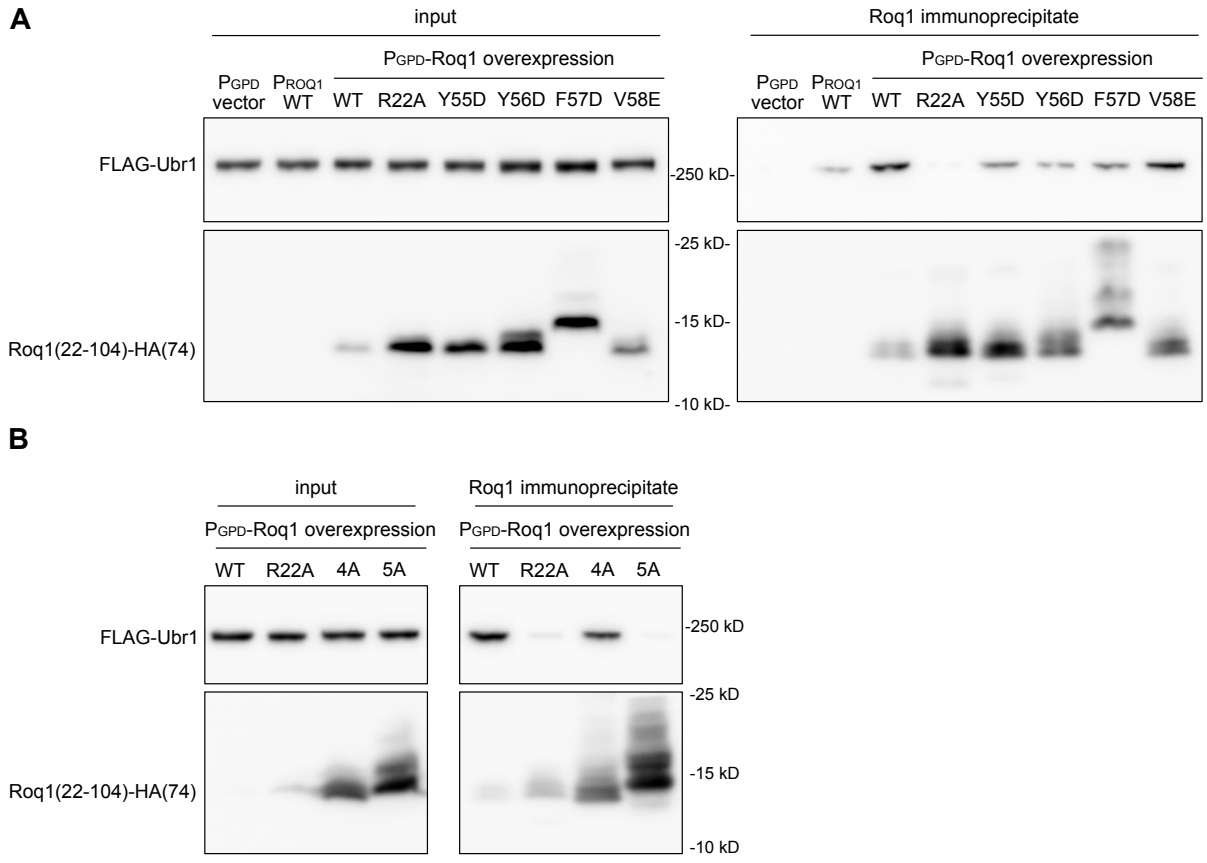

Figure 11: Roq1 requires the hydrophobic motif to bind Ubr1.

A) Western blot from total yeast cell lysates of FLAG-Ubr1 and HA-tagged Roq1 and Roq1 immunoprecipitates. Ubr1 was under control of the ADH promoter and expressed from the yeast chromosome. Roq1(22-104) variants were expressed from a plasmid under control of the GPD promoter (P_{GPD}) or the endogenous promoter (P_{ROQ1}).

As a control for unspecific binding an empty plasmid was used (P_{GPD} vector). Input samples of Ubr1 were resolved on a 7.5 % tris-gylcine gel and Roq1 input samples and immunoprecipitated samples were resolved on a 7.5-16 % tris-tricine step-gradient SDS-PAGE gel. **B**) As in A but with Roq1 variants lacking the hydrophobic motif (4A) and lacking both R22 and the hydrophobic motif (5A) with 4A = Y55A, Y56A, F57A, V58A and 5A = R22A + 4A.

I also tested whether the ubiquitin conjugating enzyme Rad6 is required for establishing the Roq1-Ubr1 interaction. Therefore, I performed the same co-immunoprecipitation experiment but with Δrad6 cells. However, the Roq1-Ubr1 complex was still formed, suggesting that Rad6 is not required for Roq1-Ubr1 binding (data not shown).
Together, the co-immunoprecipitation experiments of Roq1 and Ubr1 in yeast showed that Roq1 interacts with Ubr1 using two sites. This involves R22, which binds to the type-1 site of Ubr1, and the hydrophobic motif, which binds to a yet unknown site. Together they create synergy since the ablation of one site still allows partial binding to Ubr1 via the other.

To also test this in vitro, I applied biolayer interferometry (BLI). BLI is an optical technique for analyzing biomolecular interactions. One molecule is immobilized on a sensor, and the binding of a second molecule then causes a wavelength shift due to an increase in optical density on the sensor (Application note, Sartorius). For this, I used purified proteins and biotinylated Roq1(22-104) wild-type and variants at the single C-terminal cysteine (C103) to immobilize Roq1 on streptavidin biosensors. Purified FLAG-Ubr1 was then offered as binding partner in solution. I then measured the binding of Ubr1 to Roq1 on the sensor which was displayed as a wavelength shift. Wild-type Roq1 associated with Ubr1 whereas the R22A mutation clearly reduced binding as already suggested by my co-immunoprecipitation experiments. Moreover, the polar mutations Y55D, Y56D, F57D lead to a clear defect in binding Ubr1 whereas the V58E mutation only slightly reduced Ubr1 binding (**Figure 12A**). Thus, I have identified a mutation that deactivates Roq1 function in vivo but retains most of its Ubr1 binding capability in vitro, indicating that this residue is specifically important for Roq1 function. Furthermore, the mutation of the whole hydrophobic motif (Roq1 4A) also reduced binding. The R22A mutation has a more drastic effect on Ubr1 binding than the hydrophobic motif mutation, but Roq1 with these mutations combined (Roq1 5A) could no longer bind Ubr1 (**Figure 12B**). This indicates that probably no other binding site for Ubr1 in Roq1 exist. Taken together, the two sites, R22 and the hydrophobic motif, appear to be the two relevant Ubr1 binding determinants in Roq1.
Of note, Ubr1 did hardly dissociate once bound to Roq1. Therefore, I could unfortunately not determine binding kinetics of the Roq1-Ubr1 interaction. I also tried to immobilize His-tagged

Ubr1 on NiNTA sensors to turn the binding assay around and confirm the results obtained with Roq1 on the sensor. Unfortunately, this was not successful and hence, was not further pursued.

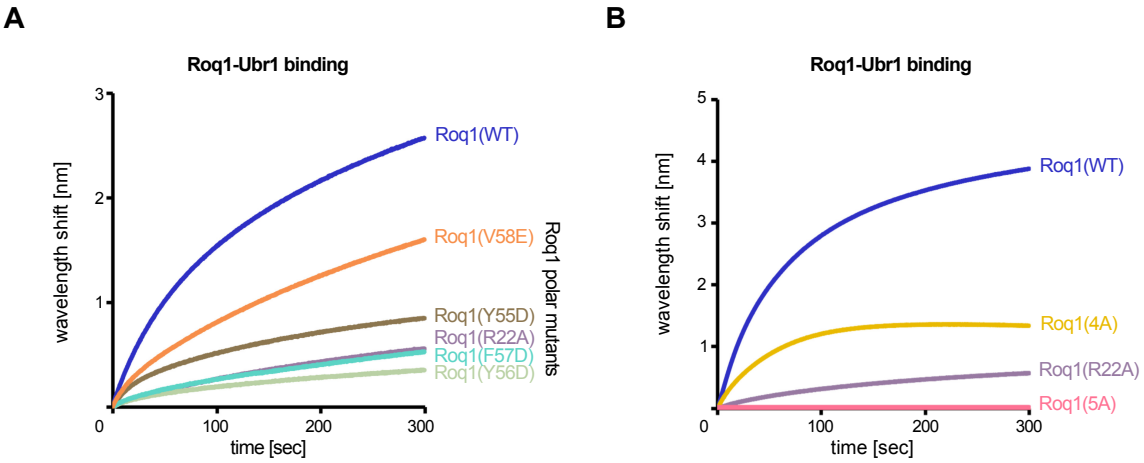

Figure 12: Roq1 binds Ubr1 in a heterobivalent manner.
A) Biolayer interferometry of immobilized Roq1 and soluble FLAG-Ubr1. Roq1(22-104) wild-type and variants were immobilized on streptavidin biosensors and binding of Ubr1 was measured at a concentration of 50 nM for 300 sec. **B)** As in A, but a different batch of biotinylated Roq1 variants and FLAG-Ubr1 was used. n = 2. 4A = Y55A, Y56A, F57A, V58A. 5A = R22A + 4A.

3.2.2 Roq1 establishes physical contact with Ubr1 via the hydrophobic motif

Apart from the N-terminus, the hydrophobic motif represents an additional site in Roq1 that is required for Ubr1 binding. However, it was not clear yet whether this motif truly makes physical contact with Ubr1. Alternatively, it could also serve as a dimerization platform. Therefore, in collaboration with my colleague Niklas Peters and with the help of Jörg Malsam (Söllner lab, BZH), we sought out to determine this with photo-crosslinking. We incorporated the unnatural photo-reactive amino acid p-benzoyl-L-phenylalanine (Bpa) at position 55 or 56 into the hydrophobic motif of Roq1(22-104)-ALFA (**Figure 13A**). Roq1 variants were expressed in *E. coli* and the complex was isolated by adding ALFA beads and Ubr1 to Roq1 after dialysis.

Crosslinking was performed by irradiating the complex with UV light after elution from ALFA beads and samples were analyzed by western blotting. As a control, we included wild-type Roq1 without incorporated Bpa, which did not crosslink with Ubr1 upon UV irradiation. Roq1 variants with Y55Bpa and Y56Bpa formed a crosslink with Ubr1 upon irradiation as they partially shifted from their low molecular weight to 250 kDa, the molecular weight of Ubr1 (**Figure 13B**). This showed that Roq1 uses the hydrophobic motif to physically bind Ubr1 and not to form a dimer.

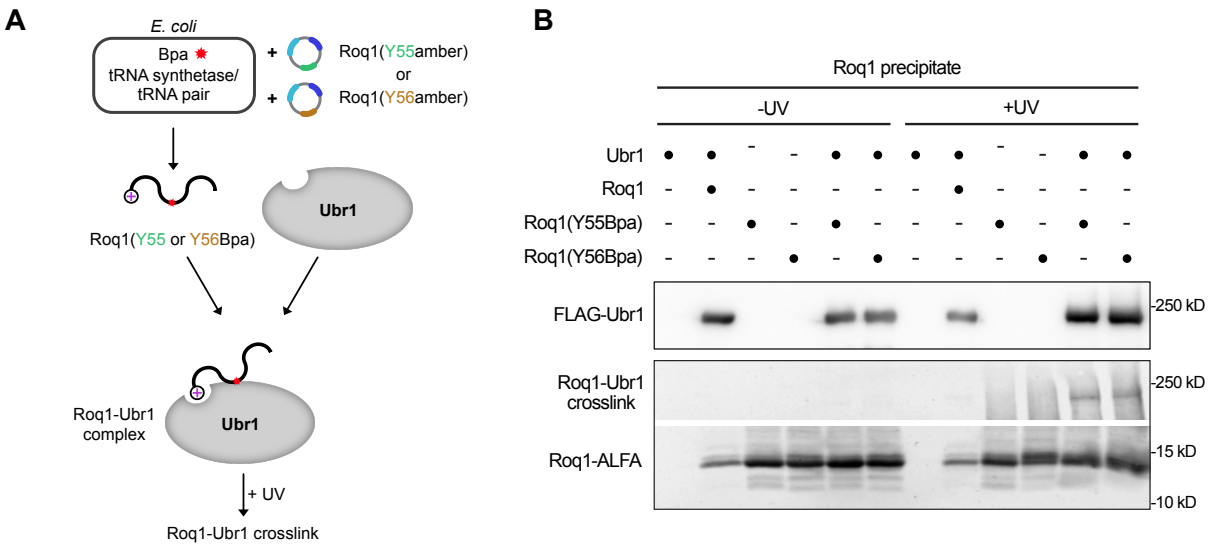

Figure 13: Roq1 establishes direct physical contact with Ubr1 via the hydrophobic motif.
A) Workflow of Roq1-Ubr1 photo-crosslinking. Roq1(22-104)-ALFA with the Y55amber or Y56amber mutation was expressed in *E. coli* and p-benzoyl-L-phenylalanine (Bpa) was incorporated via amber stop codon suppression. Roq1 variants were purified and incubated together with Ubr1 to form the Roq1-Ubr1 complex. The complex was then precipitated and irradiated with UV light in solution. Generated crosslinks were analyzed by Western blotting. **B**) Western blot of FLAG-tagged Ubr1 and ALFA-tagged Roq1(22-104) after precipitation of the Roq1-Ubr1 complex with and without irradiation by UV light as control. This experiment was performed in collaboration with Niklas Peters and Jörg Malsam.

3.3 In vitro reconstitution of SHRED

To further investigate how Roq1 uses the hydrophobic motif to reprogram Ubr1, I performed in vitro substrate ubiquitination assays with purified SHRED components. The ubiquitination assays were previously established by my colleague Niklas Peters. For this, purified Rad6 (E2 enzyme), ubiquitin, commercial Ube1 (E1 enzyme), Roq1(22-60), FLAG-Ubr1 (E3 ligase) and discrete Ubr1 substrates were incubated together at 30 °C in a PCR tube in presence of ATP. To stop the reaction sample buffer was added, samples were resolved on an SDS-PAGE gel and ubiquitination of substrates was analyzed by Western blotting. This assay allowed us to examine the effect of Roq1 on substrate ubiquitination by Ubr1. A truncated Roq1 variant was used for all in vitro ubiquitination reactions because Roq1(22-104) was itself ubiquitinated by Ubr1 in vitro (Pan et al., 2021). However, truncation of the C-terminus of Roq1(22-104) to Roq1(22-60) eliminated this problem. Therefore, we mainly used Roq1(22-60) for standard ubiquitination assays at a 10-fold molar excess of Roq1 over Ubr1 unless stated otherwise. This was motivated by an experiment from Niklas Peters showing that the amount of non-ubiquitinated substrate decreases with increasing Roq1 concentration.

3.3.1 Roq1 regulates Ubr1 in vitro

To investigate substrate ubiquitination by Ubr1 in presence of Roq1 we tested several different substrates: Niklas Peters had purified Pho8* derived from the yeast SHRED-reporter Rtn1-Pho8*-GFP, and we mainly used Pho8*-MBP as misfolded model substrate. Another SHRED substrate was the commercially available firefly luciferase, which has also been shown to be targeted by SHRED in yeast (Szoradi et al., 2018). To be recognized by Ubr1 in vitro, luciferase had to be chemically unfolded prior to a ubiquitination reaction. Besides, model N-degron substrates of Ubr1, R-GFP (as type-1 N-degron substrate) and F-GFP (as type-2 N-degron substrate), were tested. Yeast experiments have shown that Roq1 outcompetes regular type-1 N-degron substrates since they both bind the same binding site. On the other hand, Roq1 promotes the turnover of type-2 N-degron substrates (Szoradi et al., 2018). The natural Ubr1 substrate Cup9, with an internal degron, was also tested. The degradation of Cup9 in cells is typically controlled by peptides that bind to both, the type-1 and the type-2 site, releasing Ubr1 from autoinhibition (Du et al., 2002). It was unknown whether Roq1, as a type-1 site binder, also controls Cup9 ubiquitination in vitro.

In ubiquitination reactions using the misfolded Pho8*, the presence of Roq1 tremendously stimulated the ubiquitination of Pho8* by shifting the protein to a higher molecular weight. Also, non-modified Pho8* slowly vanished over time. Of note, even in absence of Roq1 Ubr1 recognized and ubiquitinated Pho8* (**Figure 14A**). Importantly, its folded counterpart, Pho8, was almost not ubiquitinated by Ubr1, neither in absence, nor in presence of Roq1 (**Figure 14B**). The same was true for chemically unfolded luciferase as misfolded substrate versus folded, native luciferase (**Figure 14C+D**). Thus, Roq1 is supposedly not just a global activator of Ubr1 but rather upregulates Ubr1 activity in a substrate-specific manner.

Another set of substrates that were tested were model N-degron Ubr1 substrates such as R-GFP and F-GFP, and Niklas Peters inquired the effect of Roq1 on their ubiquitination. In line with what is known from yeast, R-GFP ubiquitination was inhibited in presence of Roq1 (**Figure 14E**). Furthermore, occupancy of the type-1 site by Roq1 promotes the turnover of type-2 N-degron substrates (Szoradi et al., 2018). Consequently, F-GFP ubiquitination was also enhanced in presence of Roq1 in vitro (**Figure 14F**). Furthermore, I examined the effect Roq1 had on the ubiquitination of Cup9 a Ubr1 substrate with an internal degron. Typically, Cup9 ubiquitination is regulated by peptides but Roq1 as a type-1 site binder could also promote the ubiquitination of Cup9 (**Figure 14G**).

In summary, all components required to reconstitute SHRED in vitro are: Ube1 (E1), Rad6 (E2), Ubr1 (E3 ligase), ubiquitin, a Ubr1 substrate and Roq1(22-60). We have shown, that Roq1 promotes the ubiquitination of Pho8* and unfolded Luciferase but has essentially no effect on their well-folded counterparts. In the case of Cup9, Roq1 fulfills the role of a type-1 peptide and promotes the ubiquitination of Cup9. The ubiquitination of a type-1 N-degron substrate, like R-GFP, is inhibited whilst ubiquitination of a type-2 N-degron substrate, like F-GFP, is stimulated. Taken together, this suggests that Roq1 controls the substrate specificity of Ubr1 through a comprehensive reprograming mechanism.

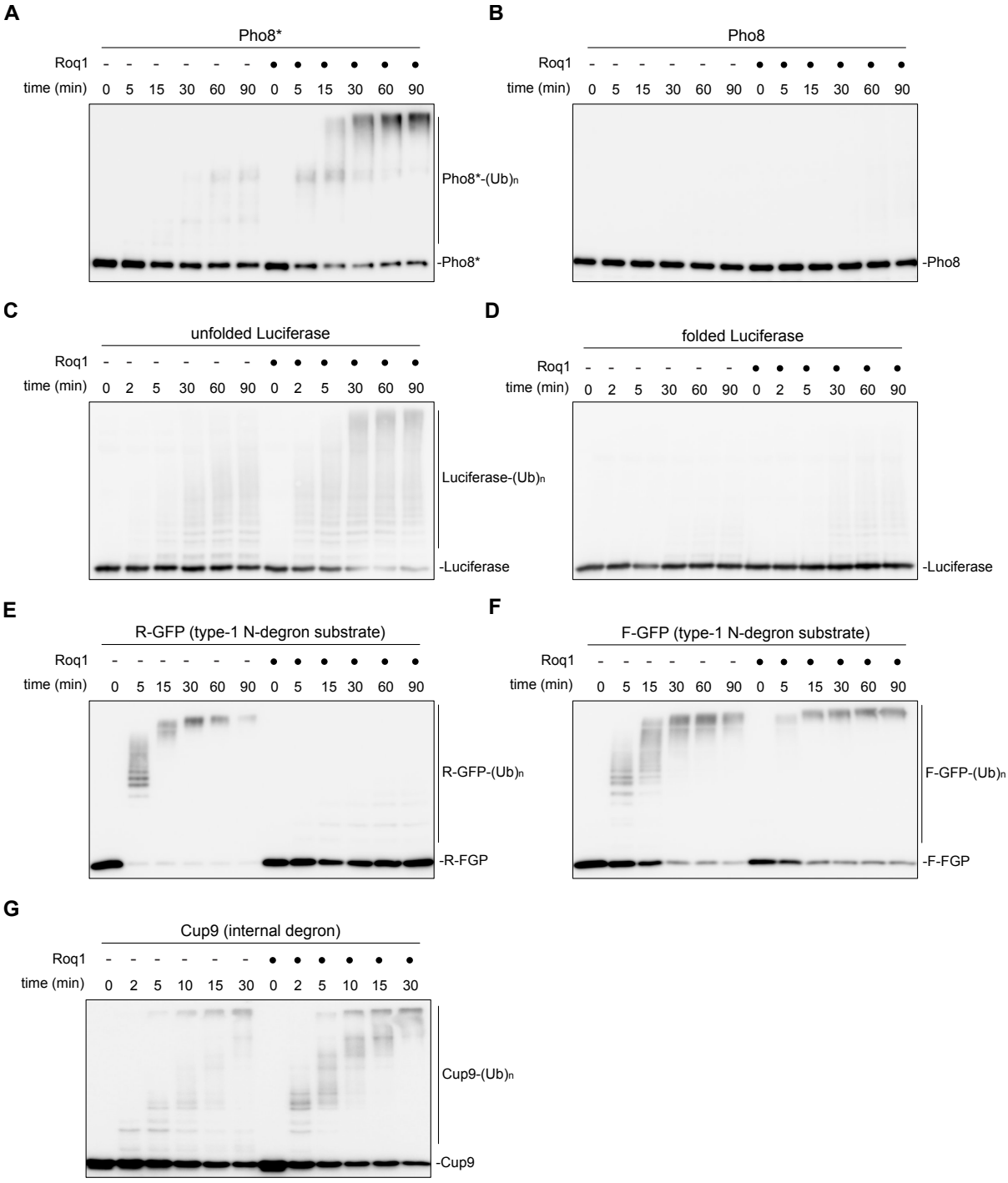

Figure 14: Roq1 reprograms Ubr1 in vitro.
A+B) Western blot of Pho8* or Pho8 from ubiquitination assays in absence and presence of Roq1(22-60). Reactions were stopped at indicated time points. **C+D**) Western blot of firefly Luciferase, chemically unfolded or folded, from ubiquitination assays in absence and presence of Roq1(22-60). Reactions were stopped at indicated time points. Experiment was performed by Niklas Peters. **E+F**) Western blot of R-GFP or F-GFP from ubiquitination assays in absence and presence of Roq1(22-60). Reactions were stopped at indicated time points. Experiment was performed by Niklas Peters. **G**) Western blot of Cup9-StrepII from ubiquitination assays in the absence and presence of Roq1(22-60). Reactions were stopped at indicated time points. Experiment from me but Cup9-StrepII protein was provided by Niklas Peters.

3.3.2 Roq1 has functions beyond a type-1 dipeptide

Through binding to the type-1 site of Ubr1, Roq1 governs the substrate specificity of Ubr1 (Szoradi et al., 2018). In general, E2 enzymes may also directly engage the target protein since they were shown to also employ an intrinsic chain-building ability (Stewart et al., 2016). To rule out that Roq1 has any other effects on substrate ubiquitination besides interacting with Ubr1, I performed a control Pho8* ubiquitination experiment with just Roq1 and absence of Ubr1. After all, this confirmed that Roq1 requires the presence of Ubr1 and does not have any effect on Pho8* ubiquitination when Ubr1 is absent (**Figure 15A**).

Moreover, substituting Roq1 with an arginine-alanine (RA) dipeptide which also binds the type-1 binding site of Ubr1 did not promote Pho8* ubiquitination (**Figure 15B**). This provides strong evidence that the simple occupancy of the type-1 site is not sufficient to reprogram Ubr1. In contrast to an RA dipeptide, Roq1 possesses an additional feature, the hydrophobic motif. This motif is required for SHRED activity in vivo and directly interacts with Ubr1. Therefore, the hydrophobic motif is likely to be required to promote misfolded substrate ubiquitination by Ubr1 in vitro.

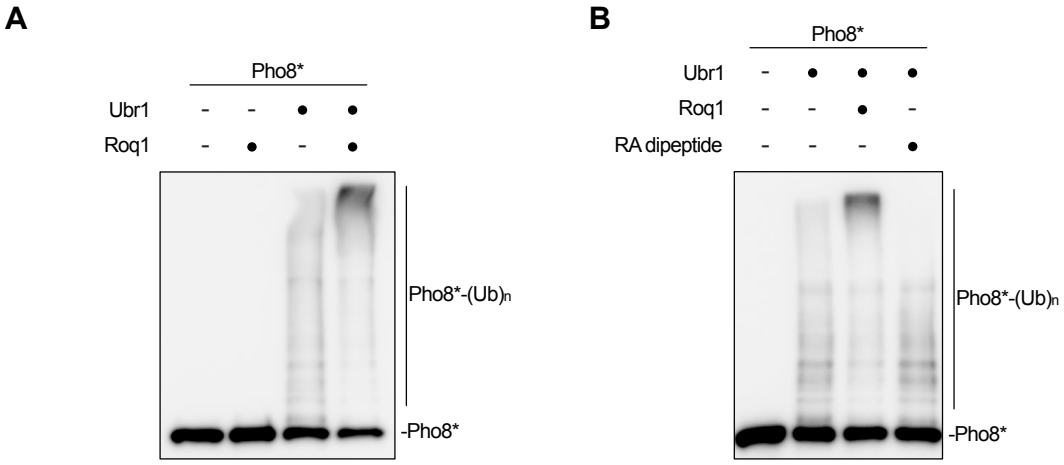

Figure 15: An RA dipeptide cannot functionally replace Roq1.
A) Western blot of Pho8* from ubiquitination assays with Roq1(22-60) after 90 min. **B**) Western blot of Pho8* from ubiquitination assays with Roq1(22-60) and RA dipeptide with a 4000-fold molar excess over Ubr1 after 90 min.

3.3.3 Regulation of Ubr1 by Roq1 via two sites

Two sites in Roq1 have been identified to be required for both SHRED-activity in vivo and Ubr1 binding in vitro: the N-terminal R22 and the hydrophobic motif. When individually mutated, both R22 and the hydrophobic motif still displayed residual Ubr1 binding with the R22A mutation having a stronger impact on the Roq1-Ubr1 interaction. Anyhow, the two binding sites seem to act synergistically. To better understand the functional interplay of the two binding sites of Roq1 and how they control Ubr1 activity, I tested and compared relevant Roq1 mutants in Pho8* ubiquitination assays. I applied Roq1 wild-type, R22A, 4A and 5A and included the RA dipeptide as control without an effect on Pho8* ubiquitination as shown before. I expected that Roq1(4A) mimics an RA dipeptide, by only occupying Ubr1's type-1 site via R22.

Roq1 wild-type promoted Pho8* ubiquitination by Ubr1 whereas Roq1 with the R22A mutation failed to do so. Interestingly, Roq1(4A, lacking the hydrophobic motif) even inhibited Pho8* ubiquitination (**Figure 16A**, lane 7 and 8). As I could see in previous co-immunoprecipitation and BLI experiments, the 4A mutation reduces the binding of Roq1 to Ubr1. Considering this, the inhibition of Pho8* ubiquitination was even more striking. It is possible that Roq1(4A) has an additional steric feature that blocks either substrate recognition by Ubr1, ubiquitin transfer or both. However, this might require the anchoring of Roq1(4A) to Ubr1 via R22. To control for this, I showed that Roq1(4A) is still able to displace R-GFP from the type-1 site of Ubr1. (**Figure 16B**, lane 4). Furthermore, the Ubr1 binding deficient variant Roq1(5A) had no effect on Pho8* ubiquitination and did no longer inhibit it (**Figure 16A**, lane 9 and 10). Thus, partial binding of Roq1(4A) to Ubr1 through R22 is required to inhibit substrate ubiquitination.
In contrast, Cup9 ubiquitination was not affected by Roq1(4A), further supporting the hypothesis that the hydrophobic motif is specifically required to enable Ubr1 to target misfolded proteins (data not shown). So, unintentionally, with Roq1(4A), I have also identified a Roq1 mutant that negatively impacts Ubr1 activity toward misfolded substrates.

Can Ubr1 activation by Roq1 somehow be restored by the combined presence of two different Roq1 variants? To answer this, I tested the effect on Pho8* ubiquitination in presence of both Roq1(R22A) to provide an intact hydrophobic motif, and Roq1(4A) or RA dipeptide to occupy the type-1 site of Ubr1 (**Figure 16C**, lane 9 and 10). However, this could not restore Ubr1

activity indicating that the correct binding of the hydrophobic motif to Ubr1 requires docking of R22 to the type-1 site of Ubr1.

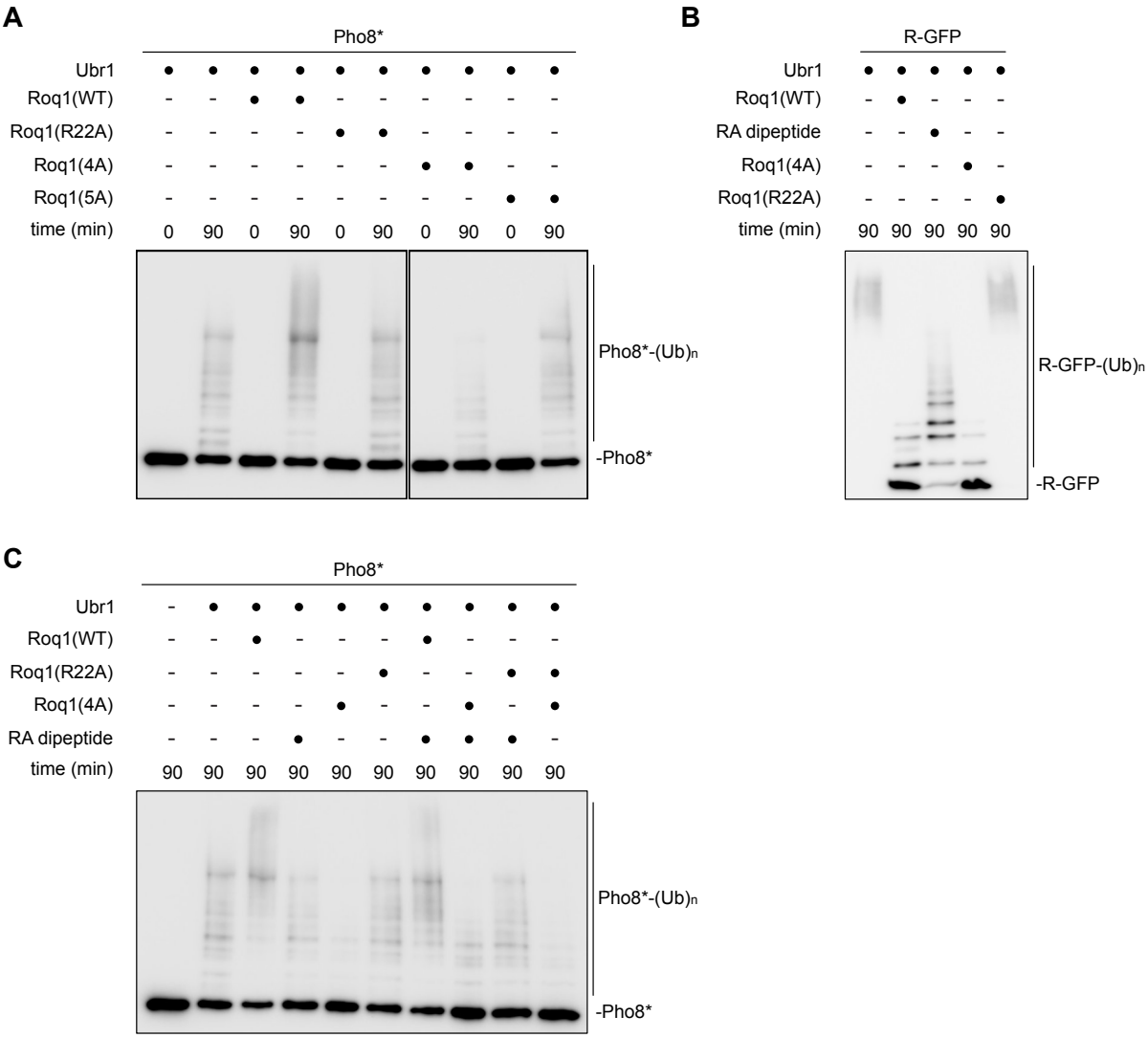

Figure 16: Roq1 lacking the hydrophobic motif inhibits Pho8* ubiquitination by Ubr1
A) Western blot of Pho8* from ubiquitination assays with Roq1(22-104) WT, R22A, 4A and 5A. Reactions were stopped at indicated time points. **B**) Western blot of R-GFP (protein provided by Niklas Peters) from ubiquitination assays with Roq1(22-104) WT, R22A, 4A and 400-fold molar excess of RA dipeptide over Ubr1 after 90 min. **C**) Western blot of Pho8* from ubiquitination assays with Roq1(22-104) WT, R22A, 4A and 400-fold molar excess of RA dipeptide over Ubr1 after 90 min. 4A = Y55A, Y56A, F57A, V58A. 5A = R22A, 4A.

3.3.4 Regulation of Ubr1 by Roq1 through its hydrophobic motif

Previously I showed that, besides binding of Ubr1, the hydrophobic motif also plays a role in Ubr1 regulation as its loss (4A mutation) results in the inhibition of Pho8* ubiquitination. Simultaneously, the 4A mutation in the hydrophobic motif reduced the binding of Roq1 to Ubr1. To specifically focus on the regulatory role of the hydrophobic motif, it was necessary to uncouple these two events. Roq1 with the V58E mutation in the hydrophobic motif, derived from the mutagenesis screen, was a suitable candidate to test this. In contrast to Roq1(4A), this mutation inactivated Roq1 function in vivo while retaining most of its Ubr1 binding capability in vitro (**Figure 17A**). Therefore, we used Roq1(V58E) and titrated this variant in ubiquitination assays.

Roq1(V58E) failed to enhance Pho8* ubiquitination by Ubr1 even at higher concentrations (**Figure 17B**), and there was only a mild stimulation of ubiquitination of unfolded Luciferase (**Figure 17C**). In contrast, Roq1(V58E) still inhibited the ubiquitination of the type-1 N-degron substrate R-GFP to the same extent as wild-type Roq1 (**Figure 17D**). Along the same line, Roq1 with the V58E mutation could still promote the ubiquitination of the type-2 N-degron substrate F-GFP and the natural substrate Cup9 just like wild-type Roq1 (**Figure 17E+F**).
In conclusion, Roq1 promotes Ubr1 activity towards the ubiquitination of misfolded substrates, such as Pho8* and unfolded Luciferase, via its hydrophobic motif. The motif is dispensable for regulating the ubiquitination of N-degron substrates such as R-GFP and F-GFP or the non-N-degron substrate Cup9 which only require binding of Roq1 to the type-1 site of Ubr1 via its N-terminal R22.

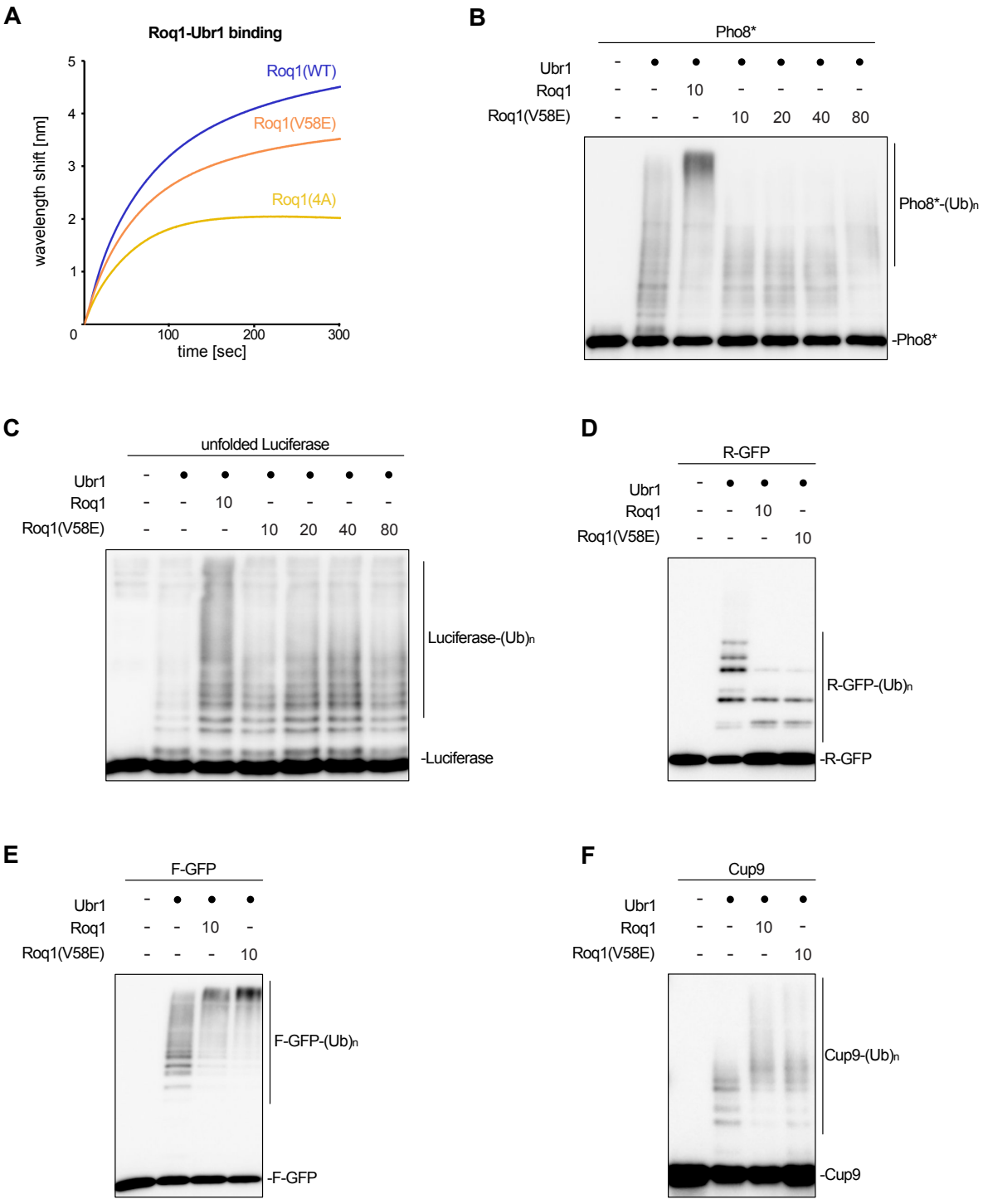

Figure 17: Roq1 selectively promotes ubiquitination of misfolded proteins through its hydrophobic motif. **A)** Biolayer interferometry of immobilized Roq1 and soluble FLAG-Ubr1. Roq1(22-104) wild-type, 4A and V58E were immobilized on streptavidin biosensors and binding of Ubr1 was measured at a concentration of 50 nM for 300 sec. n = 2. **B**) Western blot of Pho8* from ubiquitination assays with Roq1(22-60)WT or titrated amounts of Roq1(22-60)V58E after 90 min. Numbers indicate the molar excess of Roq1 over Ubr1. Experiment from Niklas Peters. **C**) As in panel B but with unfolded Luciferase after 30 min. **D**) As in panel B but with R-GFP after 15 min. Experiment from Niklas Peters. **E**) As in panel B but with F-GFP after 15 min. Experiment from Niklas Peters. **F**) As in panel B but with Cup9-StrepII after 15 min. Experiment from me but Cup9-StrepII protein was provided by Niklas Peters.

3.3.5 Roq1 does not act on Rad6 recruitment to Ubr1

Roq1 could regulate Ubr1 in several ways. A common mechanism to enhance ubiquitination of a substrate by a E3 ligase is to facilitate the binding of the ubiquitin-loaded E2 enzyme (E2~Ub) to the E3 ligase. This indirectly enhances the ubiquitin transfer from the E2 enzyme to the substrate. For example, CRLs use Nedd8, a ubiquitin-like protein, as a cofactor to bridge the existing gap between the substrate and the E2~Ub on the E3 ligase. Consequently, the recruitment of the E2 enzyme is also improved (Baek et al., 2020; Saha & Deshaies, 2008). Like Nedd8, Roq1 could enhance the recruitment of the E2 enzyme Rad6 to Ubr1 and therefore the transfer of ubiquitin. Usually, E2 enzymes are loaded with ubiquitin upon binding to the respective E3 ligase. However, it is known, that Rad6 can bind to Ubr1 even when it is not conjugated to ubiquitin (Xie & Varshavsky, 1999). To bind Rad6, Ubr1 employs two sites: the Ubc2/Rad6-binding region (U2BR) and the RING domain (Pan et al., 2021).

I investigated the interaction of unloaded Rad6 with Ubr1 in the presence and absence of Roq1. Therefore, I used purified recombinant FLAG-Ubr1 and Rad6, biotinylated Rad6 on primary amines and immobilized it on streptavidin biosensors for biolayer interferometry. I measured the binding of Ubr1 in solution with and without Roq1 to immobilized Rad6. I used Roq1 in a molar excess over Ubr1 (2:1 and 10:1) and did not observe any differences in the association of Ubr1 to Rad6 (**Figure 18**). Notably, the Rad6-Ubr1 complex did not dissociate which is why I could only analyze association kinetics. However, this indicates that Roq1 is unlikely to affect the recruitment of (unloaded) Rad6 to Ubr1.

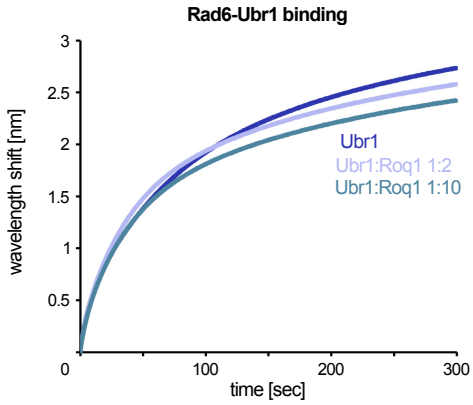

Figure 18: Roq1 does not influence the recruitment of unloaded Rad6 to Ubr1.
Biolayer interferometry of immobilized Rad6 and soluble FLAG-Ubr1. Rad6 was immobilized on streptavidin biosensors and binding of Ubr1 was measured at a concentration of 100 nM for 300 sec. Roq1(22-104) was incubated together with Ubr1 at a 2-fold (Ubr1:Roq1 1:2) or 10-fold (Ubr1:Roq1 1:10) molar excess over Ubr1. n = 2.

It is also possible that Roq1 is engaged in the recruitment of the substrate by changing the conformation of Ubr1 thereby facilitating substrate recognition. Roq1 binding could open a new substrate binding site for misfolded proteins on Ubr1, which is only hardly accessible in absence of Roq1. Consequently, Roq1 could be physically part of this new site. However, both would presumably lead to the fact that binding of substrate to Ubr1 is affected. Therefore, I also tried to immobilize Pho8* and the folded counterpart Pho8 as Ubr1 substrates on the sensor and asked whether Roq1 influenced the binding of the substrates to Ubr1 in solution. Unfortunately, this did not work for unknown reasons (data not shown). Simultaneously, Niklas Peters sought out to tackle the same hypothesis with a pulldown experiment. He used purified Pho8-MBP and Pho8*-MBP combined with Ubr1 either alone or in presence with Roq1, 1:1 or 1:10 molar excess. This revealed no enhancing effect of Roq1 on substrate binding of Ubr1 (data not shown).

3.3.6 Roq1 promotes ubiquitination of misfolded proteins by means of its hydrophobic motif

Roq1 promotes the ubiquitination of misfolded substrates, and this depends on the hydrophobic motif. How exactly the hydrophobic motif stimulates ubiquitination was still unclear. Since the recruitment of both, the E2 enzyme Rad6 and the misfolded substrate, was unaffected by Roq1, we focused on substrate ubiquitination. In previous ubiquitination assays, we could not distinguish whether Roq1 rather promotes chain initiation, chain elongation or both. Therefore, we used a commercially available lysine-free ubiquitin variant (no K ubiquitin) instead of wild-type ubiquitin in standard ubiquitination assays with misfolded Pho8*. This ubiquitin variant can be conjugated to substrate lysines through its C-terminus but can no longer form ubiquitin chains (**Figure 19A**). Ubr1 alone could attach two distinct no K ubiquitin molecules to Pho8*, appearing as two separate bands. In presence of Roq1 the number of ubiquitination sites increased up to at least five as indicated by the additional number of bands (**Figure 19B**). However, the Roq1 V58E mutation diminished this effect and the same was observed when using the RA dipeptide. This can be explained by the lack of the regulatory activity of Roq1 through the hydrophobic motif.

To further inquire the effect of the hydrophobic motif of Roq1 we tested additional substrates. The ubiquitination of the type-2 N-degron substrate F-GFP is upregulated by Roq1. Niklas Peters could show that Ubr1 by itself attached ubiquitin to five lysines within F-GFP (**Figure**

19C). With an RA dipeptide, Roq1 wild-type, or V58E, the number of ubiquitination sites increased up to six. Therefore, Roq1 had no effect beyond that of an RA dipeptide.
Simultaneously, I tested Cup9 as natural substrate with an internal degron which is regulated via the occupancy of the type-1 and type-2 site of Ubr1 (Du et al., 2002). I could observe the same for Cup9 as for F-GFP: Roq1 increased the number of ubiquitination sites, however, only to the same extend as an RA dipeptide (**Figure 19D**). This also did not dependent on the hydrophobic motif of Roq1.

To conclude, the hydrophobic motif of Roq1 has a dual function.
(1) Together with R22, it creates avidity and supports the binding strength of Roq1 to the type-1 site of Ubr1 as seen for the type-2 substrate F-GFP and the natural substrate Cup9. Notably, because of the 4000-fold molar excess of RA dipeptide and only a 10-fold molar excess of Roq1 over Ubr1, Roq1 apparently is in some way a very "strong dipeptide", a strong type-1 site binder. Thus, Roq1 is an activator for F-GFP and Cup9 ubiquitination.
(2) It selectively promotes the ubiquitination of misfolded substrates such as Pho8*. In doing so, it enhances chain initiation and increases the accessibility to more ubiquitination sites on the substrate.

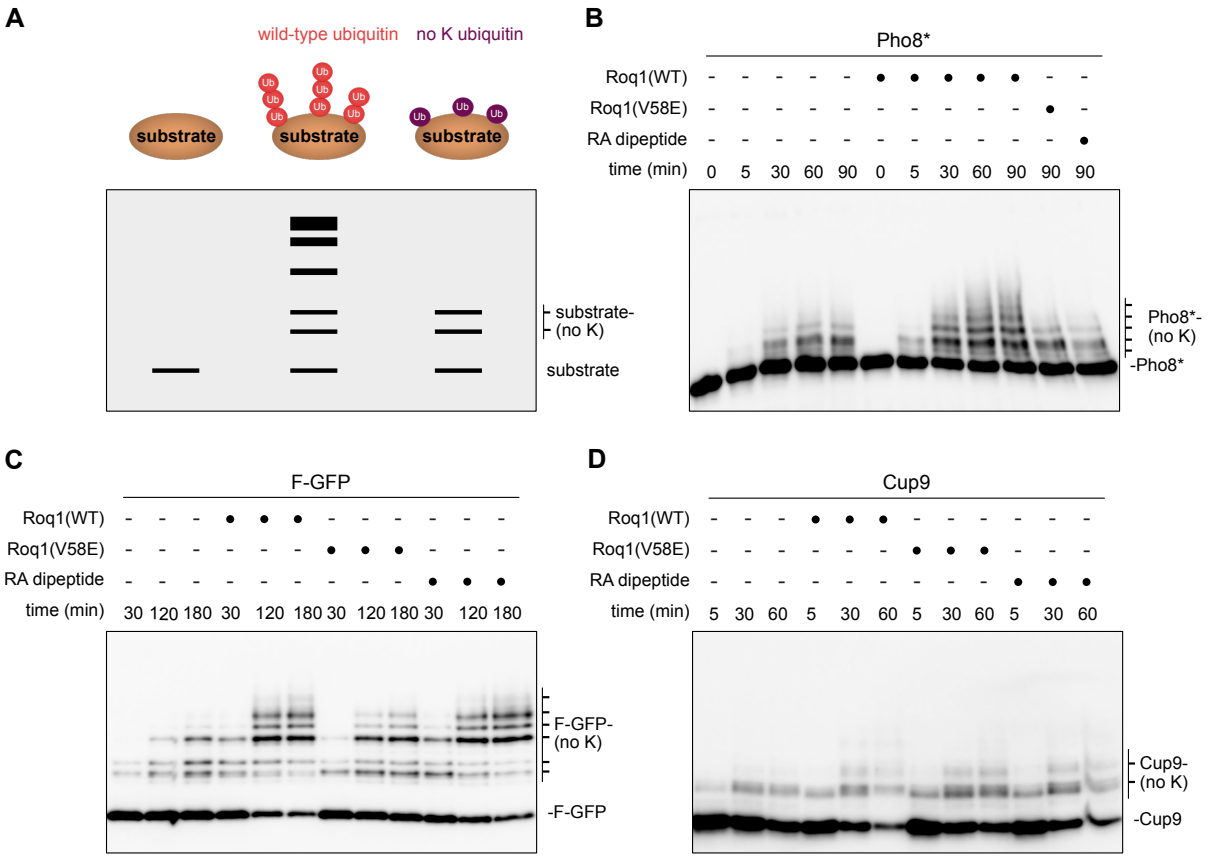

Figure 19: Roq1 promotes ubiquitin chain initiation by Ubr1.
A) Schematic of ubiquitination assays using wild-type or no K ubiquitin as ubiquitin source. **B)** Western blot of Pho8* from ubiquitination assays using no K ubiquitin as ubiquitin source and Roq1(22-60) WT, V58E and RA dipeptide at a 4000-fold molar excess over Ubr1. Reactions were stopped at indicated time points. Experiment from Niklas Peters. **C**) As in panel B but with F-GFP. Experiment from Niklas Peters. **D**) As in panel B but with Cup9-StrepII. Experiment from me but Cup9-StrepII protein was provided by Niklas Peters.

3.4 Roq1's minimal functional elements

Finally, I wanted to understand the functional architecture of Roq1 in more detail. Therefore, I aimed to break down the Roq1 sequence to its minimally required parts.

What was known so far was that the C-terminus (61-104) of Roq1 is redundant for Roq1 function in vitro as demonstrated by Niklas Peters. In cells, both Roq1(22-104) and Roq1(22-60) were SHRED-active when expressed from the strong GPD promoter (**Figure 20A**). However, when expressed from the endogenous *ROQ1* promoter Roq1(22-60) showed a SHRED defect whereas Roq1(22-104) could still induce SHRED. Therefore, presumably, the C-terminal sequence of Roq1 contributes to Roq1 stability in cells. Hence, the fact that overexpressed Roq1(22-60) is active and is also functional in vitro, shows that no functionally essential determinants are contained in that sequence. However, Roq1 requires R22 and the hydrophobic motif to regulate Ubr1 both in vivo and in vitro. To ask whether regions outside of the two determinants are dispensable, I first sought out to shorten the flexible sequence spacing R22 and the hydrophobic motif. Between R22 and the hydrophobic motif there is a stretch of 33 amino acids, and I sequentially shortened this stretch to only 15 amino acids left, generating Roq1(22 aa), my shortest Roq1 variant (**Figure 20B**). In cells, this variant still retained its function during SHRED when overexpressed, as measured by flow cytometry (**Figure 20C**). To test whether the remaining linker still contains functionally relevant parts, I replaced 10 residues of the 15 remaining amino acids from Roq1(22 aa) with a generic flexible glycine-glycine-serine (GGS) or glycine-serine-proline (GSP) sequence (**Figure 20D**). Residues immediately adjacent to R22 and the hydrophobic motif were kept. Even though GGS and GSP variants of Roq1 were inactive in vivo (data not shown), I purified Roq1(GGS), (GSP) and (22 aa) to test their function in vitro. All tested Roq1 variants were active and could still promote Pho8* ubiquitination (**Figure 20E**).
This proves that I have identified all functionally required parts of Roq1, namely R22, a short flexible linker and the hydrophobic motif (**Figure 20F**). Beyond that, I generated Roq1-derived peptides that can regulate the activity of the large E3 ligase Ubr1.

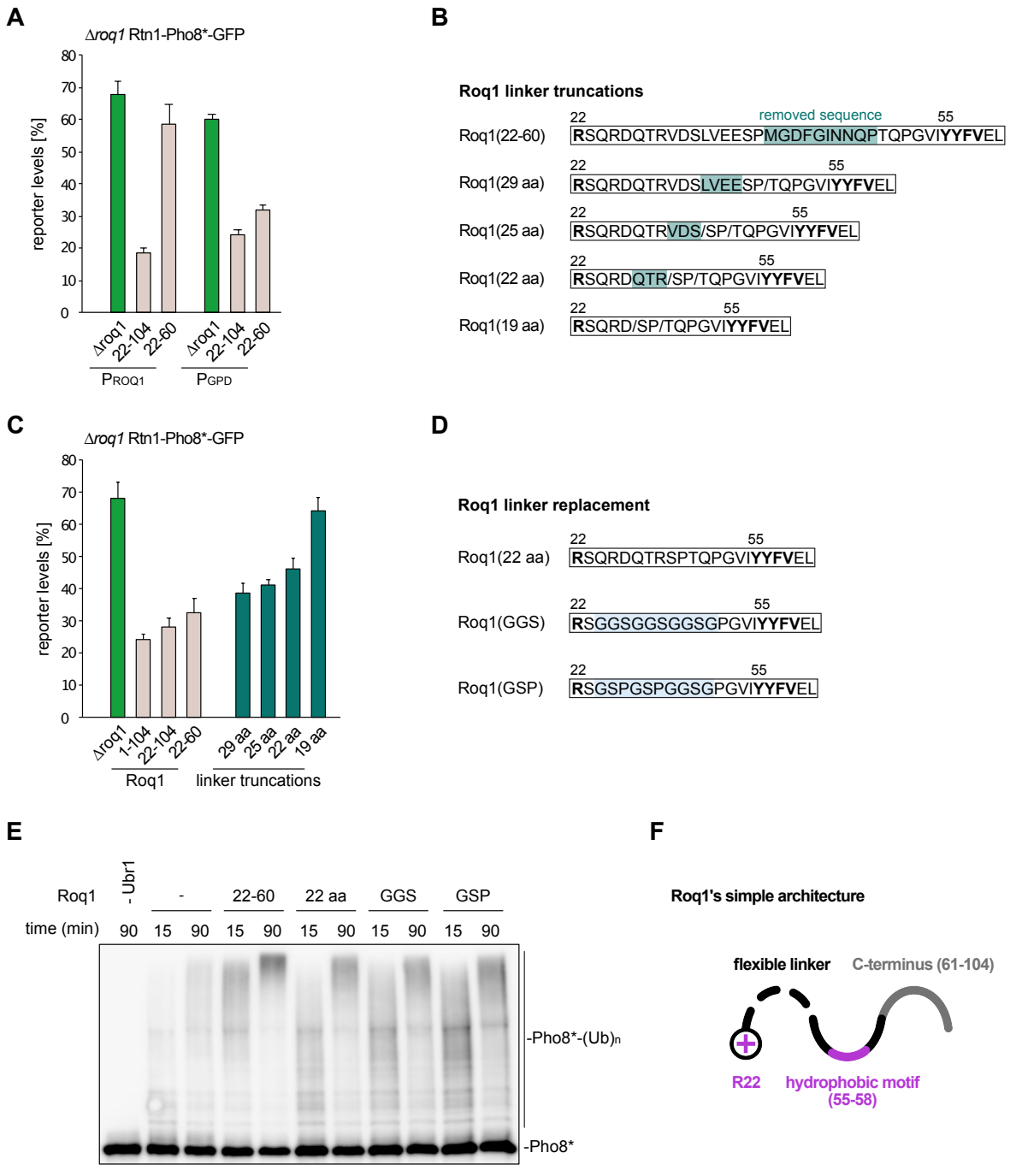

Figure 20: The minimal functional building blocks of Roq1 are R22 and the hydrophobic motif connected by a short linker.

A) Remaining reporter levels after 5 h of tunicamycin treatment measured by flow cytometry. Cells with an empty plasmid (Δroq1) were used as control and different Roq1 wild-type variants were expressed from the endogenous promoter (P_{ROQ1}) or the strong GPD promoter (P_{GPD}). Geometric mean ± SEM, n=3. **B**) Schematic of Roq1 (22-60) sequence and linker truncations highlighted in blue green. **C**) As in A but Roq1 wild-type and variants (linker truncations) were expressed under control of the strong GPD promoter. **D**) Schematic of Roq1 constructs with linker replacements highlighted in blue. GGS = glycine-glycine-serine linker, GSP = glycine-serine-proline linker. **E**) Western blot of Pho8* from ubiquitination assays with Roq1(22-60), Roq1(22 aa), Roq1(GGS) and Roq1(GSP). Reactions were stopped at indicated time points. **F**) Schematic of Roq1 and its minimal building blocks.

4. Discussion

In this work, I discovered that Roq1 reprograms Ubr1 using the hydrophobic motif, in addition to the already known N-terminal R22. By building on Oliver Pajonk's Roq1 mutagenesis screen, I identified the Y55-Y56-F57-V58 sequence in Roq1 as essential for SHRED activity in yeast. Additionally, I showed that this sequence is required to bind Ubr1 at a yet unidentified regulatory site. This interaction then drives the ubiquitination of misfolded proteins but is dispensable for regulating the ubiquitination of N-degron substrates or the natural substrate Cup9 (**Figure 21**). Therefore, Roq1 comprehensively reprograms the substrate specificity of Ubr1. Finally, I was able to dissect Roq1 into its functionally minimally required parts: the N-terminus, a short flexible linker, and the hydrophobic motif.

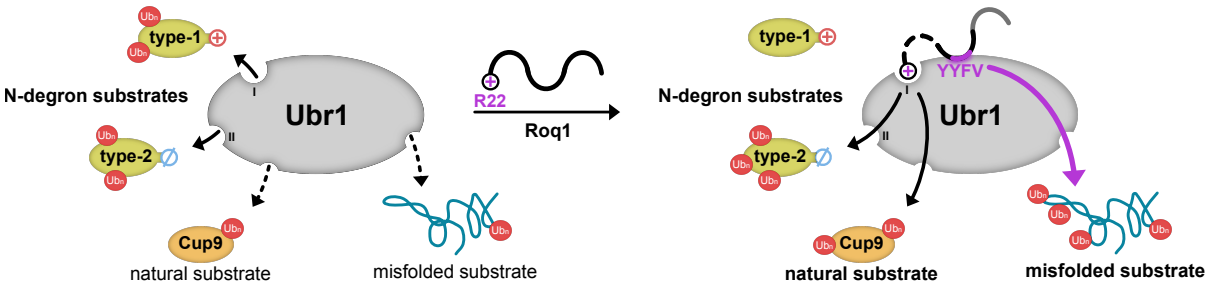

Figure 21: Model of the reprograming of Ubr1 by Roq1.
In the absence of Roq1, Ubr1 binds N-degron substrates by means of its type-1 and type-2 binding site (I + II), which recognizes either basic or bulky destabilizing N-terminal residues. The natural substrate Cup9 with an internal degron and misfolded substrates are also recognized and ubiquitinated by Ubr1. Upon binding of Roq1 to the type-1 binding site with its N-terminal R22, Roq1 inhibits the ubiquitination of type-1 N-degron substrates and promotes the ubiquitination of type-2 N-degron substrates and Cup9. Depending on the hydrophobic motif (YYFV), Roq1 can promote the ubiquitination of misfolded substrates. The architecture of Roq1 is simple: it consists of the N-terminal R22, a flexible linker (dashed line) and the hydrophobic motif (pink). The C-terminus (grey) is not required for Roq1 function in vitro.

4.1 Roq1 reprograms Ubr1 via two SLiMs

The IDP Roq1 governs the substrate specificity of Ubr1 through the use of two functional motifs: R22 at its N-terminus and the hydrophobic motif. The two motifs are short linear motifs (SLiMs) which generally can serve various functions, including as regulatory modules, proteolytic cleavage sites, sites for post-translational modification or degrons (Davey et al., 2012; Kumar et al., 2024; Van Roey et al., 2014). Roq1 binds Ubr1 via its two SLiMs as they each make physical contact with Ubr1 at different sites with individual affinities. These affinities and the bivalency together create avidity, enhancing the overall binding strength of Roq1 and Ubr1.

This may be necessary to allow Roq1 to compete with other substrates for the same binding site, the type-1 site on Ubr1, and inhibit their binding. With R22 only one single amino acid is sufficient for binding to the type-1 site. This site is very shallow and acidic and can only accommodate one residue. However, the nature of the residue at the second position has been shown to be also relevant for recognition. This residue extends into a hydrophobic pocket of the type-1 site, which preferably accommodates hydrophobic residues, but also basic and acidic residues, providing structural plasticity (Choi et al., 2010). Roq1 has a serine (S23) at position two. Supposedly, the hydrophobic motif is required to further stabilize the binding of R22 by binding to a second site in Ubr1, thereby supporting Roq1 in outcompeting regular type-1 N-degron substrates. Type-1 and type-2 peptides have both been shown to bind Ubr1 with a binding affinity (K_D) of 1 µM (Du et al., 2002). Thus, Roq1 probably has an overall K_D lower than 1 µM.

The two SLiMs of Roq1 are connected by a short flexible linker, with 15 residues being sufficient for function. The linker can be replaced by generic sequences without losing Roq1 function. Possibly, an even shorter linker might still support Roq1 function in vitro. In vivo though, a linker shorter than 15 residues led to a severe SHRED defect, possibly caused by destabilizing effects. In general, the linker may regulate the distance Roq1 can span on the Ubr1 surface after docking to the type-1 site via R22. Ubr1(1-1950 aa) measures about 12 nm x 12 nm x 6.5 nm (Pan et al., 2021). Considering that the distance from one Cα in the backbone to the next is 3.8 Å, even the small Roq1(22 aa) could still span a distance of 5.7 nm with a fully extended linker (Chakraborty et al., 2013). In theory, this enables the hydrophobic motif of Roq1(22 aa) to still cover far distances on Ubr1.

4.1.1 Multifunctionality of the SLiMs

The two SLiMs of Roq1 cooperate in binding Ubr1 but are also both multifunctional. The first SLiM of Roq1 is the Ynm3 cleavage site (IL**R**SQR), which leads to the final exposure of **R22**. This SLiM is both a cleavage site and, after cleavage, a ligand for the Ubr1 type-1 site. The second SLiM of Roq1 is the hydrophobic motif (YYFV). Importantly, I cannot exclude that neighboring residues might still contribute to Roq1 function. However, this SLiM is involved in Ubr1 binding and stability of Roq1. When residues in this sequence were changed to negatively charged residues, Roq1 was stabilized in cells suggesting that this motif may also function as a degron. Due to the unstructured nature of Roq1, the hydrophobic motif is constantly exposed and highly accessible. In addition, Roq1 is known to have a short half-life

of about five minutes, which is important to rapidly shut down SHRED activity in cells once stress subsides. In line with this, Ubr1 has been shown to play a minor role in targeting Roq1 for degradation in yeast (Szoradi et al., 2018).

4.1.2 Roq1 with a mutated hydrophobic motif impairs ubiquitination of misfolded substrates

The hydrophobic motif is required to promote misfolded substrate ubiquitination by Ubr1. Mutation of the motif resulted in only partial activation (unfolded Luciferase) or even inhibition of ubiquitination (Pho8*), depending on the substrate. Such mutations were substitutions to a glutamic acid (Roq1(V58E)) and the lack of the hydrophobic motif (Roq1(4A)). The two mutants differ in their ability of binding Ubr1. While the 4A mutation substantially reduces binding to Ubr1, the V58E mutation retains most of Roq1's Ubr1 binding ability. Consistently, changing the residues 55-57 to a charged residue also inhibited Pho8* ubiquitination (data not shown) but, unlike V58E, also binding to Ubr1 was substantially compromised (**Figure 12A**).

Roq1 is largely disordered, apart from a hydrophobic stretch in the middle of its sequence, where the hydrophobic motif is located. A polar mutation in this motif might further increase the disorder, as suggested by computational disorder predictions. Consequently, Roq1(V58E) may have a higher degree of flexibility. In general, hydrogen bonds and electrostatic interactions play a role in the formation of the initiation complex of Ubr1 with Rad6~Ub (Pan et al., 2021). It may be the case that surface-exposed polar charges in the hydrophobic motif enable Roq1(V58E) to interfere with this process. However, only the ubiquitin transfer to misfolded substrates was inhibited and not to type-2 N-degron substrates or Cup9. This may indicate that the closed conformation of Rad6~Ub on Ubr1 was not constrained. It may be more likely that the recognition or positioning of misfolded substrates for ubiquitination is altered, leading to an inhibition of Pho8* ubiquitination and only a partial activation of unfolded Luciferase ubiquitination. This suggests that the binding site for misfolded proteins is separate from those of Cup9 or the type-2 N-degron substrate. In line with this, it has been shown that disruption of the type-2 site had no impact on SHRED activity in yeast (Szoradi et al., 2018).

For Roq1(4A) AlphaFold3 predicts a denser structure which may sterically interfere with the ubiquitin transfer or binding of misfolded substrates (**Figure 22**). In general, the inhibition of substrate ubiquitination by Roq1(4A)/(V58E) could also be an artifact due to the high

concentrations used in ubiquitination assays. Possibly, these Roq1 mutants bind to other proteins in the assay and thereby manipulate the ubiquitination reaction.

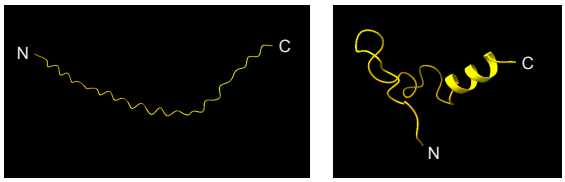

Figure 22: AlphaFold3 structure predictions of Roq1.
Roq1(22-60)(WT) and (4A) with labelled N-termini are shown in comparison. Predicted structures were analyzed using UCSF ChimeraX (Abramson et al., 2024; Meng et al., 2023). 4A = Y55A/Y56A/F57A/V58A.

Previous attempts to inactivate Ubr1 as N-recognin involve the use of a synthetic heterovalent inhibitor called RF-C11. This compound carries either an arginine or a phenylalanine at both its N- and C-terminal ends, thereby binding simultaneously to both the type-1 and the type-2 site of Ubr1. Treatment with this compound was shown to inhibit cardiac proliferation and hypertrophy in cultured cardiomyocytes (Lee et al., 2008). Intriguingly, Roq1 with a mutation of the hydrophobic motif also inactivates Ubr1 in a substrate-specific manner regarding misfolded substrates. Unlike RF-C11, Roq1(4A) only uses one binding site (type-1) and possible steric features to prevent substrate ubiquitination by Ubr1.

4.2 The Ubr1 reprograming mechanism by Roq1

It remains unclear how exactly Roq1 promotes ubiquitination of misfolded substrates by Ubr1 through its hydrophobic motif. Roq1 is unlikely to promote the recruitment of Rad6 or the misfolded substrate Pho8* to Ubr1. Rather, it stimulates chain initiation on Pho8* and therefore also chain elongation. In addition, more substrate lysines become available for ubiquitination by Ubr1. It is unlikely, that Ubr1 alone can achieve since this would require a longer incubation than with Roq1 (>90 min), which presumably is not physiological-relevant.

Roq1 does not appear to share the properties of an E4 enzyme that merely acts as an additional conjugation factor to promote chain elongation (Koegl et al., 1999). Instead, Roq1 seems to exert a more complex regulatory effect. The following scenarios how Roq1 could regulate Ubr1 are possible: Roq1 might allosterically regulate Ubr1. This means that Roq1 binding induces structural rearrangements within Ubr1 to optimally position either Rad6~Ub, the misfolded substrate, or both for more efficient ubiquitin transfer. Similarly, the ubiquitin-like molecule Nedd8 facilitates ubiquitin transfer by cullin-RING ligases (Baek et al., 2021; Saha &

Deshaies, 2008). Roq1 could also stabilize the closed conformation of Rad6~Ub upon binding to Ubr1. This would facilitate the nucleophilic attack of the substrate lysine on the C-terminus of ubiquitin and therefore the ubiquitin transfer to the substrate. To access more lysine residues, Roq1 may also increase the overall flexibility of Ubr1.

Moreover, the suggested allosteric regulation by Roq1 is also in line with the regulation of Cup9 degradation by Ubr1. Through synergistic binding of dipeptides to the type-1 and type-2 site, Ubr1 was shown to be released from autoinhibition and this uncovers the Cup9-binding site (Du et al., 2002). As well, Roq1 could lead to the release or the formation of a putative fourth substrate binding site on Ubr1. Like a natural molecular glue, Roq1 may build a new substrate-binding site on Ubr1 for *neo*-substrates (Ramachandran & Ciulli, 2021). Possibly, Roq1 may rearrange the conformation of Ubr1 such that a new substrate binding pocket for misfolded proteins is created to enhance their ubiquitination. Alternatively, Roq1 could itself be part of this pocket. However, the latter would indicate a direct interaction of Roq1 with the substrate, which Niklas Peters could not confirm in pulldown experiments.

To finally solve this puzzle, it will be fundamental to obtain the structure of the Roq1-Ubr1 complex with and without substrate. This would help to determine where the hydrophobic motif binds Ubr1 and whether this induces structural changes in Ubr1. During this project Niklas Peters had isolated the Roq1-Ubr1 complex and tried to obtain a cryo-EM structure in collaboration with Dirk Flemming from BZH. Unfortunately, they were only able to obtain low resolution data. Presumably, due to the dynamic nature of intrinsically disordered proteins, NMR would be a suitable technique (Kosol et al., 2013). It is also unknown whether Roq1 folds upon binding to Ubr1 or if it forms fuzzy complexes with R22 locked into the type-1 binding groove (Tompa & Fuxreiter, 2008). We also asked AlphaFold3 (Varadi et al., 2024) to predict other Roq1 binding sites in Ubr1 but we could not confirm these predictions in vivo (data not shown).

4.2.1 SHRED regulation in cells

The Roq1-mediated regulation of Ubr1 in vitro became clearer due to this work. However, how this translates in vivo yet remains a mystery. The SHRED-mechanism is solely based on an artificial substrate in vivo - Rtn1-Pho8*-GFP (Szoradi et al., 2018). Thus, the physiological role of SHRED is still unclear. Prior to this study, several attempts have been made to identify endogenous SHRED substrates in vivo. Ultimately, only one protein was common to all

approaches and therefore the most promising candidate: Sfa1, an alcohol dehydrogenase. In this study, I also purified Sfa1 and tested it as a substrate in ubiquitination assays. However, Sfa1 was not ubiquitinated by Ubr1 in vitro (data not shown). This raises the question of whether endogenous SHRED substrates are modified or spontaneously misfold upon stress in yeast. Consequently, only the misfolded pool of proteins would then be targeted by SHRED. In vivo degradation assays with Sfa1 and other candidates would help to understand this better. We also showed that Ubr1-mediated ubiquitination of Cup9 is promoted by Roq1 in vitro. Yet, in yeast, Roq1 has been shown to suppress Cup9 degradation (Szoradi et al., 2018). This discrepancy could be explained by the fact that in yeast many substrates are present at the same time. There may be a preference that is then dictated by Roq1. Anyways, it seems likely that Cup9 and misfolded substrates do not share the same binding site, since Roq1 binding has different effects on the two substrate categories. In general, it is possible that there are still other factors at the cellular level that regulate SHRED. The fact that Roq1 overexpression in cells triggers SHRED, however to a lesser extent than stress treatment, provides further evidence for this (Szoradi et al., 2018). It also remains unclear how cells shut down SHRED activity, and how the lysine-free Roq1(22-104) is degraded. My data suggests that the hydrophobic motif also serves as a degron in cells. However, it is yet unclear which E3 ligases are involved in Roq1 degradation. We have seen that Roq1(22-104) is also ubiquitinated in vivo implicating that Roq1 must be ubiquitinated in a lysine-independent manner (Kelsall, 2022) (Rafael Salazar, unpublished results). Generally, most IDPs are subject to the proteasome directly, without the requirement of ubiquitin (Guharoy et al., 2018). Moreover, Western blot analyses of Roq1 revealed that Roq1 frequently appears as two bands, suggesting a modification of Roq1 in vivo. It remains speculative whether this modification is relevant for SHRED in vivo. To conclude, SHRED and the reprograming of Ubr1 in cells is likely more complex than we have yet understood.

Moreover, it remains speculative whether the mechanism by which Roq1 controls Ubr1 is conserved. Ubr1 has a mammalian sequence homolog, Roq1 does not (Tasaki & Kwon, 2007). This is not surprising given the disorder of the protein, but it is possible that Roq1 has functional homologs in mammalian cells. A first step might be to test whether Roq1 can also regulate human Ubr1 in vitro.

4.2.2 Similar regulatory mechanisms

Roq1 reprograms Ubr1 via two cooperating motifs. In general, the reprograming of E3 ligases by small molecules has also been observed in other contexts and is known by the term degron mimicry. To drive infection, viruses have developed strategies to infect cells by hijacking the host UPS. One example is the viral protein ORF10 (38 aa), which causes the loss of motile cilia in the respiratory tract during a SARS-CoV-2 infection. It promotes the degradation of ciliary proteins by interacting with the E3 ligase adaptor ZYG11B of the Cul2-ElonginBC E3 ligase complex (Fonseca & Chakrabarti, 2022). Typically, $Cul2^{ZYG11B}$ recognizes its substrates via N-terminal glycine degrons (Gly/N-degrons) and ubiquitinates them for subsequent proteasomal degradation (Eldeeb et al., 2019; Timms et al., 2019). ORF10 has an N-terminal glycine residue that mimics a Gly/N-degron. Through its N-terminus ORF10 binds to $Cul2^{ZYG11B}$ and prevents the binding of target substrates while promoting the turnover of IFT46, a ciliary protein (Wang et al., 2022; Zhu et al., 2024). This mechanism is very similar to how Roq1 reprograms Ubr1 through its N-terminus and leads to the characteristic symptoms of COVID-19.

Moreover, the mechanism by which Roq1 controls Ubr1 has similarities to the regulation of inhibitors of apoptosis (IAPs) and in particular the baculoviral IAP repeat-containing protein 6 (BIRC6). BIRC6 inhibits apoptosis by binding and ubiquitinating proteolytic caspases. However, when the second mitochondria-derived activator of caspases (SMAC) is released from the mitochondrial intermembrane space it is cleaved and unleashes the proteolytic activity of caspases by binding almost irreversibly to BIRC6. Therefore, small molecule IAP antagonists, called SMAC mimetics, can now be optimized to induce apoptosis in cells (Dietz et al., 2023; Ehrmann et al., 2023; Hunkeler et al., 2023; Mace & Day, 2023). To conclude, Roq1, like SMAC, has a sequence that acts as both a cleavage site and an N-degron mimic.

Another example is the regulation of the human WDR26-CTHLH E3 ligase, where WDR26 is a non-canonical substrate receptor unit of the human C-terminal to LisH (CTLH) E3 (Mohamed et al., 2021). WDR26 binds the substrate and acts as supramolecular assembly factor (Sherpa et al., 2021). The substrate is then recognized through an internal basic motif. Inhibition occurs when the subunit YPEL5 mimics an N-terminal basic degron, blocking substrate binding, similar to how Roq1 outcompetes N-degron substrates (Gottemukkala et al., 2024).

Notably, Roq1 is the first intrinsically disordered protein described to regulate an E3 ligase, whereas ORF10, SMAC and YPEL5 rely on folded domains for their regulatory roles.

In conclusion, I showed that Roq1, even though only composed of a small number of building blocks, has a fundamental role by reprograming the E3 ligase Ubr1. With the emerging field of degradation-based therapeutics using PROTACS or molecular glues it may be possible to design other E3 ligase regulators inspired by the architecture of Roq1. Especially N-recognins, like Ubr1, which recognize single amino acids as a degradation signal, are very attractive targets for small molecule regulators.

5. Acknowledgements

In the beginning I would like to thank Sebastian for giving me the opportunity to be on one member of the SHRED team. Thank you for your supervision, your support and patience throughout my entire journey as a PhD student in your lab. Next, I would like to thank my TAC members, Frauke, Walter (and Claudio) for their expertise and their interest in my project. And many thanks to Tamas for initiating this great project!

A huge THANK YOU goes to the Schookees, past and present members, for contributing to a nice lab atmosphere and giving both scientific & moral support. Thank you, Lis(zard), Niklas, Giulia, Petra, Dimitris, Oli, Rolf, Jasmin, Aye, Klara, Natalie, Anna, Inge, Anke and Sneha. Special thanks to Rafael, who was such a talented master student. And many thanks go to Niklas, the other half of the SHRED team. You really shredded all out of SHRED. Thank you for being my lab mate and for your expertise, fruitful discussions, and support throughout.

I want to thank the people behind the scenes: the people from the *Spülküche* and the past and present ZMBH and BZH members for sharing reagents, giving technical advice, having spontaneous chats or coffee breaks – especially to the entertainers Matteo and Merlin from the 5th floor.

Another enormous THANK YOU goes to my flatmates and my friends. Especially, Sabi and Lene who were always by my side and believed in me even though they did not fully understand what exactly I was doing. I also want to thank Henrik, who chose to be part of my life during very stressful times. Finally, also many thanks to my parents and my sister.

6. References

Abramson, J., Adler, J., Dunger, J., Evans, R., Green, T., Pritzel, A., Ronneberger, O., Willmore, L., Ballard, A. J., Bambrick, J., Bodenstein, S. W., Evans, D. A., Hung, C. C., O'Neill, M., Reiman, D., Tunyasuvunakool, K., Wu, Z., Zemgulyte, A., Arvaniti, E., . . . Jumper, J. M. (2024). Accurate structure prediction of biomolecular interactions with AlphaFold 3. *Nature*, *630*(8016), 493-500. https://doi.org/10.1038/s41586-024-07487-w

An, J. Y., Seo, J. W., Tasaki, T., Lee, M. J., Varshavsky, A., & Kwon, Y. T. (2006). Impaired neurogenesis and cardiovascular development in mice lacking the E3 ubiquitin ligases UBR1 and UBR2 of the N-end rule pathway. *Proc Natl Acad Sci U S A*, *103*(16), 6212-6217. https://doi.org/10.1073/pnas.0601700103

Andreasson, C., Fiaux, J., Rampelt, H., Mayer, M. P., & Bukau, B. (2008). Hsp110 is a nucleotide-activated exchange factor for Hsp70. *J Biol Chem*, *283*(14), 8877-8884. https://doi.org/10.1074/jbc.M710063200

Aoki, D., Awazu, A., Fujii, M., Uewaki, J. I., Hashimoto, M., Tochio, N., Umehara, T., & Tate, S. I. (2020). Ultrasensitive Change in Nucleosome Binding by Multiple Phosphorylations to the Intrinsically Disordered Region of the Histone Chaperone FACT. *J Mol Biol*, *432*(16), 4637-4657. https://doi.org/10.1016/j.jmb.2020.06.011

Arai, M., Sugase, K., Dyson, H. J., & Wright, P. E. (2015). Conformational propensities of intrinsically disordered proteins influence the mechanism of binding and folding. *Proc Natl Acad Sci U S A*, *112*(31), 9614-9619. https://doi.org/10.1073/pnas.1512799112

Baek, K., Krist, D. T., Prabu, J. R., Hill, S., Klugel, M., Neumaier, L. M., von Gronau, S., Kleiger, G., & Schulman, B. A. (2020). NEDD8 nucleates a multivalent cullin-RING-UBE2D ubiquitin ligation assembly. *Nature*, *578*(7795), 461-466. https://doi.org/10.1038/s41586-020-2000-y

Baek, K., Scott, D. C., & Schulman, B. A. (2021). NEDD8 and ubiquitin ligation by cullin-RING E3 ligases. *Curr Opin Struct Biol*, *67*, 101-109. https://doi.org/10.1016/j.sbi.2020.10.007

Balaji, V., & Hoppe, T. (2020). Regulation of E3 ubiquitin ligases by homotypic and heterotypic assembly. *F1000Res*, *9*. https://doi.org/10.12688/f1000research.21253.1

Balchin, D., Hayer-Hartl, M., & Hartl, F. U. (2016). In vivo aspects of protein folding and quality control. *Science*, *353*(6294), aac4354. https://doi.org/10.1126/science.aac4354

Battaglia, M., Olvera-Carrillo, Y., Garciarrubio, A., Campos, F., & Covarrubias, A. A. (2008). The enigmatic LEA proteins and other hydrophilins. *Plant Physiol*, *148*(1), 6-24. https://doi.org/10.1104/pp.108.120725

Berlow, R. B., Dyson, H. J., & Wright, P. E. (2022). Multivalency enables unidirectional switch-like competition between intrinsically disordered proteins. *Proc Natl Acad Sci U S A*, *119*(3). https://doi.org/10.1073/pnas.2117338119

Brower, C. S., & Varshavsky, A. (2009). Ablation of arginylation in the mouse N-end rule pathway: loss of fat, higher metabolic rate, damaged spermatogenesis, and neurological perturbations. *PLoS One*, *4*(11), e7757. https://doi.org/10.1371/journal.pone.0007757

Brzovic, P. S., Rajagopal, P., Hoyt, D. W., King, M. C., & Klevit, R. E. (2001). Structure of a BRCA1-BARD1 heterodimeric RING-RING complex. *Nat Struct Biol*, *8*(10), 833-837. https://doi.org/10.1038/nsb1001-833

Buchberger, A., Bukau, B., & Sommer, T. (2010). Protein quality control in the cytosol and the endoplasmic reticulum: brothers in arms. *Mol Cell*, *40*(2), 238-252. https://doi.org/10.1016/j.molcel.2010.10.001

Buetow, L., & Huang, D. T. (2016). Structural insights into the catalysis and regulation of E3 ubiquitin ligases. *Nat Rev Mol Cell Biol*, *17*(10), 626-642. https://doi.org/10.1038/nrm.2016.91

Bulatov, E., & Ciulli, A. (2015). Targeting Cullin-RING E3 ubiquitin ligases for drug discovery: structure, assembly and small-molecule modulation. *Biochem J*, *467*(3), 365-386. https://doi.org/10.1042/BJ20141450

Byrd, C., Turner, G. C., & Varshavsky, A. (1998). The N-end rule pathway controls the import of peptides through degradation of a transcriptional repressor. *EMBO J*, *17*(1), 269-277. https://doi.org/10.1093/emboj/17.1.269

Cai, H., Kauffman, S., Naider, F., & Becker, J. M. (2006). Genomewide screen reveals a wide regulatory network for di/tripeptide utilization in Saccharomyces cerevisiae. *Genetics*, *172*(3), 1459-1476. https://doi.org/10.1534/genetics.105.053041

Cenciarelli, C., Chiaur, D. S., Guardavaccaro, D., Parks, W., Vidal, M., & Pagano, M. (1999). Identification of a family of human F-box proteins. *Curr Biol*, *9*(20), 1177-1179. https://doi.org/10.1016/S0960-9822(00)80020-2

Cermakova, K., & Hodges, H. C. (2023). Interaction modules that impart specificity to disordered protein. *Trends Biochem Sci*, *48*(5), 477-490. https://doi.org/10.1016/j.tibs.2023.01.004

Chakraborty, S., Venkatramani, R., Rao, B. J., Asgeirsson, B., & Dandekar, A. M. (2013). Protein structure quality assessment based on the distance profiles of consecutive backbone Calpha atoms. *F1000Res*, *2*, 211. https://doi.org/10.12688/f1000research.2-211.v3

Chaugule, V. K., Burchell, L., Barber, K. R., Sidhu, A., Leslie, S. J., Shaw, G. S., & Walden, H. (2011). Autoregulation of Parkin activity through its ubiquitin-like domain. *EMBO J*, *30*(14), 2853-2867. https://doi.org/10.1038/emboj.2011.204

Chen, B., Retzlaff, M., Roos, T., & Frydman, J. (2011). Cellular strategies of protein quality control. *Cold Spring Harb Perspect Biol*, *3*(8), a004374. https://doi.org/10.1101/cshperspect.a004374

Chiti, F., & Dobson, C. M. (2006). Protein misfolding, functional amyloid, and human disease. *Annu Rev Biochem*, *75*, 333-366. https://doi.org/10.1146/annurev.biochem.75.101304.123901

Choi, W. S., Jeong, B. C., Joo, Y. J., Lee, M. R., Kim, J., Eck, M. J., & Song, H. K. (2010). Structural basis for the recognition of N-end rule substrates by the UBR box of ubiquitin ligases. *Nat Struct Mol Biol*, *17*(10), 1175-1181. https://doi.org/10.1038/nsmb.1907

Ciechanover, A. (1994). The ubiquitin-mediated proteolytic pathway: mechanisms of action and cellular physiology. *Biol Chem Hoppe Seyler*, *375*(9), 565-581. https://doi.org/10.1515/bchm3.1994.375.9.565

Ciechanover, A., & Schwartz, A. L. (1998). The ubiquitin-proteasome pathway: the complexity and myriad functions of proteins death. *Proc Natl Acad Sci U S A*, *95*(6), 2727-2730. https://doi.org/10.1073/pnas.95.6.2727

Cook, W. J., Martin, P. D., Edwards, B. F., Yamazaki, R. K., & Chau, V. (1997). Crystal structure of a class I ubiquitin conjugating enzyme (Ubc7) from Saccharomyces cerevisiae at 2.9 angstroms resolution. *Biochemistry*, *36*(7), 1621-1627. https://doi.org/10.1021/bi962639e

Cotton, T. R., & Lechtenberg, B. C. (2020). Chain reactions: molecular mechanisms of RBR ubiquitin ligases. *Biochem Soc Trans*, *48*(4), 1737-1750. https://doi.org/10.1042/BST20200237

Cowan, A. D., & Ciulli, A. (2022). Driving E3 Ligase Substrate Specificity for Targeted Protein Degradation: Lessons from Nature and the Laboratory. *Annu Rev Biochem*, *91*, 295-319. https://doi.org/10.1146/annurev-biochem-032620-104421

Dang, N. X., & Hincha, D. K. (2011). Identification of two hydrophilins that contribute to the desiccation and freezing tolerance of yeast (Saccharomyces cerevisiae) cells. *Cryobiology*, *62*(3), 188-193. https://doi.org/10.1016/j.cryobiol.2011.03.002

Davey, N. E., Cyert, M. S., & Moses, A. M. (2015). Short linear motifs - ex nihilo evolution of protein regulation. *Cell Commun Signal*, *13*, 43. https://doi.org/10.1186/s12964-015-0120-z

Davey, N. E., Van Roey, K., Weatheritt, R. J., Toedt, G., Uyar, B., Altenberg, B., Budd, A., Diella, F., Dinkel, H., & Gibson, T. J. (2012). Attributes of short linear motifs. *Mol Biosyst*, *8*(1), 268-281. https://doi.org/10.1039/c1mb05231d

Deshaies, R. J., & Joazeiro, C. A. (2009). RING domain E3 ubiquitin ligases. *Annu Rev Biochem*, *78*, 399-434. https://doi.org/10.1146/annurev.biochem.78.101807.093809

Dietz, L., Ellison, C. J., Riechmann, C., Cassidy, C. K., Felfoldi, F. D., Pinto-Fernandez, A., Kessler, B. M., & Elliott, P. R. (2023). Structural basis for SMAC-mediated antagonism of caspase inhibition by the giant ubiquitin ligase BIRC6. *Science*, *379*(6637), 1112-1117. https://doi.org/10.1126/science.ade8840

Dingwall, C., & Laskey, R. A. (1991). Nuclear targeting sequences--a consensus? *Trends Biochem Sci*, *16*(12), 478-481. https://doi.org/10.1016/0968-0004(91)90184-w

Dissmeyer, N., Rivas, S., & Graciet, E. (2018). Life and death of proteins after protease cleavage: protein degradation by the N-end rule pathway. *New Phytol*, *218*(3), 929-935. https://doi.org/10.1111/nph.14619

Dou, H., Buetow, L., Hock, A., Sibbet, G. J., Vousden, K. H., & Huang, D. T. (2012). Structural basis for autoinhibition and phosphorylation-dependent activation of c-Cbl. *Nat Struct Mol Biol*, *19*(2), 184-192. https://doi.org/10.1038/nsmb.2231

Du, F., Navarro-Garcia, F., Xia, Z., Tasaki, T., & Varshavsky, A. (2002). Pairs of dipeptides synergistically activate the binding of substrate by ubiquitin ligase through dissociation of its autoinhibitory domain. *Proc Natl Acad Sci U S A*, *99*(22), 14110-14115. https://doi.org/10.1073/pnas.172527399

Dubiel, W., & Gordon, C. (1999). Ubiquitin pathway: another link in the polyubiquitin chain? *Curr Biol*, *9*(15), R554-557. https://doi.org/10.1016/s0960-9822(99)80353-4

Duda, D. M., Borg, L. A., Scott, D. C., Hunt, H. W., Hammel, M., & Schulman, B. A. (2008). Structural insights into NEDD8 activation of cullin-RING ligases: conformational control of conjugation. *Cell*, *134*(6), 995-1006. https://doi.org/10.1016/j.cell.2008.07.022

Dyson, H. J., & Wright, P. E. (2005). Intrinsically unstructured proteins and their functions. *Nat Rev Mol Cell Biol*, *6*(3), 197-208. https://doi.org/10.1038/nrm1589

Ehrmann, J. F., Grabarczyk, D. B., Heinke, M., Deszcz, L., Kurzbauer, R., Hudecz, O., Shulkina, A., Gogova, R., Meinhart, A., Versteeg, G. A., & Clausen, T. (2023). Structural basis for regulation of apoptosis and autophagy by the BIRC6/SMAC complex. *Science*, *379*(6637), 1117-1123. https://doi.org/10.1126/science.ade8873

Eisele, F., & Wolf, D. H. (2008). Degradation of misfolded protein in the cytoplasm is mediated by the ubiquitin ligase Ubr1. *FEBS Lett*, *582*(30), 4143-4146. https://doi.org/10.1016/j.febslet.2008.11.015

Eldeeb, M., Esmaili, M., & Fahlman, R. (2019). Degradation of proteins with N-terminal glycine. *Nat Struct Mol Biol*, *26*(9), 761-763. https://doi.org/10.1038/s41594-019-0291-1

Eldeeb, M. A., Leitao, L. C. A., & Fahlman, R. P. (2018). Emerging branches of the N-end rule pathways are revealing the sequence complexities of N-termini dependent protein degradation. *Biochem Cell Biol*, *96*(3), 289-294. https://doi.org/10.1139/bcb-2017-0274

Feltham, R., Bettjeman, B., Budhidarmo, R., Mace, P. D., Shirley, S., Condon, S. M., Chunduru, S. K., McKinlay, M. A., Vaux, D. L., Silke, J., & Day, C. L. (2011). Smac mimetics activate the E3 ligase activity of cIAP1 protein by promoting RING domain dimerization. *J Biol Chem*, *286*(19), 17015-17028. https://doi.org/10.1074/jbc.M111.222919

Finley, D. (2009). Recognition and processing of ubiquitin-protein conjugates by the proteasome. *Annu Rev Biochem*, *78*, 477-513. https://doi.org/10.1146/annurev.biochem.78.081507.101607

Finley, D., Chen, X., & Walters, K. J. (2016). Gates, Channels, and Switches: Elements of the Proteasome Machine. *Trends Biochem Sci*, *41*(1), 77-93. https://doi.org/10.1016/j.tibs.2015.10.009

Fischer, E. S., Bohm, K., Lydeard, J. R., Yang, H., Stadler, M. B., Cavadini, S., Nagel, J., Serluca, F., Acker, V., Lingaraju, G. M., Tichkule, R. B., Schebesta, M., Forrester, W. C., Schirle, M., Hassiepen, U., Ottl, J., Hild, M., Beckwith, R. E., Harper, J. W., . . . Thoma, N. H. (2014). Structure of the DDB1-CRBN E3 ubiquitin ligase in complex with thalidomide. *Nature*, *512*(7512), 49-53. https://doi.org/10.1038/nature13527

Fonseca, B. F., & Chakrabarti, L. A. (2022). A close shave: How SARS-CoV-2 induces the loss of cilia. *J Cell Biol*, *221*(7). https://doi.org/10.1083/jcb.202206023

Forster, F., Lasker, K., Nickell, S., Sali, A., & Baumeister, W. (2010). Toward an integrated structural model of the 26S proteasome. *Mol Cell Proteomics*, *9*(8), 1666-1677. https://doi.org/10.1074/mcp.R000002-MCP201

Fredrickson, E. K., & Gardner, R. G. (2012). Selective destruction of abnormal proteins by ubiquitin-mediated protein quality control degradation. *Semin Cell Dev Biol*, *23*(5), 530-537. https://doi.org/10.1016/j.semcdb.2011.12.006

Fredrickson, E. K., Rosenbaum, J. C., Locke, M. N., Milac, T. I., & Gardner, R. G. (2011). Exposed hydrophobicity is a key determinant of nuclear quality control degradation. *Mol Biol Cell*, *22*(13), 2384-2395. https://doi.org/10.1091/mbc.E11-03-0256

Giangreco, G., Malabarba, M. G., & Sigismund, S. (2021). Specialised endocytic proteins regulate diverse internalisation mechanisms and signalling outputs in physiology and cancer. *Biol Cell*, *113*(4), 165-182. https://doi.org/10.1111/boc.202000129

Gibson, D. G. (2011). Enzymatic assembly of overlapping DNA fragments. *Methods Enzymol*, *498*, 349-361. https://doi.org/10.1016/B978-0-12-385120-8.00015-2

Glickman, M. H., & Ciechanover, A. (2002). The ubiquitin-proteasome proteolytic pathway: destruction for the sake of construction. *Physiol Rev*, *82*(2), 373-428. https://doi.org/10.1152/physrev.00027.2001

Gottemukkala, K. V., Chrustowicz, J., Sherpa, D., Sepic, S., Vu, D. T., Karayel, O., Papadopoulou, E. C., Gross, A., Schorpp, K., von Gronau, S., Hadian, K., Murray, P. J., Mann, M., Schulman, B. A., & Alpi, A. F. (2024). Non-canonical substrate

recognition by the human WDR26-CTLH E3 ligase regulates prodrug metabolism. *Mol Cell*, *84*(10), 1948-1963 e1911. https://doi.org/10.1016/j.molcel.2024.04.014

Grabbe, C., & Dikic, I. (2009). Functional roles of ubiquitin-like domain (ULD) and ubiquitin-binding domain (UBD) containing proteins. *Chem Rev*, *109*(4), 1481-1494. https://doi.org/10.1021/cr800413p

Guharoy, M., Lazar, T., & Tompa, P. (2018). Disordered Substrates of the 20S Proteasome Link Degradation with Phase Separation. *Proteomics*, *18*(21-22), e1800276. https://doi.org/10.1002/pmic.201800276

Heck, J. W., Cheung, S. K., & Hampton, R. Y. (2010). Cytoplasmic protein quality control degradation mediated by parallel actions of the E3 ubiquitin ligases Ubr1 and San1. *Proc Natl Acad Sci U S A*, *107*(3), 1106-1111. https://doi.org/10.1073/pnas.0910591107

Hershko, A., & Ciechanover, A. (1998). The ubiquitin system. *Annu Rev Biochem*, *67*, 425-479. https://doi.org/10.1146/annurev.biochem.67.1.425

Hicke, L., Schubert, H. L., & Hill, C. P. (2005). Ubiquitin-binding domains. *Nat Rev Mol Cell Biol*, *6*(8), 610-621. https://doi.org/10.1038/nrm1701

Hochstrasser, M. (1995). Ubiquitin, proteasomes, and the regulation of intracellular protein degradation. *Curr Opin Cell Biol*, *7*(2), 215-223. https://doi.org/10.1016/0955-0674(95)80031-x

Hochstrasser, M. (1996). Protein degradation or regulation: Ub the judge. *Cell*, *84*(6), 813-815. https://doi.org/10.1016/s0092-8674(00)81058-2

Holehouse, A. S., & Kragelund, B. B. (2024). The molecular basis for cellular function of intrinsically disordered protein regions. *Nat Rev Mol Cell Biol*, *25*(3), 187-211. https://doi.org/10.1038/s41580-023-00673-0

Hoppe, T. (2005). Multiubiquitylation by E4 enzymes: 'one size' doesn't fit all. *Trends Biochem Sci*, *30*(4), 183-187. https://doi.org/10.1016/j.tibs.2005.02.004

Hunkeler, M., Jin, C. Y., & Fischer, E. S. (2023). Structures of BIRC6-client complexes provide a mechanism of SMAC-mediated release of caspases. *Science*, *379*(6637), 1105-1111. https://doi.org/10.1126/science.ade5750

Hwang, C. S., Shemorry, A., Auerbach, D., & Varshavsky, A. (2010). The N-end rule pathway is mediated by a complex of the RING-type Ubr1 and HECT-type Ufd4 ubiquitin ligases. *Nat Cell Biol*, *12*(12), 1177-1185. https://doi.org/10.1038/ncb2121

Hwang, C. S., Shemorry, A., & Varshavsky, A. (2009). Two proteolytic pathways regulate DNA repair by cotargeting the Mgt1 alkylguanine transferase. *Proc Natl Acad Sci U S A*, *106*(7), 2142-2147. https://doi.org/10.1073/pnas.0812316106

Hwang, C. S., & Varshavsky, A. (2008). Regulation of peptide import through phosphorylation of Ubr1, the ubiquitin ligase of the N-end rule pathway. *Proc Natl Acad Sci U S A*, *105*(49), 19188-19193. https://doi.org/10.1073/pnas.0808891105

Ikeda, F., & Dikic, I. (2008). Atypical ubiquitin chains: new molecular signals. 'Protein Modifications: Beyond the Usual Suspects' review series. *EMBO Rep*, *9*(6), 536-542. https://doi.org/10.1038/embor.2008.93

Ishida, T., & Ciulli, A. (2021). E3 Ligase Ligands for PROTACs: How They Were Found and How to Discover New Ones. *SLAS Discov*, *26*(4), 484-502. https://doi.org/10.1177/2472555220965528

Ito, T., Ando, H., Suzuki, T., Ogura, T., Hotta, K., Imamura, Y., Yamaguchi, Y., & Handa, H. (2010). Identification of a primary target of thalidomide teratogenicity. *Science*, *327*(5971), 1345-1350. https://doi.org/10.1126/science.1177319

Itoh, Y., Ishikawa, M., Naito, M., & Hashimoto, Y. (2010). Protein knockdown using methyl bestatin-ligand hybrid molecules: design and synthesis of inducers of ubiquitination-mediated degradation of cellular retinoic acid-binding proteins. *J Am Chem Soc*, *132*(16), 5820-5826. https://doi.org/10.1021/ja100691p

Janke, C., Magiera, M. M., Rathfelder, N., Taxis, C., Reber, S., Maekawa, H., Moreno-Borchart, A., Doenges, G., Schwob, E., Schiebel, E., & Knop, M. (2004). A versatile toolbox for PCR-based tagging of yeast genes: new fluorescent proteins, more markers and promoter substitution cassettes. *Yeast*, *21*(11), 947-962. https://doi.org/10.1002/yea.1142

Jin, J., Cardozo, T., Lovering, R. C., Elledge, S. J., Pagano, M., & Harper, J. W. (2004). Systematic analysis and nomenclature of mammalian F-box proteins. *Genes Dev*, *18*(21), 2573-2580. https://doi.org/10.1101/gad.1255304

Kelsall, I. R. (2022). Non-lysine ubiquitylation: Doing things differently. *Front Mol Biosci*, *9*, 1008175. https://doi.org/10.3389/fmolb.2022.1008175

Koegl, M., Hoppe, T., Schlenker, S., Ulrich, H. D., Mayer, T. U., & Jentsch, S. (1999). A novel ubiquitination factor, E4, is involved in multiubiquitin chain assembly. *Cell*, *96*(5), 635-644. https://doi.org/10.1016/s0092-8674(00)80574-7

Komander, D., & Rape, M. (2012). The ubiquitin code. *Annu Rev Biochem*, *81*, 203-229. https://doi.org/10.1146/annurev-biochem-060310-170328

Kosol, S., Contreras-Martos, S., Cedeno, C., & Tompa, P. (2013). Structural characterization of intrinsically disordered proteins by NMR spectroscopy. *Molecules*, *18*(9), 10802-10828. https://doi.org/10.3390/molecules180910802

Kronke, J., Udeshi, N. D., Narla, A., Grauman, P., Hurst, S. N., McConkey, M., Svinkina, T., Heckl, D., Comer, E., Li, X., Ciarlo, C., Hartman, E., Munshi, N., Schenone, M., Schreiber, S. L., Carr, S. A., & Ebert, B. L. (2014). Lenalidomide causes selective degradation of IKZF1 and IKZF3 in multiple myeloma cells. *Science*, *343*(6168), 301-305. https://doi.org/10.1126/science.1244851

Kumar, M., Gouw, M., Michael, S., Samano-Sanchez, H., Pancsa, R., Glavina, J., Diakogianni, A., Valverde, J. A., Bukirova, D., Calyseva, J., Palopoli, N., Davey, N. E., Chemes, L. B., & Gibson, T. J. (2020). ELM-the eukaryotic linear motif resource in 2020. *Nucleic Acids Res*, *48*(D1), D296-D306. https://doi.org/10.1093/nar/gkz1030

Kumar, M., Michael, S., Alvarado-Valverde, J., Zeke, A., Lazar, T., Glavina, J., Nagy-Kanta, E., Donagh, J. M., Kalman, Z. E., Pascarelli, S., Palopoli, N., Dobson, L., Suarez, C. F., Van Roey, K., Krystkowiak, I., Griffin, J. E., Nagpal, A., Bhardwaj, R., Diella, F., . . . Gibson, T. J. (2024). ELM-the Eukaryotic Linear Motif resource-2024 update. *Nucleic Acids Res*, *52*(D1), D442-D455. https://doi.org/10.1093/nar/gkad1058

Kurgan, L. (2022). Resources for computational prediction of intrinsic disorder in proteins. *Methods*, *204*, 132-141. https://doi.org/10.1016/j.ymeth.2022.03.018

Labbadia, J., & Morimoto, R. I. (2015). The biology of proteostasis in aging and disease. *Annu Rev Biochem*, *84*, 435-464. https://doi.org/10.1146/annurev-biochem-060614-033955

Lee, M. J., Pal, K., Tasaki, T., Roy, S., Jiang, Y., An, J. Y., Banerjee, R., & Kwon, Y. T. (2008). Synthetic heterovalent inhibitors targeting recognition E3 components of the N-end rule pathway. *Proc Natl Acad Sci U S A*, *105*(1), 100-105. https://doi.org/10.1073/pnas.0809681105

Longtine, M. S., McKenzie, A., 3rd, Demarini, D. J., Shah, N. G., Wach, A., Brachat, A., Philippsen, P., & Pringle, J. R. (1998). Additional modules for versatile and economical PCR-based gene deletion and modification in Saccharomyces cerevisiae. *Yeast*, *14*(10), 953-961. https://doi.org/10.1002/(SICI)1097-0061(199807)14:10<953::AID-YEA293>3.0.CO;2-U

Mace, P. D., & Day, C. L. (2023). A massive machine regulates cell death. *Science*, *379*(6637), 1093-1094. https://doi.org/10.1126/science.adg9605

Mace, P. D., Linke, K., Feltham, R., Schumacher, F. R., Smith, C. A., Vaux, D. L., Silke, J., & Day, C. L. (2008). Structures of the cIAP2 RING domain reveal conformational changes associated with ubiquitin-conjugating enzyme (E2) recruitment. *J Biol Chem*, *283*(46), 31633-31640. https://doi.org/10.1074/jbc.M804753200

Markova, M., Pivovarova, O., Hornemann, S., Sucher, S., Frahnow, T., Wegner, K., Machann, J., Petzke, K. J., Hierholzer, J., Lichtinghagen, R., Herder, C., Carstensen-Kirberg, M., Roden, M., Rudovich, N., Klaus, S., Thomann, R., Schneeweiss, R., Rohn, S., & Pfeiffer, A. F. (2017). Isocaloric Diets High in Animal or Plant Protein Reduce Liver Fat and Inflammation in Individuals With Type 2 Diabetes. *Gastroenterology*, *152*(3), 571-585 e578. https://doi.org/10.1053/j.gastro.2016.10.007

Matta-Camacho, E., Kozlov, G., Li, F. F., & Gehring, K. (2010). Structural basis of substrate recognition and specificity in the N-end rule pathway. *Nat Struct Mol Biol*, *17*(10), 1182-1187. https://doi.org/10.1038/nsmb.1894

Meng, E. C., Goddard, T. D., Pettersen, E. F., Couch, G. S., Pearson, Z. J., Morris, J. H., & Ferrin, T. E. (2023). UCSF ChimeraX: Tools for structure building and analysis. *Protein Sci*, *32*(11), e4792. https://doi.org/10.1002/pro.4792

Meszaros, B., Kumar, M., Gibson, T. J., Uyar, B., & Dosztanyi, Z. (2017). Degrons in cancer. *Sci Signal*, *10*(470). https://doi.org/10.1126/scisignal.aak9982

Meszaros, B., Samano-Sanchez, H., Alvarado-Valverde, J., Calyseva, J., Martinez-Perez, E., Alves, R., Shields, D. C., Kumar, M., Rippmann, F., Chemes, L. B., & Gibson, T. J. (2021). Short linear motif candidates in the cell entry system used by SARS-CoV-2 and their potential therapeutic implications. *Sci Signal*, *14*(665). https://doi.org/10.1126/scisignal.abd0334

Metzger, M. B., Pruneda, J. N., Klevit, R. E., & Weissman, A. M. (2014). RING-type E3 ligases: master manipulators of E2 ubiquitin-conjugating enzymes and ubiquitination. *Biochim Biophys Acta*, *1843*(1), 47-60. https://doi.org/10.1016/j.bbamcr.2013.05.026

Mohamed, W. I., Park, S. L., Rabl, J., Leitner, A., Boehringer, D., & Peter, M. (2021). The human GID complex engages two independent modules for substrate recruitment. *EMBO Rep*, *22*(11), e52981. https://doi.org/10.15252/embr.202152981

Mumberg, D., Muller, R., & Funk, M. (1995). Yeast vectors for the controlled expression of heterologous proteins in different genetic backgrounds. *Gene*, *156*(1), 119-122. https://doi.org/10.1016/0378-1119(95)00037-7

Munro, S., & Pelham, H. R. (1987). A C-terminal signal prevents secretion of luminal ER proteins. *Cell*, *48*(5), 899-907. https://doi.org/10.1016/0092-8674(87)90086-9

Narendra, D., Tanaka, A., Suen, D. F., & Youle, R. J. (2008). Parkin is recruited selectively to impaired mitochondria and promotes their autophagy. *J Cell Biol*, *183*(5), 795-803. https://doi.org/10.1083/jcb.200809125

Oh, J. H., Hyun, J. Y., & Varshavsky, A. (2017). Control of Hsp90 chaperone and its clients by N-terminal acetylation and the N-end rule pathway. *Proc Natl Acad Sci U S A*, *114*(22), E4370-E4379. https://doi.org/10.1073/pnas.1705898114

Pan, M., Zheng, Q., Wang, T., Liang, L., Mao, J., Zuo, C., Ding, R., Ai, H., Xie, Y., Si, D., Yu, Y., Liu, L., & Zhao, M. (2021). Structural insights into Ubr1-mediated N-degron polyubiquitination. *Nature*, *600*(7888), 334-338. https://doi.org/10.1038/s41586-021-04097-8

Pan, Z. Q., Kentsis, A., Dias, D. C., Yamoah, K., & Wu, K. (2004). Nedd8 on cullin: building an expressway to protein destruction. *Oncogene*, *23*(11), 1985-1997. https://doi.org/10.1038/sj.onc.1207414

Petroski, M. D., & Deshaies, R. J. (2005). Function and regulation of cullin-RING ubiquitin ligases. *Nat Rev Mol Cell Biol*, *6*(1), 9-20. https://doi.org/10.1038/nrm1547

Piatkov, K. I., Brower, C. S., & Varshavsky, A. (2012). The N-end rule pathway counteracts cell death by destroying proapoptotic protein fragments. *Proc Natl Acad Sci U S A*, *109*(27), E1839-1847. https://doi.org/10.1073/pnas.1207786109

Pickart, C. M. (2001). Mechanisms underlying ubiquitination. *Annu Rev Biochem*, *70*, 503-533. https://doi.org/10.1146/annurev.biochem.70.1.503

Pickart, C. M., & Fushman, D. (2004). Polyubiquitin chains: polymeric protein signals. *Curr Opin Chem Biol*, *8*(6), 610-616. https://doi.org/10.1016/j.cbpa.2004.09.009

Plechanovova, A., Jaffray, E. G., Tatham, M. H., Naismith, J. H., & Hay, R. T. (2012). Structure of a RING E3 ligase and ubiquitin-loaded E2 primed for catalysis. *Nature*, *489*(7414), 115-120. https://doi.org/10.1038/nature11376

Prasad, R., Kawaguchi, S., & Ng, D. T. (2010). A nucleus-based quality control mechanism for cytosolic proteins. *Mol Biol Cell*, *21*(13), 2117-2127. https://doi.org/10.1091/mbc.e10-02-0111

Ramachandran, S., & Ciulli, A. (2021). Building ubiquitination machineries: E3 ligase multi-subunit assembly and substrate targeting by PROTACs and molecular glues. *Curr Opin Struct Biol*, *67*, 110-119. https://doi.org/10.1016/j.sbi.2020.10.009

Rao, H., Uhlmann, F., Nasmyth, K., & Varshavsky, A. (2001). Degradation of a cohesin subunit by the N-end rule pathway is essential for chromosome stability. *Nature*, *410*(6831), 955-959. https://doi.org/10.1038/35073627

Robinson, M. S. (2004). Adaptable adaptors for coated vesicles. *Trends Cell Biol*, *14*(4), 167-174. https://doi.org/10.1016/j.tcb.2004.02.002

Robustelli, P., Piana, S., & Shaw, D. E. (2020). Mechanism of Coupled Folding-upon-Binding of an Intrinsically Disordered Protein. *J Am Chem Soc*, *142*(25), 11092-11101. https://doi.org/10.1021/jacs.0c03217

Sabari, B. R., Dall'Agnese, A., & Young, R. A. (2020). Biomolecular Condensates in the Nucleus. *Trends Biochem Sci*, *45*(11), 961-977. https://doi.org/10.1016/j.tibs.2020.06.007

Saha, A., & Deshaies, R. J. (2008). Multimodal activation of the ubiquitin ligase SCF by Nedd8 conjugation. *Mol Cell*, *32*(1), 21-31. https://doi.org/10.1016/j.molcel.2008.08.021

Sakamoto, K. M., Kim, K. B., Kumagai, A., Mercurio, F., Crews, C. M., & Deshaies, R. J. (2001). Protacs: chimeric molecules that target proteins to the Skp1-Cullin-F box complex for ubiquitination and degradation. *Proc Natl Acad Sci U S A*, *98*(15), 8554-8559. https://doi.org/10.1073/pnas.141230798

Schagger, H. (2006). Tricine-SDS-PAGE. *Nat Protoc*, *1*(1), 16-22. https://doi.org/10.1038/nprot.2006.4

Schmidt, R. M., Schessner, J. P., Borner, G. H., & Schuck, S. (2019). The proteasome biogenesis regulator Rpn4 cooperates with the unfolded protein response to promote ER stress resistance. *Elife*, *8*. https://doi.org/10.7554/eLife.43244

Schuler, B., Borgia, A., Borgia, M. B., Heidarsson, P. O., Holmstrom, E. D., Nettels, D., & Sottini, A. (2020). Binding without folding - the biomolecular function of disordered polyelectrolyte complexes. *Curr Opin Struct Biol*, *60*, 66-76. https://doi.org/10.1016/j.sbi.2019.12.006

Sherpa, D., Chrustowicz, J., Qiao, S., Langlois, C. R., Hehl, L. A., Gottemukkala, K. V., Hansen, F. M., Karayel, O., von Gronau, S., Prabu, J. R., Mann, M., Alpi, A. F., & Schulman, B. A. (2021). GID E3 ligase supramolecular chelate assembly configures multipronged ubiquitin targeting of an oligomeric metabolic enzyme. *Mol Cell*, *81*(11), 2445-2459 e2413. https://doi.org/10.1016/j.molcel.2021.03.025

Shiba-Fukushima, K., Imai, Y., Yoshida, S., Ishihama, Y., Kanao, T., Sato, S., & Hattori, N. (2012). PINK1-mediated phosphorylation of the Parkin ubiquitin-like domain primes mitochondrial translocation of Parkin and regulates mitophagy. *Sci Rep*, *2*, 1002. https://doi.org/10.1038/srep01002

Simonetta, K. R., Taygerly, J., Boyle, K., Basham, S. E., Padovani, C., Lou, Y., Cummins, T. J., Yung, S. L., von Soly, S. K., Kayser, F., Kuriyan, J., Rape, M., Cardozo, M., Gallop, M. A., Bence, N. F., Barsanti, P. A., & Saha, A. (2019). Prospective discovery of small molecule enhancers of an E3 ligase-substrate interaction. *Nat Commun*, *10*(1), 1402. https://doi.org/10.1038/s41467-019-09358-9

Singer, M. A., & Lindquist, S. (1998). Multiple effects of trehalose on protein folding in vitro and in vivo. *Mol Cell*, *1*(5), 639-648. https://doi.org/10.1016/s1097-2765(00)80064-7

Singhal, S., Mehta, J., Desikan, R., Ayers, D., Roberson, P., Eddlemon, P., Munshi, N., Anaissie, E., Wilson, C., Dhodapkar, M., Zeddis, J., & Barlogie, B. (1999). Antitumor activity of thalidomide in refractory multiple myeloma. *N Engl J Med*, *341*(21), 1565-1571. https://doi.org/10.1056/NEJM199911183412102

Stewart, M. D., Ritterhoff, T., Klevit, R. E., & Brzovic, P. S. (2016). E2 enzymes: more than just middle men. *Cell Res*, *26*(4), 423-440. https://doi.org/10.1038/cr.2016.35

Stolz, A., Besser, S., Hottmann, H., & Wolf, D. H. (2013). Previously unknown role for the ubiquitin ligase Ubr1 in endoplasmic reticulum-associated protein degradation. *Proc Natl Acad Sci U S A*, *110*(38), 15271-15276. https://doi.org/10.1073/pnas.1304928110

Swatek, K. N., & Komander, D. (2016). Ubiquitin modifications. *Cell Res*, *26*(4), 399-422. https://doi.org/10.1038/cr.2016.39

Szoradi, T., Schaeff, K., Garcia-Rivera, E. M., Itzhak, D. N., Schmidt, R. M., Bircham, P. W., Leiss, K., Diaz-Miyar, J., Chen, V. K., Muzzey, D., Borner, G. H. H., & Schuck, S. (2018). SHRED Is a Regulatory Cascade that Reprograms Ubr1 Substrate Specificity for Enhanced Protein Quality Control during Stress. *Mol Cell*, *70*(6), 1025-1037 e1025. https://doi.org/10.1016/j.molcel.2018.04.027

Tan, X., Calderon-Villalobos, L. I., Sharon, M., Zheng, C., Robinson, C. V., Estelle, M., & Zheng, N. (2007). Mechanism of auxin perception by the TIR1 ubiquitin ligase. *Nature*, *446*(7136), 640-645. https://doi.org/10.1038/nature05731

Tanaka, A., Cleland, M. M., Xu, S., Narendra, D. P., Suen, D. F., Karbowski, M., & Youle, R. J. (2010). Proteasome and p97 mediate mitophagy and degradation of mitofusins induced by Parkin. *J Cell Biol*, *191*(7), 1367-1380. https://doi.org/10.1083/jcb.201007013

Tang, X., Orlicky, S., Lin, Z., Willems, A., Neculai, D., Ceccarelli, D., Mercurio, F., Shilton, B. H., Sicheri, F., & Tyers, M. (2007). Suprafacial orientation of the SCFCdc4 dimer accommodates multiple geometries for substrate ubiquitination. *Cell*, *129*(6), 1165-1176. https://doi.org/10.1016/j.cell.2007.04.042

Tasaki, T., & Kwon, Y. T. (2007). The mammalian N-end rule pathway: new insights into its components and physiological roles. *Trends Biochem Sci*, *32*(11), 520-528. https://doi.org/10.1016/j.tibs.2007.08.010

Tasaki, T., Mulder, L. C., Iwamatsu, A., Lee, M. J., Davydov, I. V., Varshavsky, A., Muesing, M., & Kwon, Y. T. (2005). A family of mammalian E3 ubiquitin ligases that contain the UBR box motif and recognize N-degrons. *Mol Cell Biol*, *25*(16), 7120-7136. https://doi.org/10.1128/MCB.25.16.7120-7136.2005

Tasaki, T., Sriram, S. M., Park, K. S., & Kwon, Y. T. (2012). The N-end rule pathway. *Annu Rev Biochem*, *81*, 261-289. https://doi.org/10.1146/annurev-biochem-051710-093308

Timms, R. T., Zhang, Z., Rhee, D. Y., Harper, J. W., Koren, I., & Elledge, S. J. (2019). A glycine-specific N-degron pathway mediates the quality control of protein N-myristoylation. *Science*, *365*(6448). https://doi.org/10.1126/science.aaw4912

Tompa, P., & Fuxreiter, M. (2008). Fuzzy complexes: polymorphism and structural disorder in protein-protein interactions. *Trends Biochem Sci*, *33*(1), 2-8. https://doi.org/10.1016/j.tibs.2007.10.003

Tompa, P., Schad, E., Tantos, A., & Kalmar, L. (2015). Intrinsically disordered proteins: emerging interaction specialists. *Curr Opin Struct Biol*, *35*, 49-59. https://doi.org/10.1016/j.sbi.2015.08.009

Tong, H., Hateboer, G., Perrakis, A., Bernards, R., & Sixma, T. K. (1997). Crystal structure of murine/human Ubc9 provides insight into the variability of the ubiquitin-conjugating system. *J Biol Chem*, *272*(34), 21381-21387. https://doi.org/10.1074/jbc.272.34.21381

Turner, G. C., Du, F., & Varshavsky, A. (2000). Peptides accelerate their uptake by activating a ubiquitin-dependent proteolytic pathway. *Nature*, *405*(6786), 579-583. https://doi.org/10.1038/35014629

van der Lee, R., Buljan, M., Lang, B., Weatheritt, R. J., Daughdrill, G. W., Dunker, A. K., Fuxreiter, M., Gough, J., Gsponer, J., Jones, D. T., Kim, P. M., Kriwacki, R. W., Oldfield, C. J., Pappu, R. V., Tompa, P., Uversky, V. N., Wright, P. E., & Babu, M. M.

(2014). Classification of intrinsically disordered regions and proteins. *Chem Rev*, *114*(13), 6589-6631. https://doi.org/10.1021/cr400525m

Van Roey, K., Gibson, T. J., & Davey, N. E. (2012). Motif switches: decision-making in cell regulation. *Curr Opin Struct Biol*, *22*(3), 378-385. https://doi.org/10.1016/j.sbi.2012.03.004

Van Roey, K., Uyar, B., Weatheritt, R. J., Dinkel, H., Seiler, M., Budd, A., Gibson, T. J., & Davey, N. E. (2014). Short linear motifs: ubiquitous and functionally diverse protein interaction modules directing cell regulation. *Chem Rev*, *114*(13), 6733-6778. https://doi.org/10.1021/cr400585q

Varadi, M., Bertoni, D., Magana, P., Paramval, U., Pidruchna, I., Radhakrishnan, M., Tsenkov, M., Nair, S., Mirdita, M., Yeo, J., Kovalevskiy, O., Tunyasuvunakool, K., Laydon, A., Zidek, A., Tomlinson, H., Hariharan, D., Abrahamson, J., Green, T., Jumper, J., . . . Velankar, S. (2024). AlphaFold Protein Structure Database in 2024: providing structure coverage for over 214 million protein sequences. *Nucleic Acids Res*, *52*(D1), D368-D375. https://doi.org/10.1093/nar/gkad1011

Varshavsky, A. (2008). Discovery of cellular regulation by protein degradation. *J Biol Chem*, *283*(50), 34469-34489. https://doi.org/10.1074/jbc.X800009200

Varshavsky, A. (2011). The N-end rule pathway and regulation by proteolysis. *Protein Sci*, *20*(8), 1298-1345. https://doi.org/10.1002/pro.666

Vittal, V., Stewart, M. D., Brzovic, P. S., & Klevit, R. E. (2015). Regulating the Regulators: Recent Revelations in the Control of E3 Ubiquitin Ligases. *J Biol Chem*, *290*(35), 21244-21251. https://doi.org/10.1074/jbc.R115.675165

Wang, L., Liu, C., Yang, B., Zhang, H., Jiao, J., Zhang, R., Liu, S., Xiao, S., Chen, Y., Liu, B., Ma, Y., Duan, X., Guo, Y., Guo, M., Wu, B., Wang, X., Huang, X., Yang, H., Gui, Y., . . . Li, W. (2022). SARS-CoV-2 ORF10 impairs cilia by enhancing CUL2ZYG11B activity. *J Cell Biol*, *221*(7). https://doi.org/10.1083/jcb.202108015

Ward, J. J., Sodhi, J. S., McGuffin, L. J., Buxton, B. F., & Jones, D. T. (2004). Prediction and functional analysis of native disorder in proteins from the three kingdoms of life. *J Mol Biol*, *337*(3), 635-645. https://doi.org/10.1016/j.jmb.2004.02.002

Winston, J. T., Koepp, D. M., Zhu, C., Elledge, S. J., & Harper, J. W. (1999). A family of mammalian F-box proteins. *Curr Biol*, *9*(20), 1180-1182. https://doi.org/10.1016/S0960-9822(00)80021-4

Winter, G. E., Buckley, D. L., Paulk, J., Roberts, J. M., Souza, A., Dhe-Paganon, S., & Bradner, J. E. (2015). DRUG DEVELOPMENT. Phthalimide conjugation as a strategy for in vivo target protein degradation. *Science*, *348*(6241), 1376-1381. https://doi.org/10.1126/science.aab1433

Wolff, S., Weissman, J. S., & Dillin, A. (2014). Differential scales of protein quality control. *Cell*, *157*(1), 52-64. https://doi.org/10.1016/j.cell.2014.03.007

Worthylake, D. K., Prakash, S., Prakash, L., & Hill, C. P. (1998). Crystal structure of the Saccharomyces cerevisiae ubiquitin-conjugating enzyme Rad6 at 2.6 A resolution. *J Biol Chem*, *273*(11), 6271-6276. https://doi.org/10.1074/jbc.273.11.6271

Xia, Z., Turner, G. C., Hwang, C. S., Byrd, C., & Varshavsky, A. (2008). Amino acids induce peptide uptake via accelerated degradation of CUP9, the transcriptional repressor of the PTR2 peptide transporter. *J Biol Chem*, *283*(43), 28958-28968. https://doi.org/10.1074/jbc.M803980200

Xia, Z., Webster, A., Du, F., Piatkov, K., Ghislain, M., & Varshavsky, A. (2008). Substrate-binding sites of UBR1, the ubiquitin ligase of the N-end rule pathway. *J Biol Chem*, *283*(35), 24011-24028. https://doi.org/10.1074/jbc.M802583200

Xie, Y., & Varshavsky, A. (1999). The E2-E3 interaction in the N-end rule pathway: the RING-H2 finger of E3 is required for the synthesis of multiubiquitin chain. *EMBO J*, *18*(23), 6832-6844. https://doi.org/10.1093/emboj/18.23.6832

Yang, Y., Arseni, D., Zhang, W., Huang, M., Lovestam, S., Schweighauser, M., Kotecha, A., Murzin, A. G., Peak-Chew, S. Y., Macdonald, J., Lavenir, I., Garringer, H. J., Gelpi, E., Newell, K. L., Kovacs, G. G., Vidal, R., Ghetti, B., Ryskeldi-Falcon, B., Scheres, S. H. W., & Goedert, M. (2022). Cryo-EM structures of amyloid-beta 42 filaments from human brains. *Science*, *375*(6577), 167-172. https://doi.org/10.1126/science.abm7285

Young, T. S., Ahmad, I., Yin, J. A., & Schultz, P. G. (2010). An enhanced system for unnatural amino acid mutagenesis in E. coli. *J Mol Biol*, *395*(2), 361-374. https://doi.org/10.1016/j.jmb.2009.10.030

Zanzoni, A., Ribeiro, D. M., & Brun, C. (2019). Understanding protein multifunctionality: from short linear motifs to cellular functions. *Cell Mol Life Sci*, *76*(22), 4407-4412. https://doi.org/10.1007/s00018-019-03273-4

Zengerle, M., Chan, K. H., & Ciulli, A. (2015). Selective Small Molecule Induced Degradation of the BET Bromodomain Protein BRD4. *ACS Chem Biol*, *10*(8), 1770-1777. https://doi.org/10.1021/acschembio.5b00216

Zenker, M., Mayerle, J., Lerch, M. M., Tagariello, A., Zerres, K., Durie, P. R., Beier, M., Hulskamp, G., Guzman, C., Rehder, H., Beemer, F. A., Hamel, B., Vanlieferinghen, P., Gershoni-Baruch, R., Vieira, M. W., Dumic, M., Auslender, R., Gil-da-Silva-Lopes, V. L., Steinlicht, S., . . . Reis, A. (2005). Deficiency of UBR1, a ubiquitin ligase of the N-end rule pathway, causes pancreatic dysfunction, malformations and mental retardation (Johanson-Blizzard syndrome). *Nat Genet*, *37*(12), 1345-1350. https://doi.org/10.1038/ng1681

Zhang, S., Chang, L., Alfieri, C., Zhang, Z., Yang, J., Maslen, S., Skehel, M., & Barford, D. (2016). Molecular mechanism of APC/C activation by mitotic phosphorylation. *Nature*, *533*(7602), 260-264. https://doi.org/10.1038/nature17973

Zhang, Y., Lin, S., Peng, J., Liang, X., Yang, Q., Bai, X., Li, Y., Li, J., Dong, W., Wang, Y., Huang, Y., Pei, Y., Guo, J., Zhao, W., Zhang, Z., Liu, M., & Zhu, A. J. (2022).

Amelioration of hepatic steatosis by dietary essential amino acid-induced ubiquitination. *Mol Cell*, *82*(8), 1528-1542 e1510. https://doi.org/10.1016/j.molcel.2022.01.021

Zhao, W., Zhang, Y., Lin, S., Li, Y., Zhu, A. J., Shi, H., & Liu, M. (2023). Identification of Ubr1 as an amino acid sensor of steatosis in liver and muscle. *J Cachexia Sarcopenia Muscle*, *14*(3), 1454-1467. https://doi.org/10.1002/jcsm.13233

Zheng, N., Schulman, B. A., Song, L., Miller, J. J., Jeffrey, P. D., Wang, P., Chu, C., Koepp, D. M., Elledge, S. J., Pagano, M., Conaway, R. C., Conaway, J. W., Harper, J. W., & Pavletich, N. P. (2002). Structure of the Cul1-Rbx1-Skp1-F boxSkp2 SCF ubiquitin ligase complex. *Nature*, *416*(6882), 703-709. https://doi.org/10.1038/416703a

Zheng, N., & Shabek, N. (2017). Ubiquitin Ligases: Structure, Function, and Regulation. *Annu Rev Biochem*, *86*, 129-157. https://doi.org/10.1146/annurev-biochem-060815-014922

Zheng, N., Zhou, Q., Wang, Z., & Wei, W. (2016). Recent advances in SCF ubiquitin ligase complex: Clinical implications. *Biochim Biophys Acta*, *1866*(1), 12-22. https://doi.org/10.1016/j.bbcan.2016.05.001

Zhu, K., Song, L., Wang, L., Hua, L., Luo, Z. Wang, T., Qin, B., Yuan, S., Gao, X., Mi, W, Cui, S. (2024). SARS-CoV-2 ORF10 hijacking ubiquitination machinery reveals potential unique drug targeting sites: *Acta Pharm Sin B*, 14(9), 4164-4173. https://doi.org/10.1016/j.apsb.2024.05.018

7. List of Figures

8. List of Tables